UC Berkeley
Research Reports

Title
Experimental Automatic Lateral Control System For An Automobile

Permalink
https://escholarship.org/uc/item/5d50p418

Authors
Peng, Huei
Zhang, Wei-bin
Arai, Alan
et al.

Publication Date
1992

eScholarship.org Powered by the California Digital Library
University of California

CALIFORNIA PATH PROGRAM
INSTITUTE OF TRANSPORTATION STUDIES
UNIVERSITY OF CALIFORNIA, BERKELEY

Experimental Automatic Lateral Control System for an Automobile

Huei Peng, Wei-Bin Zhang, Alan Arai, Ye Lin, Thomas Hessburg, Peter Devlin, Masayoshi Tomizuka, and Steven Shladover

PATH Research Report
UCB-ITS-PRR-92-11

This work was performed as part of the California PATH Program of the University of Califomia, in cooperation with the State of California, Business, Transportation, and Housing Agency, Department of Transportation, and the United States Department of Transportation, Federal Highway Administration.

The contents of this report reflect the views of the authors who are responsible for the facts and the accuracy of the data presented herein. The contents do not necessarily reflect the official views or policies of the State of California. This report does not constitute a standard, specification, or regulation.

November 1992

ISSN 1055-1425

This paper has been mechanically scanned. Some errors may have been inadvertently introduced.

CONTENTS

FIGURES

TABLES

FOREWORD

This report summarizes an experimental effort in integrating and testing a vehicle lateral control system. This project is being conducted as a collaborative effort between California's Partners for Advanced Transit and Highways (PATH) Program at the University of California, Berkeley and IMRA America, Inc. The portion of the work conducted by PATH is sponsored by the State of California, Business, Transportation, and Housing Agency, Department of Transportation (Caltrans). This project was conducted at the Richmond Field Station (RFS) of the University of California at Berkeley (UCB). The duration of the project was 17 months beginning in January, 1991.

The project researchers include Mr. Wei-Bin Zhang, Dr. Ye Lin, Mr. Peter Devlin, and Dr. Steven Shladover of PATH; Professor Masayoshi Tomizuka, Mr. Huei Peng, and Mr. Thomas Hessburg of the Mechanical Engineering Department of UCB; and Mr. Alan Arai of IMRA. In addition, a steering committee was formed to provide guidance to the researchers throughout the project. This committee consisted of representatives from Caltrans (Mr. Roy Bushey), PATH (Dr. Steven Shladover), IMRA (Mr. Michael Dearing, followed by Mr. Takashi Omitsu) and Parsons Transportation Associates (Mr. Robert Parsons)

Other participants who made significant contributions were Mr. Charles Price and Mr. Sompol Chatusripitak of Caltrans, for their direct involvement in the test track construction and many of the project milestones; Mr. Larry Bell of RFS, for the coordination of the design and construction of the test track; and Mr. Yoshiyuki Yasui, for his assistance in the procurement of the DSP system. We would also like to acknowledge Ms. Mimi Huie and Mr. David Ashuckian of CALTRANS for their assistance in the project.

EXECUTIVE SUMMARY

The project described in this report is a cooperative effort between the California Partners for Advanced Transit and Highway (PATH) Program and IMRA America, Inc. The project focused on an experimental study of a lateral control system for a full scaled automobile.

Previous PATH program work on vehicle lateral control has emphasized **a** concept of cooperative vehicle lateral control system using a roadway reference system and a preview controller to perform "intelligent" steering. During the past several years, PATH has been developing a reference/sensing system for passing much of the information required for preview steering control. Extensive work has been performed in establishing the theory behind the technology through computer simulation and experiments [2, 3, 4, 5].

IMRA has also been conducting research and development on automatic vehicle control. IMRA researchers, in partnership with university researchers, have been studying vehicle dynamics using computer modelling and simulation. Based on the promising results from the simulation studies, IMRA developed and installed a prototype of a control augmentation system for steering on an automobile.

Due to their mutual interest in automatic vehicle control, PATH and IMRA agreed to jointly conduct an experimental project. This project was started in January 1991 and completed in May 1992.

The objective of this project was to prove the concept of an automated lateral control system with a full scale automobile using the components developed by PATH and IMRA. The system components include a discrete roadway reference system, on-vehicle magnetic sensing system, a computer control system and a hydraulic actuator. The test vehicle and the actuator were provided by IMRA, the sensing and control systems and the test facility are provided by PATH. The project was conducted at the University of California at Berkeley, Richmond Field Station.

The test conditions investigated were limited to low vehicle speeds (I 60 km/hr). In additional to nominal conditions (dry road, tires at standard pressure), the system's performance was also investigated with low tire pressure (30% of nominal in the front two tires), wet road conditions, offset magnetic markers (maximum of about 2 cm), missing magnetic markers, and increased vehicle load (additional 227 kgf). Two control algorithms

were developed for the tests: Proportional-Integral-Derivative (PID) control, and Frequency Shaped Linear Quadratic (FSLQ) control. In both cases, a preview action was found to be necessary. The system's performance was evaluated using lateral deviation and lateral acceleration.

The following conclusions were made based on the results of the experiments on the components and the overall system:

1. The experimental results indicate that the PATH concept of a cooperative lateral control system using discrete magnetic reference/sensing system can produce good control response. A system using this concept can acquire reliable and accurate vehicle state and road geometry information. By using the road geometry information, preview control logic can perform anticipatory steering maneuvers before curve sections, thus the tracking error can be reduced and ride quality can be improved.

2. The experiments on the magnetic reference/sensing system indicate that the accuracy of the lateral measurement provides adequate precision and is robust at different vehicle speeds up to 70 km/hr.

3. FSLQ and PID control test results indicate that both control algorithms perform satisfactorily under the conditions tested. Comparing the two algorithms, it was concluded that the FSLQ control algorithm can provide better ride comfort than that achieved using the PID controller.

4. The steering actuator system with the series configuration was found to perform adequately under the conditions tested. The steering angle range of the actuator was a limitation, however the curve radii used in the tests were much smaller than would be found on an open highway, the intended target for the system.

5. The closed loop experiments show that the system performed satisfactory under nominal and the tested non-ideal conditions at low vehicle speeds. The test vehicle can be controlled within ±20 cm on both straight and curved sections of test path #1 (with a radius of 74 m) at a speed of 50 km/hr. Tighter control was performed on the reverse curves in test path #2 at speeds up to 60 km/hr. Both test data and passenger perception indicate that the ride quality was good even when the vehicle went through the 74 m radius curve at a speed of 50 km/hr.

Analysis of the test results in this report also led to the recommendations for future research. These recommendations include additional development of the components and full scale experiments under adverse conditions and at higher speeds.

1. INTRODUCTION

The purpose of an automated vehicular lateral control system is to automatically steer or to assist a driver in steering the vehicle. The automated steering functions may include lane keeping, lane changing, merging and diverging. Previous studies indicate that reliable and tight lane tracking performance can be achieved by applying automated lateral control systems. Consequently, both capacity and safety benefits are expected [1].

1.1 Project Background

During the past thirty years, many efforts have been directed toward the investigation of automated lateral control systems. As a result, a number of systems have been developed or simulated. However, only a few full scale systems have been tested in a real road/vehicle environment. Most of the studies focused on the lane keeping problem.

Based on a technology assessment of the previous research efforts in vehicle lateral control, PATH developed a concept of a cooperative lateral control system using a roadway reference/sensing system and a preview controller [2, 3, 4]. This concept has been implemented using a discrete magnetic reference/sensing system and preview controller. This system has been tested by computer simulation and by utilizing a scaled experimental vehicle [5].

IMRA has also been conducting research on automatic vehicle control. IMRA researchers, in partnership with university researchers, have been studying vehicle dynamics using computer modelling and simulation. Based on the promising results from the simulation studies, IMRA developed a steering control augmentation system prototype for an automobile.

Due to their mutual interest in automatic vehicle control, PATH and IMRA agreed to combine their efforts to conduct this experimental research project. The objective of this project is to prove the concept of an automated lateral control system for a full scale automobile using practical hardware and appropriate software. The test vehicle and actuator were developed by IMRA. The magnetic reference and control systems were developed by PATH. This project was conducted at the Richmond Field Station of the University of California, Berkeley.

1.2 Report Overview

This report describes the development and testing of an experimental lateral guidance system for an automobile. The objective of the project was accomplished through the development of various components, integration and debugging of the experimental system, and a series of experiments on the components and the integrated system. Intermediate results were reported in two papers [6, 7]. This report summarizes the accomplishments of this research project.

Section 2 outlines the system concept. The system configuration, the major components and the control algorithms are described.

Section 3 describes the experiments on the components. First of all, comparisons between the independent measurement system and the discrete magnetic reference/sensing system verified the accuracy of the magnetic reference/sensing system. Secondly, this section describes tire tests performed to characterize the road/tire forces necessary for developing the tire model used in the computer simulation of the vehicle system. Vehicle simulations were used to predict the response of the test vehicle using the control algorithms described in section 2.6. Lastly, this section presents the results of the open loop experiments which were conducted to verify the accuracy of the vehicle model used for simulation and to evaluate the performance characteristics of the steering system.

Section 4 describes the closed loop experiments. Closed loop experiments were conducted at low vehicle speeds (20 km/hr to 70 km/hr) under both nominal and some adverse conditions such as increased load, reduced tire pressure, misaligned or missing markers, and a wet road surface.

Section 5 concludes the report with an assessment of the cooperative lateral control system concept. Based on the test results, further recommendations are given for the next phase of testing.

2. EXPERIMENTAL SYSTEM

A lateral control system requires four basic components: a roadway reference system, on-vehicle sensing systems, a controller, and a steering actuator. The roadway reference system together with the on-vehicle sensing systems provide the necessary information regarding the vehicle state and some road geometry characteristics. The controller processes the information from the sensors and produces the steering commands. The steering actuator steers the vehicle following the steering commands.

In the PATH/IMRA experiments, a cooperative lateral control concept is used. This concept allows the vehicle to receive both vehicle state and road geometry information from a discrete magnetic reference system consisting of a series of permanent magnetic markers buried in the roadway. The on-board sensing system measures the lateral deviation of the vehicle relative to the markers and decodes upcoming road geometry information. The lateral controller incorporates preview control logic to steer the vehicle based on the vehicle's measured tracking error and upcoming road curvature to achieve both improved tracking accuracy and better ride quality. Figure 2.1 shows a block diagram of the experimental system.

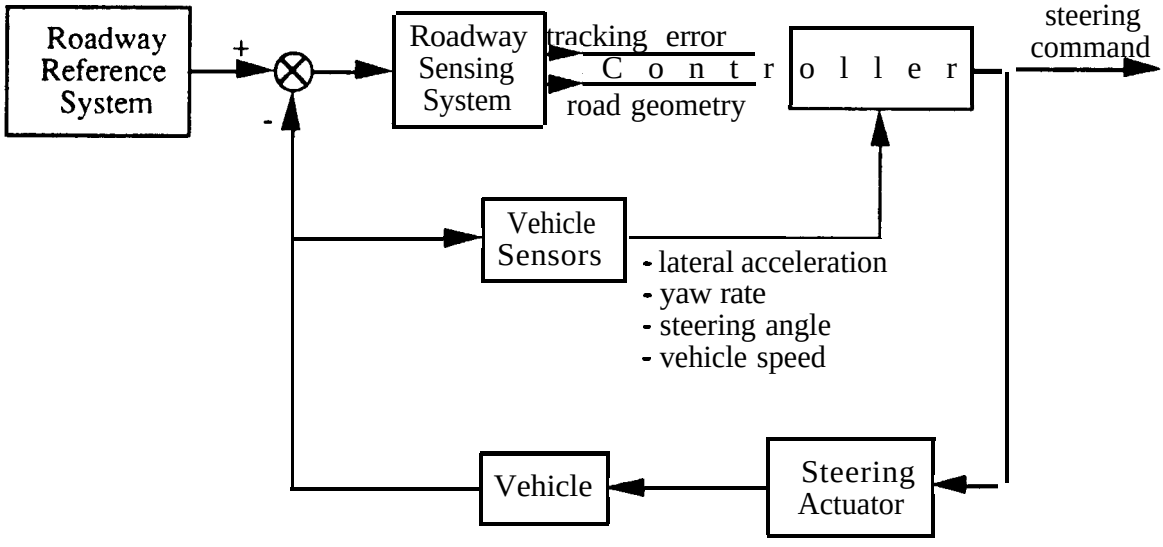

Figure 2.1 Experimental System Block Diagram

2.1 Experimental Vehicle

The vehicle platform selected was a 1988 Toyota Celica Turbo All-Trac. Figure 2.2 is a photograph of the test vehicle at the test track. Figure 2.3 shows a schematic of the test

vehicle. The following sections describe the various components of the test vehicle system and the test facility. A list of the measurement and computer equipment is included in

Figure 2.2 Test Vehicle at the Test Track

2.2 Discrete Magnetic Reference/Sensing System

A roadway reference/sensing system provides the vehicle's displacement relative to the center of the traffic lane and the road geometry information to a lateral controller in order to perform the lane keeping function. An assessment of current technology indicated that a roadway reference/sensing system can be implemented by using either active or passive roadway components together with appropriate on-vehicle sensing devices [2]. A variety of techniques were assessed, including optical, acoustic, radar, and other sensing devices. Previous PATH studies investigated the characteristics of a discrete magnetic reference/sensing system. The system provides an adequate measurement range of the vehicle's lateral displacement. Road geometry information may be encoded in the highway. Both the on-vehicle sensors and the roadway magnetic markers are inexpensive. The system will also function under a wide variety of weather conditions. Therefore, the reference/sensing system using discrete magnetic markers was determined to have potential for practical application on existing roadways.

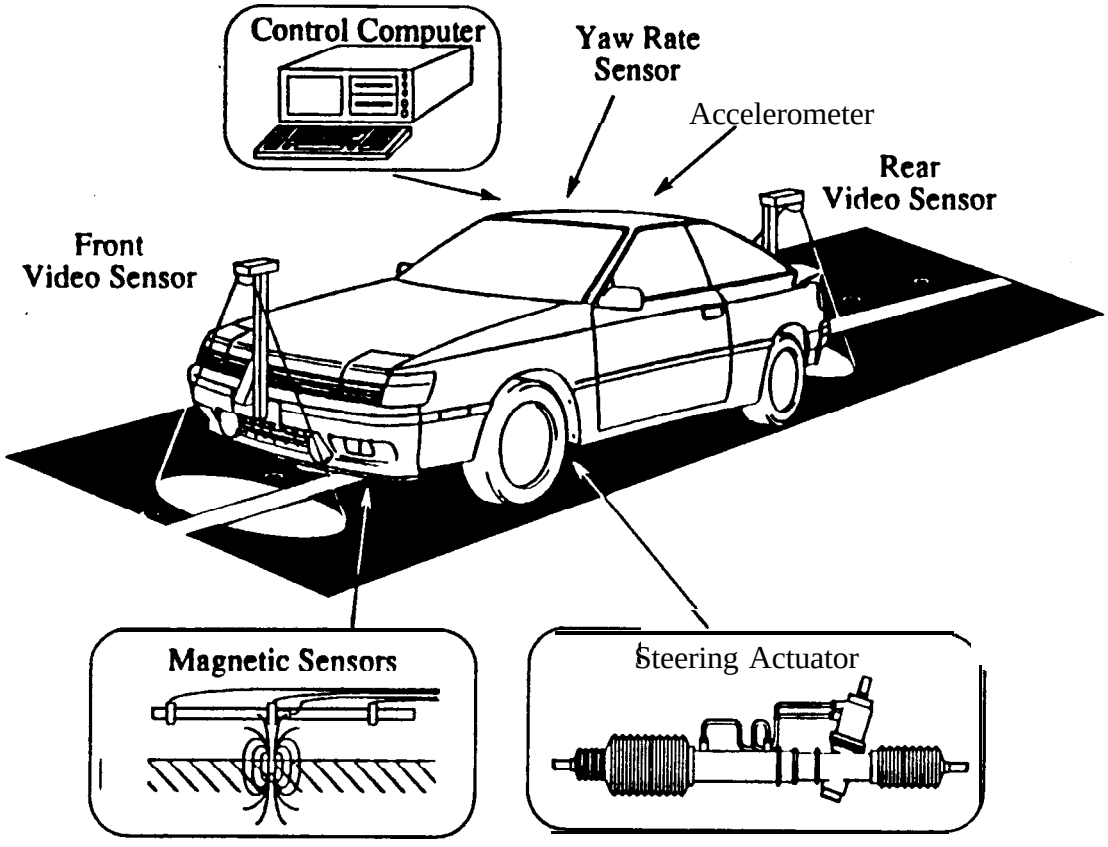

Figure 2.3 Test Vehicle Schematic

Figure 2.4 illustrates the signal flow path of the magnetic marker reference/sensing system. The reference system consists of a series of permanent magnets installed at one meter intervals along the center of a traffic lane. The magnetic field of each marker is sensed to determine the lateral location of the vehicle relative to the center of the desired path. By alternating the polarities of the magnets road geometry information, such as radius and length of curvature, can be passed to the vehicle. A preview of road geometry information has been determined to be an important input for vehicle lateral control [3, 5, 8].

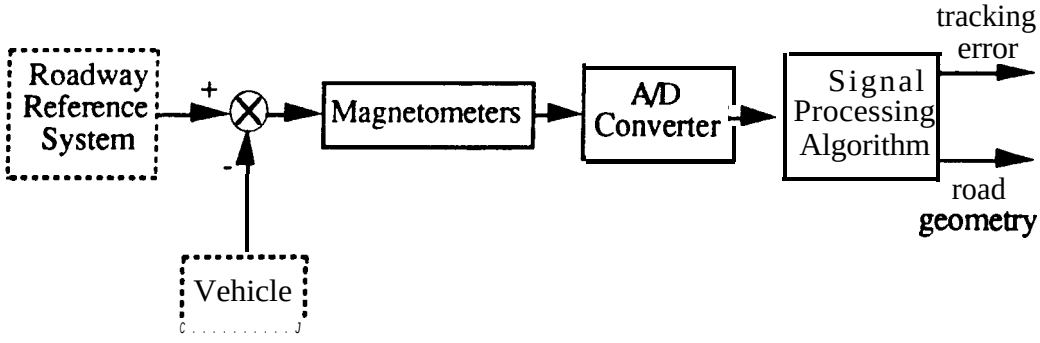

Figure 2.4 Magnetic Marker Reference/Sensing Block Diagram

The magnetic sensing system for the **PATH/IMRA** experimental system includes an array of four Hall-effect magnetometer probes mounted beneath the front bumper of the vehicle, 15 cm above the roadway surface (Figure 2.5). Two magnetometer probes are located on the longitudinal axis of the vehicle. One magnetometer measures the vertical component of the magnetic field, the other measures the horizontal component. The other two probes both measure the vertical component of the magnetic field and are mounted on each side of the longitudinal'axis of the vehicle, 30 cm from the central sensors. Figure 2.6 illustrates the arrangement of the magnetic sensors. Each probe is connected to a receiver by a shielded cable. Each magnetometer is powered by a 9 V battery. The output voltage range is ± 2 V which corresponds to a full scale of ± 3500 milligauss.

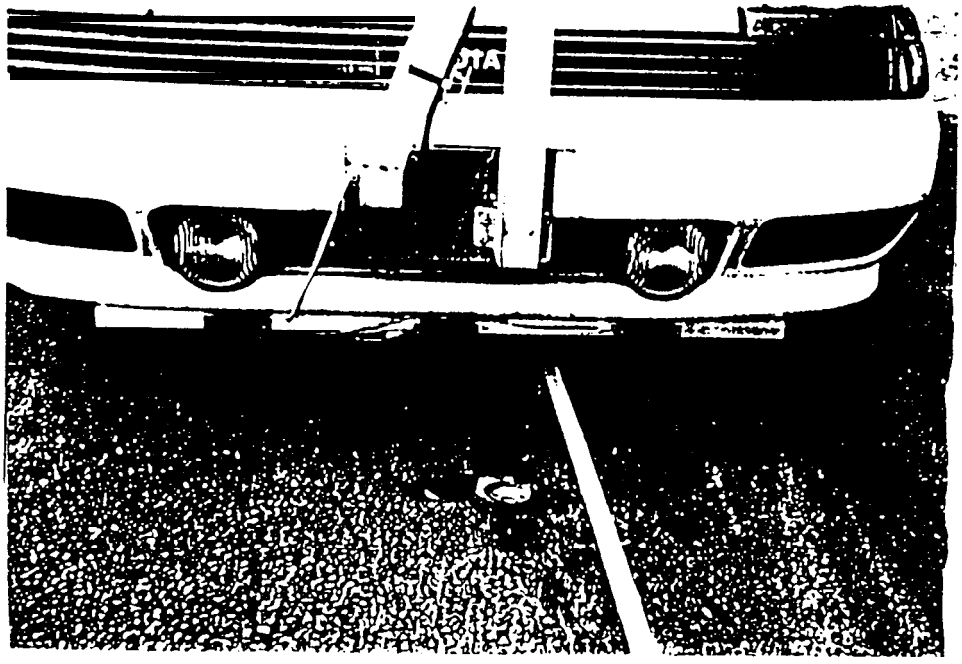

Figure 2.5 Magnetic Sensor Array on Test Vehicle

The signals acquired from the sensors are digitized using an analog-to-digital (A/D) converter before being processed by the controller computer. In the experiments described in this report, the signals acquired by the magnetic sensing system are not filtered. Instead, the probes of the magnetic sensors are isolated from possible magnetic field sources and the cables are shielded. The resulting low level of signal noise was found to have no effect on the accuracy of the measurement of lateral displacement.

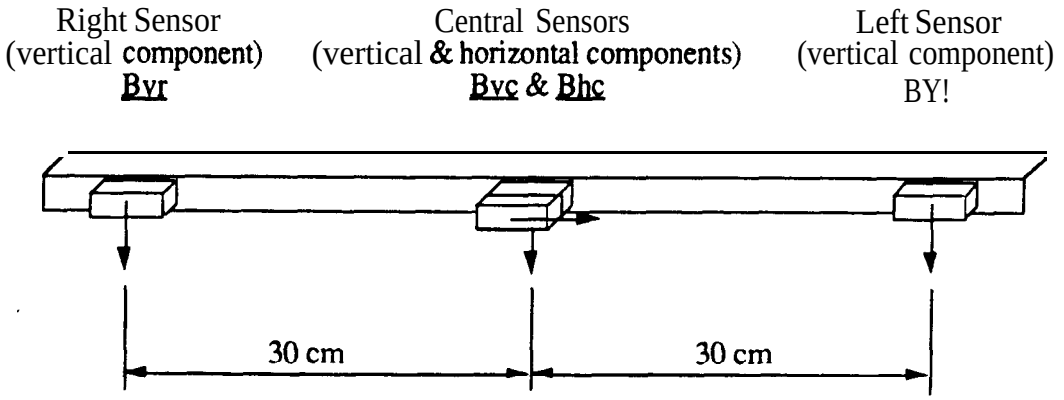

Figure 2.6 Magnetic Sensor Array

The sensing system was designed for a sensing range of approximately 80 cm with a region of high resolution near the center of the vehicle (within ±25 cm) and a region of coarse resolution outside the central region (> 25 cm from the vehicle center). The assumption behind this design was that under most operating conditions the vehicle would be controlled within ±25 cm of the desired path. The simulation results indicated that the degradation of the measurement resolution at larger vehicle deviations does not affect the overall performance of the lateral control system because in conditions of large lateral deviations the lateral controller only needs to know that the vehicle is "too far away from the lane center".

The signal processing algorithm uses different sets of logic statements for each of the two regions of resolution. PATH has conducted previous studies to derive an algorithm for extracting accurate vehicle deviation information from the measured magnetic field. The analysis and experiments indicate that the lateral deviation measurement is sensitive to both the horizontal and vertical distance variation between the magnetic marker and the sensor. To eliminate the influence of the vertical movement of the vehicle on the lateral deviation measurement, both the vertical and horizontal components of the magnetic field must be measured. The relationship between the lateral displacement of the sensor and the measurement of the magnetic field was determined by experiment [3] (also included as Appendix B). An algorithm has been developed based on this relationship which determines the magnetic field of the marker and uses a look-up table for translating the magnetic field measurement into a value for the vehicle's lateral displacement. The simulation analysis and bench experiments indicate that the algorithm can provide adequate resolution and accuracy.

The processing logic for the coarse resolution region is rather simple. Because less accuracy is required, only the vertical component of the magnetic field is measured in the coarse resolution region. The sensors that correspond to these signals, Bvr and Bvl, are shown in Figure 2.6. The distance between the outboard sensors and the central sensors was chosen to be about half the measurement range of the vertical component magnetometer, 30 cm. Figure 2.7 shows the magnetic field profiles measured by the four magnetometers as a function of the position of a magnetic marker relative to the magnetometer array (note that the earth field and other distortions in the magnetic field have been subtracted to produce Figure 2.7). Because of the symmetry of the vertical component of the magnetic field there would be an ambiguity in the measurement of the lateral position if only the vertical component was used. To eliminate this ambiguity, the horizontal component of the magnetic field measured by the one of the central sensors (Bhc, see Figure 2.6) is used in combination with the measurement Bvr or Bvl. The processing is performed in two steps: 1) determine the outboard sensor closest to the magnetic marker, 2) estimate the lateral position.

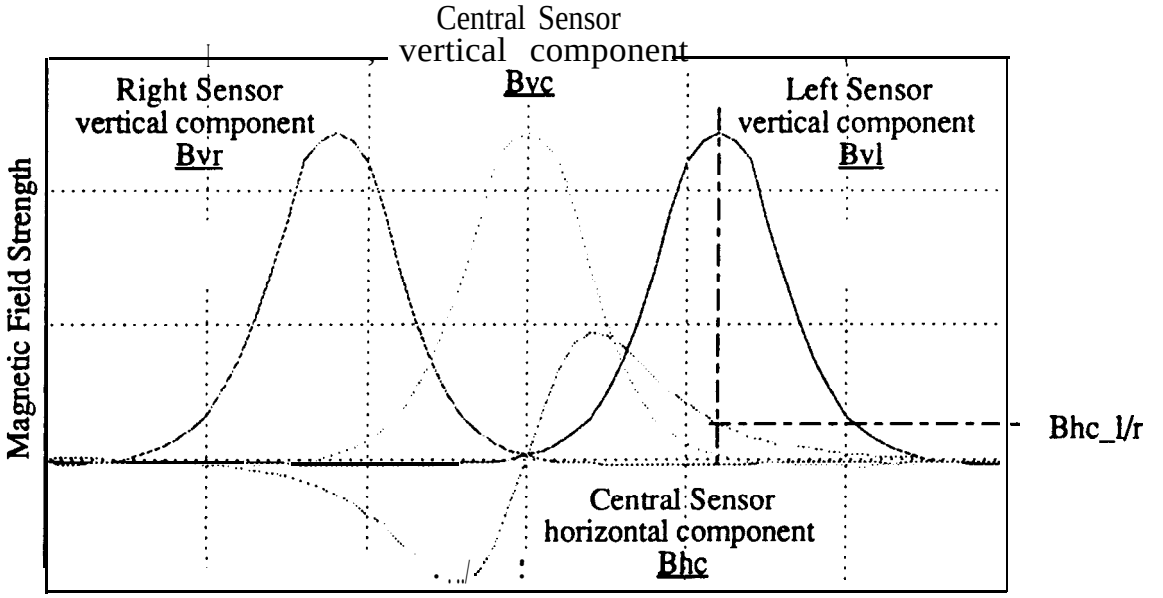

Figure 2.7 Magnetic Field Profiles

The axis of symmetry of the vertical component of the magnetic field is the border between the two ranges of ambiguity, the inner range closer to the central sensors and the outer range farther from the central sensors. Bhc is used to determine whether the marker is in

the inner or outer range of the outboard sensor. A threshold, Bhc_l/r, is determined by measuring the horizontal component of the magnetic field at a lateral distance of 30 cm and height of 15 cm from the magnetic marker.

A look-up table, Table 2.1, is used to determine the lateral displacement from the magnetic field measurement. The look-up table was developed from bench test data using a fixed sensor height of 15 cm. Interpolation is used to determine the deviation between values in the table. Since the variation in the sensor height is not included in the look-up table, the accuracy is lower.

Table 2.1 Coarse Resolution Look-up Table

vertical magnetic field	vehicle's lateral displacement	
	$\|Bhc\| > Bhc\_l/r$	$\|Bhc\| \leq Bhc\_l/r$
Bvll (Bvrl)	Y1	Y7
Bvl2 (Bvr2)	Y2	Y6
Bvl3 (Bvr3)	Y3	Y5
Bvl4 (Bvr4)	Y4	

A binary code has also been developed to encode the road geometry information into the roadway reference system using the magnetic markers. The vehicle reads and records the polarities of the magnetic markers as it travels along the road and decodes the road geometry information after a message is completed. Due to the limited length of the test track, only identifying numbers for the curvatures, e.g. Curve #1, are coded into the roadway reference system. Road geometry information for various curvatures is stored in a database. The control algorithm determines the geometry information from the coded curvature identification number for preview control. In coding the curvature identification numbers, parity checking is used for error detection. In an actual highway installation, more information would be included in the magnetic marker sequence code and less information would be stored in the on-board database. For example, a length of 50 m would be necessary to code the road geometry for a curve of radius 1100 m and length of 700 m, assuming a magnetic marker spacing of 1 m and information resolution of 1 m.

2.3 Other Sensors and Measurement Systems

Other sensors required for lateral control include an accelerometer and yaw rate sensor. In addition, an independent measurement system is used for evaluating the overall system performance and calibrating the magnetic reference/sensing system. The steering angle and vehicle speed are also required as inputs for the control algorithm.

2.3.1 Accelerometer

An accelerometer mounted inside the vehicle, approximately 12 cm behind the vehicle mass center, is used to measure the lateral acceleration of the vehicle. The accelerometer is powered by 12 V. Figure 2.8 shows the approximate location of the accelerometer.

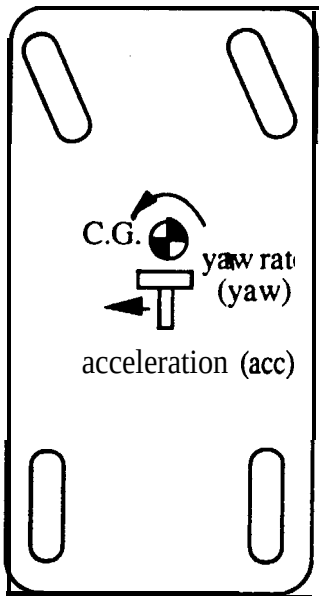

Figure 2.8 Yaw Rate and Accelerometer Positions

2.3.2 Angular Rate Sensor

An angular rate sensor is mounted inside the vehicle near the mass center to measure the vehicle's yaw rate. The angular rate sensor is powered by ±15 V. Figure 2.8 shows the approximate location of the yaw rate sensor.

2.3.3 Independent Measurement System

The independent measurement system is used to evaluate the performance of the vehicle control system and calibrate the magnetic measurement/sensing system. Therefore, it must have a similar dynamic range and an error less than 1% of the full range compared to the magnetic reference/sensing system. Since this system will not be used as the primary

feedback input for the control, it does not-need to be practical for all real world conditions. Cost was an important criterion in the selection process. After evaluating a variety of technologies including radio frequency, buried wire reference, optical and video, an Allen-Bradley line scan video camera system was selected.

Two cameras are mounted on the front and rear of the test vehicle 110 cm above the roadway surface. Reflective tape was placed on the roadway parallel to the magnetic reference system. The video system scans the roadway at predetermined intervals. Edge detection circuitry and a signal processing algorithm in the camera's electronics determine the distance between the center of the camera field of view and the center of the reference tape, from which the vehicle's lateral deviation is derived. The independent measurement system is powered by 24 V. Prior to performing the magnetic reference/sensing system verification tests, the independent measurement system was statically calibrated and verified. Dynamic verification test results indicated that the standard deviation of this independent measurement system is less than 0.4 cm. A more detailed description of the independent measurement system and the calibration results are reported in Appendix C.

2.3.4 Steering Angle Measurement

Two potentiometers mounted within the steering system are used to measure the steering angle (Figure 2.9). One potentiometer measures the displacement of the steering actuator. The other potentiometer measures the rotation of the steering wheel. The combination of these two measurements provides the front wheel steering angle. Appendix D describes the calibration method.

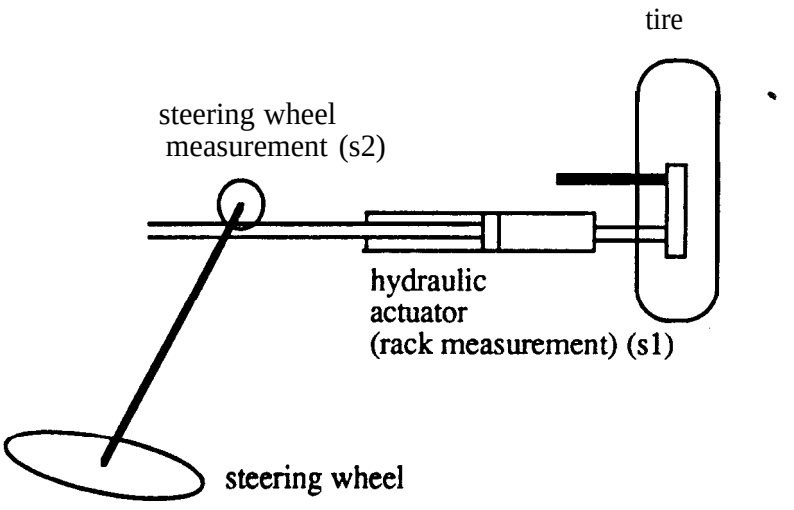

Figure 2.9 Steering Angle Sensor Positions

2.3.5 Vehicle Speed Measurement

The vehicle speed can be estimated by using the magnetic field measurement. As the vehicle passes over a magnetic marker the vertical component of the magnetic field peaks. Since the spacing between each magnet is fixed at 1 m, the time intervals between each successive signal peak can be used to estimate the vehicle's speed. To increase estimation accuracy, three successive time intervals are used in final computation as follows:

$$V = \frac{3000}{(t_k + t_{k-1} + d-2)} \text{ [m/s]} \qquad (2.1)$$

where t_k is the time it takes the vehicle to reach the current magnetic marker from the previous magnetic marker, in msec.

2.4 Lateral Control Computer

The lateral control computer is based on a TMS320C30 Digital Signal Processor (DSP). Initially, the lateral control computer system was specified as the DSP system mounted in an external PC chassis. The external chassis was to be connected to a laptop computer as the user interface through a PC bus extension. However, after reviewing the design and the available components, the PC bus extension was determined to be a weak and unreliable link in the computer system. To eliminate this weak link, the DSP system was installed in a portable computer with the necessary number of expansion slots.

The Kontron IP Lite 386 is a ruggedized portable computer. The DSP executes the signal processing and control codes. The 386 computer is used to debug the programs, to download control codes to the DSP and to upload the test data through a DSP link. The 386 computer also acts as the user interface. An analog input board with 32 A/D channels was installed in the 386 to add to the 2 A/D-D/A channels on the DSP system board. A signal conditioning board was also installed in the 386 computer which preprocesses incoming measurement signals by providing offsets and gains, and filtering some of the signals according to the predefined bandwidth, Further details are included in Appendix E.

It should be noted that a DSP system was chosen to provide sufficient computational power for possible functional expansion in the future. It was found that the real-time control program uses less than 10% of the computational capacity of the DSP system.

2.5 Power Supplies

A power inverter is mounted in the trunk of the vehicle to supply power to the control computer, DC power supply, and 24V power supply. The DC power supply is installed in the vehicle to provide ±15 V and 10 V for the sensors.

2.6 Test Track

A T-shaped, asphalt test road was built at the UCB Richmond Field Station for low speed testing of the lateral control system (Figure 2.10). While the test track is incorporated with the other Field Station roads, it is closed to traffic during the duration of the vehicle testing phase. Much of the test track design was defined by a previously existing dirt road at the site. Another consideration was the many trees along the side of the road. The total length of the test track is approximately 480 m and the width is approximately 5 m. The road was built without superelevation or crown.

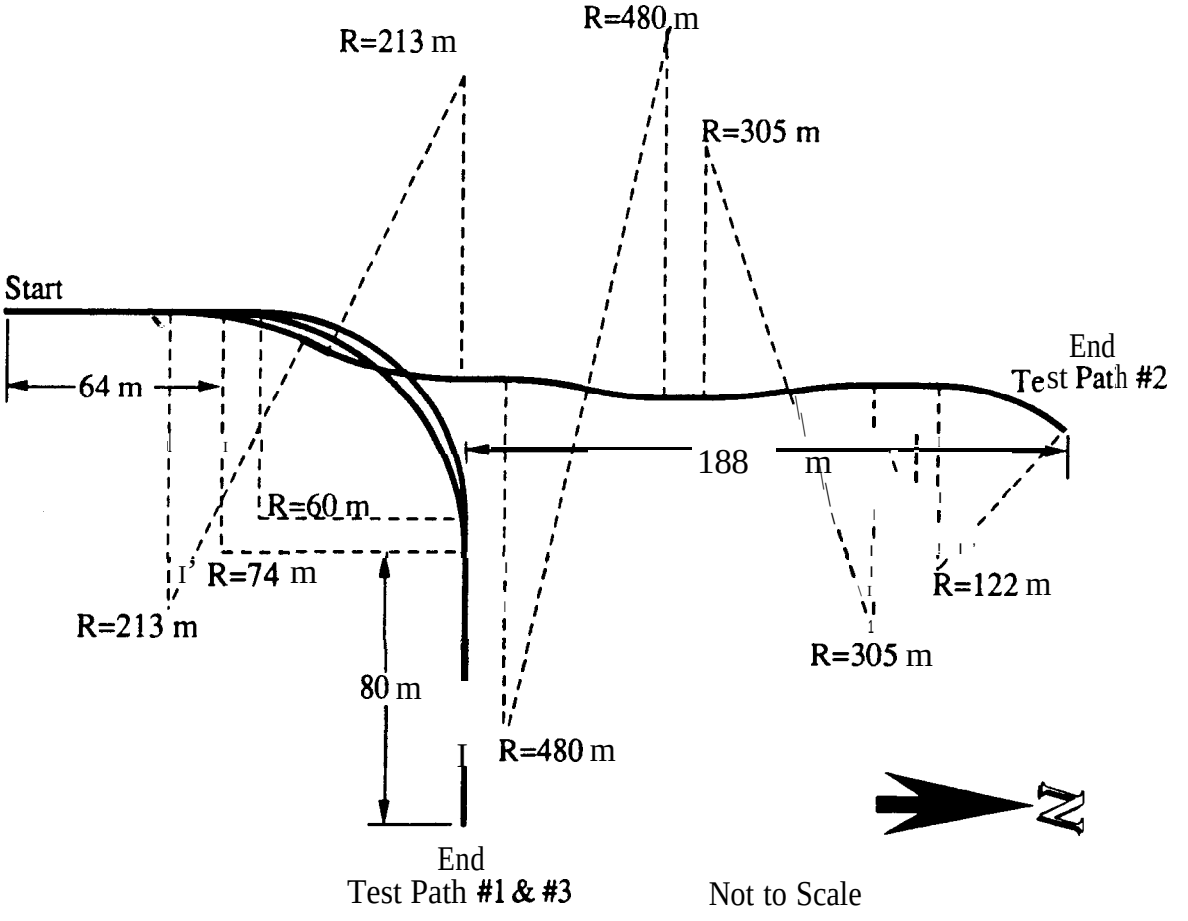

Figure 2.10 Test Track Layout

The test track includes two 90° curves (test paths #1 and #3) and a reverse curve section (test path #2). The two 90° curves have radii of 60 m and 74 m. The reverse curve section is a series of three curve pairs with radii of 213 m, 488 m, and 305 m, with a single 122 m curve at the end. A short straight section separates each curve pair. The lateral displacement between each curve pair is approximately 1.5 m.

Standard ceramic magnets are used for the desired path markers. The magnets are housed in plastic capsules (Figure 2.11). Each capsule contains a stack of magnets 10 cm tall and 2.3 cm in diameter. The capsules are installed at 1 m increments along the center of the three test track paths. The capsules were installed after the road was paved, by coring holes at the desired positions. Sand was placed in the bottom of each hole to bring it up to the correct height. The capsule was then fixed in place using epoxy and quick-set concrete.

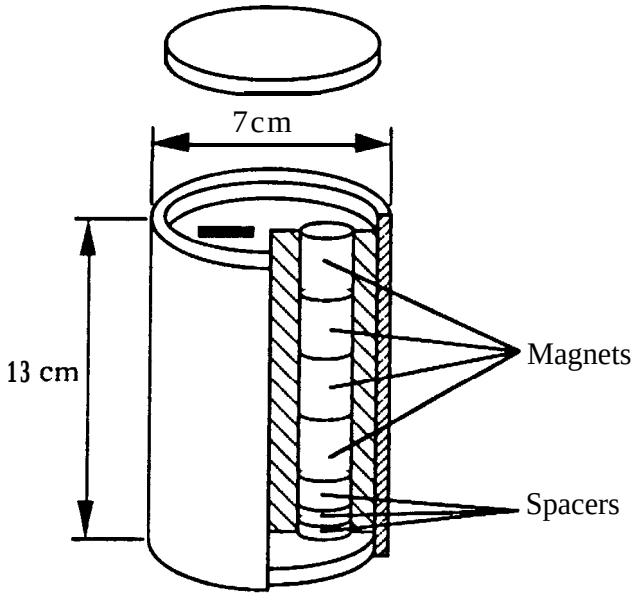

Figure 2.11 Magnetic Marker Capsule

The reason for using capsules is to allow for testing on the effects of different magnet placement tolerances. The inner plug of the capsule rotates to provide a lateral adjustment of approximately 2.5 cm. The capsule also includes several spacers (with a total height of 2.5 cm) below the magnet. These plastic spacers allow the depth of the magnets to be adjusted.

One inch wide reflective tape used as the independent measurement system reference was placed on the road 10 cm from the magnetic marker path. The offset is necessary to keep the tape off the capsules. This offset required that the cameras be mounted on the car with

the same offset relative to the magnetometers. This offset prevented testing in both directions on the test track. In the curved sections, the tape was placed as straight line segments between markers. The error due to this approximation was determined to be insignificant.

2.7 Steering Actuator

The steering actuator steers the vehicle's front wheels based on the command signals received from the controller computer. The steering actuator positioning is controlled by the steering actuator controller which interfaces with the lateral control computer.

The steering actuator, developed by IMRA, is based on the standard power assisted rack and pinion steering system. A hydraulic servo is incorporated between the power-assisted rack motion and the front tires, as shown in Figure 2.12. In this design, the computer controlled steering input is in series with the driver's steering input. The controlled steering angle range is limited to approximately 10% of the full range of the standard steering system. The series control arrangement and the limited range of the computer controlled steering angle allow the driver to override the computer controlled input at any time. This design allows the steering actuator to augment the driver's steering performance on a typical highway and as such should be limited in the latitude of its control. Further analysis from the viewpoints of safety, human factors and system dynamics is necessary to determine the steering angle range needed for automated steering under various operating conditions.

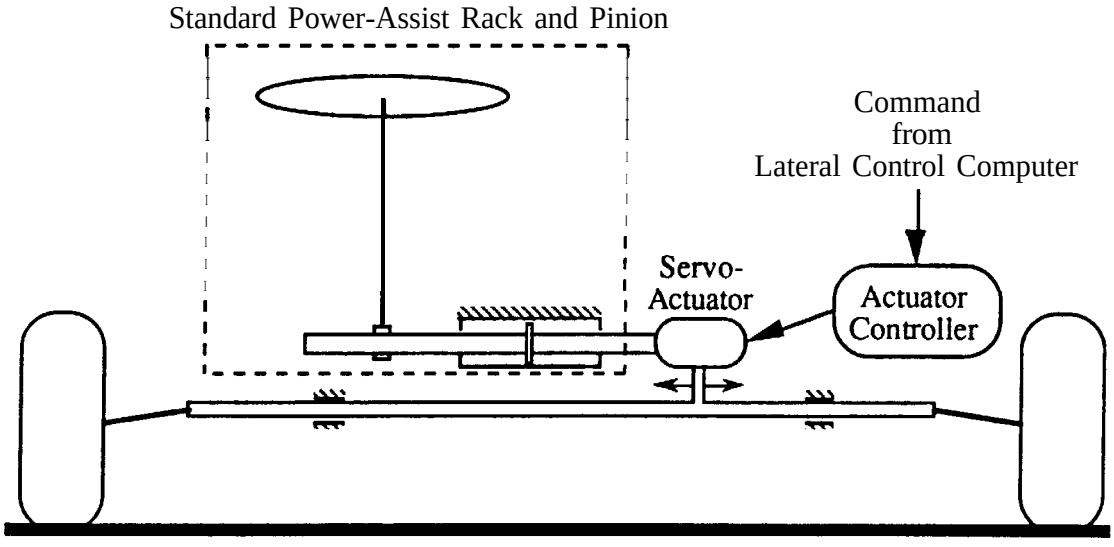

Figure 2.12 Steering Actuator Schematic

Due to the series arrangement of the steering actuator, it is necessary to fix the steering wheel to prevent it from rotating. The original design followed the philosophy of the augmentation role of the steering actuator and anticipated that the augmentation would be in addition to the driver's choice of steering wheel positions. However, for research purposes of greater accuracy, it was decided to eliminate the driver's influence from the steering control loop. A spring-loaded detent mechanism was designed to attach to the steering column housing (Figure 2.13). A groove in the steering column shaft locks the position of the steering column when the keys are removed from the ignition. The spring pushes a round plunger into this groove to fix the position of the steering column. The rotational position of the groove in the steering column shaft may be adjusted relative to the tire steering angle since the upper shaft is connected to the lower shaft through a 22 tooth spline (The spline connection is used for the telescoping function of the steering wheel column.). The angular position of the detent may be further adjusted by rotating the detent housing since it is attached to the steering column housing through slotted holes. The spring preload is set to allow the driver to overcome the detent force and take control of the steering of the vehicle.

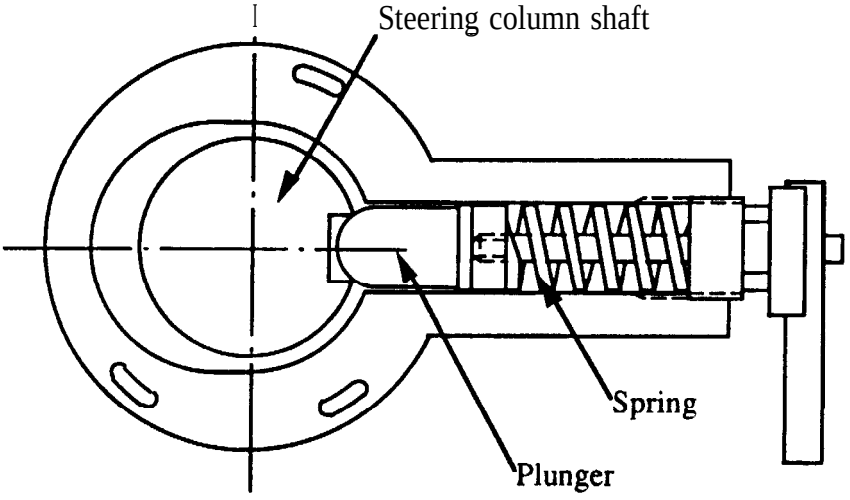

Figure 2.13 Steering Column Detent Mechanism

Despite the presence of the steering column detent, there is still an uncontrolled degree of freedom in the steering system. A torsion bar in the power assist flow control valve is used to control the power-assist hydraulic pressure based on the torque applied to the steering wheel. This torsion bar is also in series with the steering actuator and driver's steering input. Stops in the flow control valve around the torsion bar limit its rotation. The torsion bar rotation influences the tire steering angle by a maximum of approximately 0.5°. A

sensor measures this value and adds it to the actuator position measurement to determine the true steering angle at the front tires. The combined measurement of the actuator position and the steering wheel/torsion bar rotation completely describes changes in the steering angle at the tire and has been shown to be satisfactory for control.

A steering angle larger than the range allowed in this design is needed to negotiate the 90°, 74 m radius curve at vehicle speeds greater than 40 km/hr. In the state of California, the recommended minimum radius of curvature for freeways is 1524 m in rural areas and 914 m in urban areas [9]. Therefore, the curves in this track are much sharper than would be encountered on a freeway. In order to negotiate the 74 m radius curve in test path #1, the actuator's center position was shifted to a non-zero steering angle. As a result, the maximum computer controlled steering angle in the negative direction was increased and the maximum computer controlled steering angle in the positive direction was reduced. This permitted the car to be able to negotiate the turn, but prohibited it from going through the curve in the reverse direction without shifting the offset in the opposite direction.

2.8 Control Algorithm

The feedback and feedforward controllers for the automatic lane following problem are designed based on a linear model (Appendix F). The Frequency-Shaped Linear Quadratic (FSLQ) control theory is utilized to include the tracking error, passenger ride quality, and robustness with respect to high frequency unmodeled dynamics in the performance index. The preview control theory is then introduced to design the feedforward controller for the FSLQ augmented system. By adding a feedforward component, the gain of the feedback controller can be reduced. The automatic steering problem is formulated as a regulation problem, and future exogenous inputs (road curvature and superelevation) of the system are assumed to be known if the absolute position of the car on the highway (test track) is available.

The vehicle dynamics depend on the tire cornering stiffness, Cs, which dominates the characteristics of the tire-road interaction; the load, m, Iz; and forward speed, V. The value of Cs is affected by many factors. In addition to the tire slip ratio and the tire slip angle, the value depends on the tire pressure, load, velocity, camber angle, temperature, and most of all, road surface conditions [10, 11]. The cornering stiffness, Cs, and velocity, V, are the dominant parameters. They vary over a wide range which prohibits the use of fixed-gain controllers. At this stage of the testing, the feedback and feedforward gains were scheduled with respect to vehicle speed only to improve the tracking performance when the vehicle

speed varies. The feedback and feedforward controllers were tested by computer simulation using a complex vehicle model (see Appendix F) before being implemented on the test vehicle.

2.8.1 Frequency Shaped Linear Quadratic (FSLQ) Control Law

The FSLQ control theory [12,13] provides a controller design tool for linear systems based on the 'minimization of a quadratic performance index, which includes frequency as a parameter. The performance index of the automatic lateral control problem is formulated as follows:

$$J = \frac{1}{2\pi}\int_{-\infty}^{\infty} \left[a^*(j\omega)\frac{q_a^2}{1+\lambda_a^2\omega^2}a(j\omega) + y_s^*(j\omega)\frac{q_y^2}{1+\lambda_y^2\omega^2}y_s(j\omega) + (\dot{\varepsilon}(j\omega)-\dot{\varepsilon}_d(j\omega))^*\frac{q_\varepsilon^2}{1+\lambda_\varepsilon^2\omega^2}(\dot{\varepsilon}(j\omega)-\dot{\varepsilon}_d(j\omega)) + y_s^*(j\omega)\frac{q_i^2}{(j\omega)^2}y_s(j\omega) + \delta^*(j\omega)R\delta(j\omega)\right] d\omega \tag{2.2}$$

where ω is the angular frequency and a is the difference between the measured lateral acceleration $\ddot{y}_a$ and its desired value. * denotes the complex conjugate. $y_s, \dot{\varepsilon}, \dot{\varepsilon}_d$ and δ are all defined in the linear model (Appendix F).

In other words, only the variation of the lateral acceleration from its desired value is penalized. By properly choosing the values of λ_a, the first term in Eq. (2.2) can be used to represent the ride quality. The values of λ_y and λ_ε are chosen to shape the performance index so that the controller is less responsive to the measurement noise (high frequency), while the tracking performance (low frequency) is not sacrificed. Refer to [14] for details.

The FSLQ problem is reformulated by transforming the original system into a state augmented system (see Appendix G). The FSLQ problem is then solved as a standard LQ problem. The parameters of the performance index used in the tests are listed in Table 2.2 for reference, where RC describes the road surface conditions which dominates the road-tire force interaction. More details will be explained in 3.2.5.2.

Table 2.2 Parameters of the FSLQ Controller

	test path #1	test path #2
λ_a	0.005305	0.005305
λ_y	0.23	0.23
λ_ε	0.23	0.23
q_ε	$\frac{0.1}{RC^{0.2}}$	$\frac{0.1}{RC^{0.2}}$
q_a	$\frac{0.01}{RC^{0.2}}$	$\frac{0.007}{RC^{0.2}}$
q_y	$\frac{0.08}{RC^{0.2}}$	$\frac{0.15}{RC^{0.2}}$
q_i	$\frac{0.003}{RC^{0.3}}$	$\frac{0.003}{RC^{0.3}}$

2.8.2 Deterministic Preview Control Algorithm

When future road curvature information is available, the tracking performance can be further improved by properly incorporating this information in the control law. The optimal preview control problem is to minimize a quadratic performance index:

$$J(t) = \frac{1}{2}\int_t^\infty \underline{x}_e^T(\tau)Q\underline{x}_e(\tau) + \underline{\delta}^T(\tau)R\underline{\delta}(\tau)\,d\tau \tag{2.3}$$

The linear vehicle system has the form:

$$\dot{\underline{x}}_e(t) = A_e\underline{x}_e(t) + B_e\underline{\delta}(t) + D_e\underline{w}(t) \tag{2.4}$$

where $\dot{\underline{x}}_e, A_e, B_e$ and D_e are augmented state vector, state matrix, input matrix and disturbance matrix, respectively, and $\underline{w}$ is the disturbance (road curvature) in a future section of time.

In other words, the problem is to determine how to use the future disturbance information (over a finite period) to "invert" the vehicle dynamic equation to achieve better tracking performance in curved section of the road. The procedure to solve the preview control

problem is described in A.ppendix H. For more details, please refer to [4]. The optimal preview control algorithm was found to have the following form:

$$\delta_{opt}(t) = -R^{-1}B_e^T[\, K(t)x_e(t) + \int_0^{t_{la}} F_1(t,\tau)w(t,\tau)\,d\tau + F_2(t)\,w(t + t_{la})\,] \qquad (2.5)$$

The preview, control law consists of three terms, one feedback term and two feedforward terms. The feedback gains, K(t), and feedforward gains, $F_1(t,\tau)$, $F_2(t)$, are solved by using the Dynamic Programming technique [4]. The feedback term is exactly the same as the FSLQ feedback control algorithm without the preview assumption [4]. The second term is the preview action which deals with the disturbance signal (road curvature) within the preview segment. The third term is the preview action which copes with the disturbance beyond the preview segment. The feedforward terms are initiated before the vehicle reaches a curve and reduce the tracking error significantly.

In the closed-loop test, the feedback and feedforward gains are computed for selected vehicle speeds (30.5, 39.5, 48.5 and 57.5 km/hr) and cornering stiffnesses (30000, 33000, 36000, 39000 and 42000 N/rad), and stored in memory for gain scheduling purposes.

The state variable estimations are obtained from a Luenberger observer [15], with poles assigned at -7.5 $\pm$ 3j and -7 $\pm$ 2j. The observer gains are computed for the same cornering stiffnesses as above, and slightly higher vehicle speeds (25, 34, 43, 52, and 61 km/hr). The rationale for using the higher vehicle speeds is explained in section 4.1.

The preview time used in the experiments is 1 second. By ending the road geometry information code 20 m before the beginning of the curve, the vehicle will receive the entire message more than 1 second before the curve for all vehicle speeds lower than 72 km/hr. A 25-step summation is used instead of the integration in Eq. (2.5).

2.8.3 PID Controller

A PID controller contains proportional, integral and derivative terms in the feedback equation. This PID controller is designed to compare with the FSLQ controller in the closed-loop test. The gains of the PID controller are obtained by placing closed-loop poles in a target region, checking the performance by simulation, and fine tuning by trial and error during the vehicle tests. Speed-dependent gains are used to ensure that the tracking

performance is acceptable for all test speeds. The following gains were found to generate satisfactory results:

$$\begin{aligned} k_p &= -0.005V + 0.19 \\ k_i &= 0.001 \\ k_d &= 0.038V + 0.0033 \end{aligned} \tag{2.6}$$

where

$$\delta_{opt}(k) = -[k_p \times y_s + k_d \times (y_s(k) - y_s(k-1)) + k_i \times \sum y_s] \tag{2.7}$$

It should be noted that the PID control law shown in Eq. (2.7) is only a feedback algorithm. It was found from the closed-loop tests that the tracking performance is unacceptably large if there is no feedforward action (preview). Therefore, the two feedforward terms in Eq. (2.5) are used together with the PID controller in Eq. (2.7) throughout the closed-loop test. However, the feedforward terms in Eq. (2.5) are determined with respect to a certain choice of q_y, q_ε, q_e and qi. More study is required to determine the appropriate preview control gains to use with the PID control algorithm.

It was found in the experiments that the gains of the FSLQ controller are easy to tune and those gains that work in the simulations also work in the experiments. The reason is that the tuning of the weighting factors in the FSLQ performance index involves trade-offs between physical quantities (tracking error, steering angle and lateral acceleration). On the other hand, the tuning of the PID gains does not correspond to any physical quantities and relies on the designer's intuition and evaluation of the system performance. Also, it was found that the PID gains which work very well in the simulations may produce unacceptable performance with the vehicle system. Therefore, the PID gains require more experimental tuning than the FSLQ gains.

2.9 Man/Machine Interface

The driver is always in control of the accelerator and brake of the test vehicle. It is the driver's responsibility to monitor the safety of the vehicle system during testing operations. The design of the spring-loaded detent allows the driver to take control of the steering at any time during the test, even when the lateral control algorithm is functioning. A switch is located next to the gear shift lever that allows the driver to cut the power to the steering

actuator at any time. Cutting the power to the steering actuator will freeze it at its latest position. With the actuator off, the driver can take any necessary evasive maneuvers without interference from the steering actuator. In order to assist the driver in monitoring the performance of the vehicle system during a test, a display panel was installed next to the speedometer. The display panel shows three types of information: An LED indicates when the control computer is actively sending commands to the steering actuator. Another LED alerts the driver when the vehicle is too far from the magnetic markers in the road to make reliable measurements of the lateral deviation. An analog meter displays the lateral deviation as measured by the magnetic reference/sensing system.

3. EXPERIMENTS ON COMPONENTS

3.1 Verification of the Magnetic Reference/Sensing System

The magnetic reference/sensing system was verified using the independent measurement system. Verification tests were performed on test path #1. The vehicle was steered manually over the reflective tape on the road in a slowly waving path. The control computer simultaneously acquired signals from both magnetic sensors and the front camera. In processing the two test results, signals acquired from magnetic markers were used for synchronization so that only the data from the independent measurement system which corresponded to the magnetic marker positions were kept. The two data were then compared to determine the error of the magnetic reference/sensing system relative to the independent measurement system. Figure 3.1 shows a comparison between the magnetic sensing system and the independent measurement system. It is noted that the maximum error of the magnetic reference system relative to the independent measurement system was approximately 0.015 m. The standard deviation of the error was less than 0.01 m. The experimental data verifies that the accuracy of the magnetic reference/sensing system is acceptable.

3.2 Tire Model

A tire model has been developed based on test data from a YOKOHAMA P205/60R1487H steel-belt radial tire, the same tire used on the test vehicle. The tire pressure was 206.8 kPa throughout the tire tests. The curve fit model proposed by Bakker and Pacejka is used for the lateral and longitudinal tire force equations. A correction formula developed by Bakker and Pacejka is then utilized so that the tire model developed from separate longitudinal and lateral force tests can be used for combined traction (braking) and cornering maneuvers. A simple scaling factor is used to modify the tire force equations to represent road friction variations. The new tire model is then incorporated in the computer simulation program to predict the responses of the test vehicle.

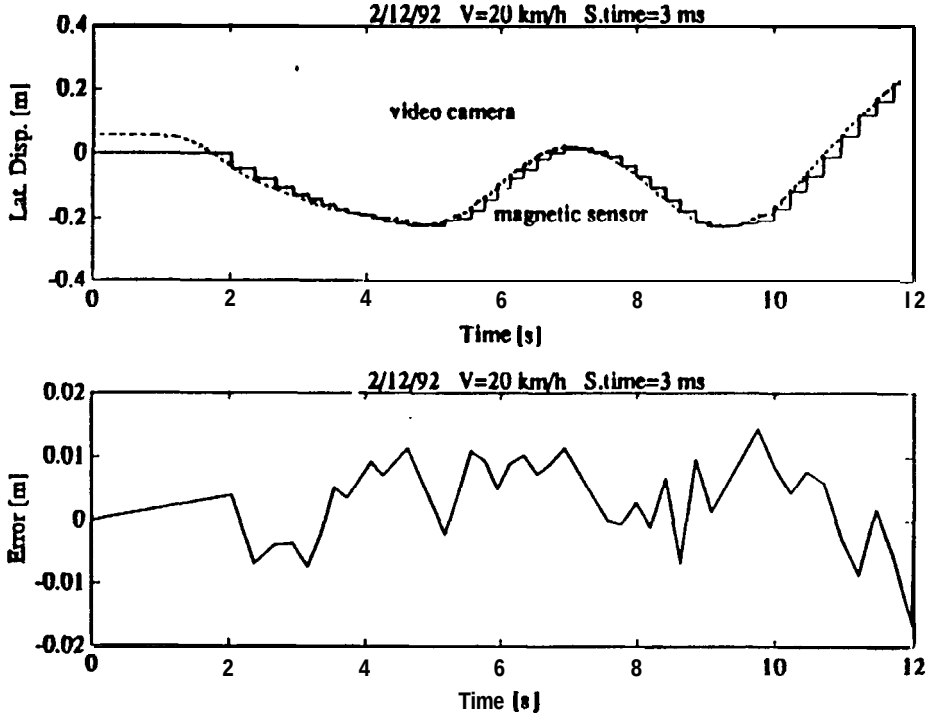

Figure 3.1 Reference Sensing System Comparison

3.2.1 Test Procedure

Data from two types of tire tests were used to develop the tire model. The DRS (Drive/Retard Slip ratio) test measures the longitudinal force characteristics of the tire by applying a driving torque to the tire while the tire slip angle, a, is kept at zero. The SWP (slip angle SWeeP) test measures the tire lateral force characteristics by steering the tire while keeping the driving torque (T_s) applied to the tire at zero (see [16] for details). Notice there are no combined traction and cornering maneuvers (turning the tire and applying tire shaft torque at the same time), which call for the modifications described in section 3.2.6. The DRS tests were performed under the following conditions (see Figure 3.2):

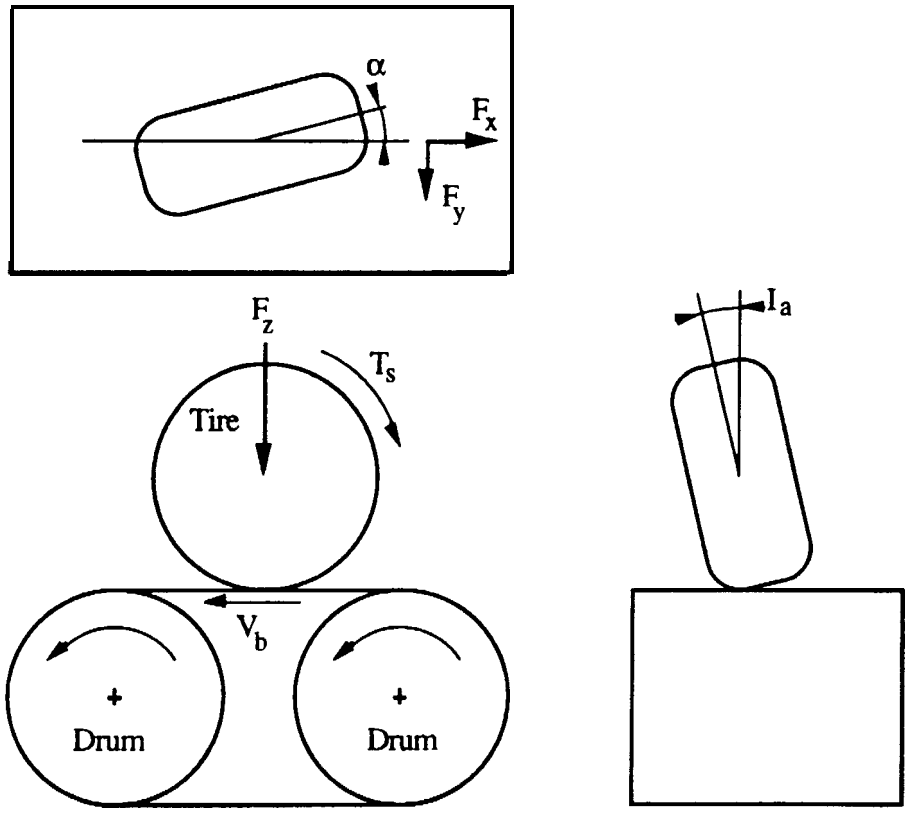

Figure 3.2 Tire Test Set Up

1) The tire slip angle, a, and inclination angle, Ia, were kept at zero and the test bed speed, V_b, was kept constant (80 km/hr in all tests).

2) For three different vertical loads, F_z, (1935N, 2580N, and 3225N), the driving torque, T_s, was applied using a trapezoidal time profile. The maximum values of the

driving torque were chosen such that the maximum longitudinal force generated, F_x, was approximately 1 to 1.1 times F_z.

3) The variables listed in Table 3.1 were measured and recorded.

Table 3.1 Variables Measured in the Tire Tests

parameter	meaning	parameter	meaning
Rl (mm)	tire radius	Tach (RPM)	tire angular speed
Ts (N-m)	shaft torque	Fx (N)	longitudinal force
Fy (N)	lateral force	Fz (N)	normal force
Mx (N-m)	overturning moment	Mz (N-m)	self-aligning torque
α (deg)	slip angle	Ia (deg)	inclination angle
Vb (km/hr)	test bed speed		

The procedure of the SWP test is described as follows:

1) The shaft torque, T_s, and inclination angle, Ia, were kept at zero and the test bed speed, V_b, was kept constant (80 km/hr).

2) For nine different vertical loads, F_z, (60N, 650N, 1300N, 1950N, 2600N, 3250N, 3900N, 4550N, and 5200N), the slip angle, a, was varied using a triangular time profile.

3) All variables listed in Table 3.1 were measured, except that another tire angular speed measurement, Spindl, was recorded instead of Tach.

3.2.2 Longitudinal Tire Force

The longitudinal tire force characteristic is strongly related to the tire slip ratio, s. The definition of the tire slip ratio is:

$$s \equiv \frac{\omega r - V}{V} \tag{3.1}$$

where ω is the tire angular speed, r is the tire radius and V is the tire translational speed. The tire longitudinal force, F_x, is zero when the tire slip ratio, s, is zero, and is positive when s is greater than zero. In other words, if the vehicle is driving at a constant speed the tire circumferential speed, ωr, has to be larger than the tire translational speed V to overcome the wind resistance force. The definition in Eq. (3.1) was not used with the test data because of a problem in the tire angular speed measurement (Tach). Instead, the alternative definition is used:

$$s = \frac{\text{Tach} - \text{Tach}(0)}{\text{Tach}(0)} \tag{3.2}$$

where Tach(0) is the tachometer reading corresponding to zero slip ratio. Note that a small T_s has to be applied to make s (F,) zero. The values of Tach(0) for the three DRS tests are 644.50, 645.36, and 646.76 RPM, respectively.

The longitudinal force equation can be obtained by fitting the test data according to the following two equations:

$$F_x = f(F_z, \alpha, s) \tag{3.3}$$

$$\frac{F_x}{F_z} = f(F_z, \alpha, s) \tag{3.4}$$

If the test data are fit according to Eq. (3.3), a group of curves (for different F_z's) is produced. Fitting the data using Eq. (3.4) produces only one curve, the normalized longitudinal force. Using the normalized longitudinal force would simplify the model. However, a "structural error" is introduced as a result of the unnecessary approximation of the normalization. Thus, to better utilize the test data, the original data were fit using Eq. (3.3).

The tire test test data revealed that the longitudinal force characteristics in the traction and braking directions are not symmetric. Therefore, two different equations are used to fit the data for $s > 0$ and for $s < 0$.

3.2.3 Lateral Tire Force

The lateral tire force characteristic is mainly determined by the tire slip angle, a. However, when the driving torque, T_s, is zero, the longitudinal force, F_x, will not be zero when the tire steering angle is swept on the test bed. Steering the tire generates longitudinal force as well as lateral force. To provide more insight, the tire lateral force, F_y, is plotted as functions of a. Different symbols are used to indicate the data points for different slip ratios.

Because of experimental set-up problems the sensor output, Tach, could not be measured when the driving torque, T_s, was zero. Another measurement, Spindl, which is quite noisy, had to be used in the lateral (SWP) test analysis. The original definition of the slip ratio is used in the following form:

$$s = \frac{12\pi \times 10^{-6} \times R_l \times \text{Spindle} - V_b}{V_b} \qquad (3.5)$$

where R_l is the tire radius in mm, Spindl is the tire angular speed in RPM and V_b is the test bed speed in km/hr.

As with the longitudinal tire force, the original lateral force test data were used for the tire model rather than the normalized lateral tire force. The lateral force characteristic was found to be symmetric for $a > 0$ and $a < 0$. Therefore, one equation is used.

3.2.4 Curve Fitting

Bakker's curve fit formula [17, 18] was chosen for the following reasons:

1) Bakker's modeling equations are easy to use and the effects of the coefficients on the geometry of the resulting curve are clear. Therefore, it is relatively simple, compared with other models [19, 20], to tune the coefficients of the equations to fit the test results (see [17] for details).

2) Bakker proposed a modification method for the force equations when both traction and cornering actions are present. This method has been validated by experiments [18]. Although Bakker's method can be used on the force equations from other models, we used Bakker's tire force curve fit formula and force modification method together for consistency.

Baker's tire model assumes the following:

$$F_x = D_x \sin(C_x \tan^{-1}(B_x\phi_x)) + S_{vx} \quad (3.6)$$

$$F_y = D_y \sin(C_y \tan^{-1}(B_y\phi_y)) + S_{vy} \quad (3.7)$$

$$\phi_x = (1-E_x)(s + S_{hx}) + \frac{E_x}{B_x}\tan^{-1}(B_x(s + S_{hx})) \quad (3.8)$$

$$\phi_y = (1-E_y)(\alpha + S_{hy}) + \frac{E_y}{B_y}\tan^{-1}(B_y(\alpha + S_{hy})) \quad (3.9)$$

The coefficients for the longitudinal and lateral forces are:

$$B_y = 0.22 + \frac{5200 - F_z}{40000} \qquad C_y = 1.26 + \frac{F_z - 5200}{32750} \quad (3.10)$$

$$D_y = -0.00003F_z^2 + 1.0096F_z - 22.73 \qquad E_y = -1.6$$

$$s_{hy} = 0 \qquad s_{vy} = 0$$

$(s > 0)$

$$B_x = 22 + \frac{F_z - 1940}{645} \qquad C_x = 1.35 - \frac{F_z - 194}{16125} \quad (3.11)$$

$$D_x = 2000 + \frac{F_z - 194}{0.956} \qquad E_x = -3.6$$

$$s_{hx} = 0 \qquad s_{vx} = 0$$

$(s \leq 0)$

$$B_x = 22 + \frac{F_z - 1940}{430} \qquad C_x = 1.35 - \frac{F_z - 194}{16125} \quad (3.12)$$

$$D_x = 1750 + \frac{F_z - 194}{0.956} \qquad E_x = 0.1$$

$$s_{hx} = 0 \qquad s_{vx} = 0$$

where the units of F_x, F_y and F_z are Newtons and a is in degrees.

The tire force curves produced from these coefficients are shown in Figures 3.3 and 3.4. Only minor differences between the test data and the fitted curves are observed, even when α (or s) is large.

3.2.5 Modifications

One important point to keep in mind is that the DRS tests were performed by applying a driving torque with the tire at zero slip angle, and the SWP tests were performed with the tire swept left and right while no driving torque was applied. However, under normal driving conditions the traction or braking torque and the tire steering angle are often applied simultaneously. Therefore, the above force equations must be modified to describe combined lateral and longitudinal maneuvers. Furthermore, the surface material of the test bed can be substantially different from the road surface material on the test track, and the surface properties of the test track may also vary due to water, temperature variation, etc. Therefore, Eqs. (3.6) and (3.7) must be modified to include these factors.

3.2.5.1 Combined traction and cornering maneuvers

Bakker proposed the following method to modify Eqs. (3.6) and (3.7) when both traction torque and slip angle are applied to the tire:

1) Suppose the longitudinal and lateral tire force equations have already been obtained separately from traction-only and cornering-only tests. The force equations are described by:

$$F_x = f_{x0}(s, F_z) \tag{3.13}$$

$$F_y = f_{y0}(\alpha, F_z) \tag{3.14}$$

2) Define the normalized slip factors s^* and α^* as follows:

$$s^* = \frac{s}{s_m} \tag{3.15}$$

$$\alpha^* = \frac{\alpha}{\alpha_m} \tag{3.16}$$

where s_m and α_m are the values of s and α where F_x and F_y achieve their peak values respectively.

3) Define the correction factor σ^*:

$$\sigma^* = \sqrt{(s^*)^2 + (\alpha^*)^2} \tag{3.17}$$

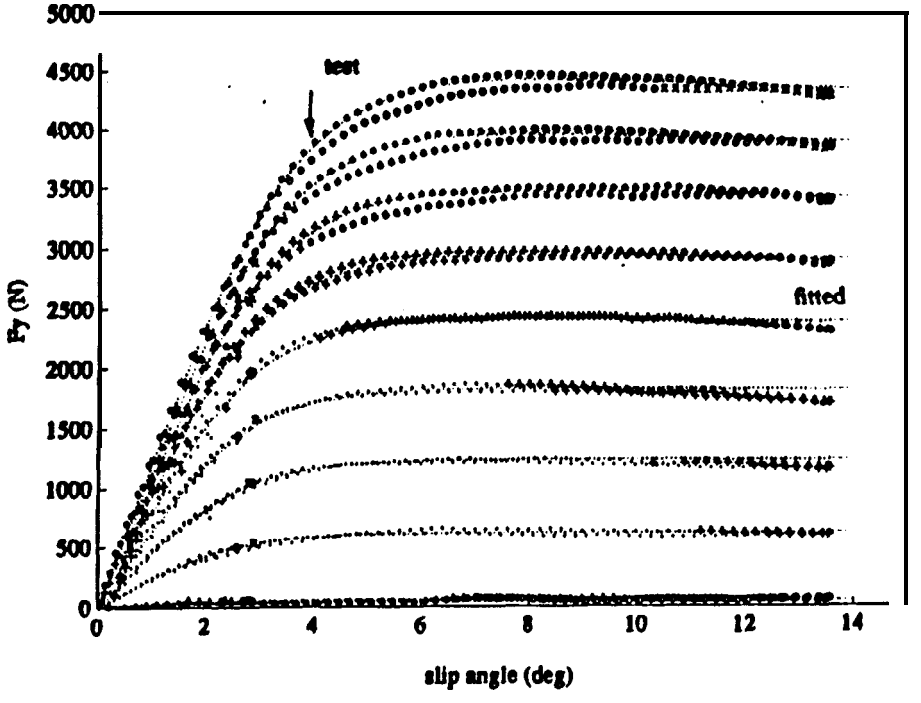

Figure 3.3 Lateral Tire Force Curve

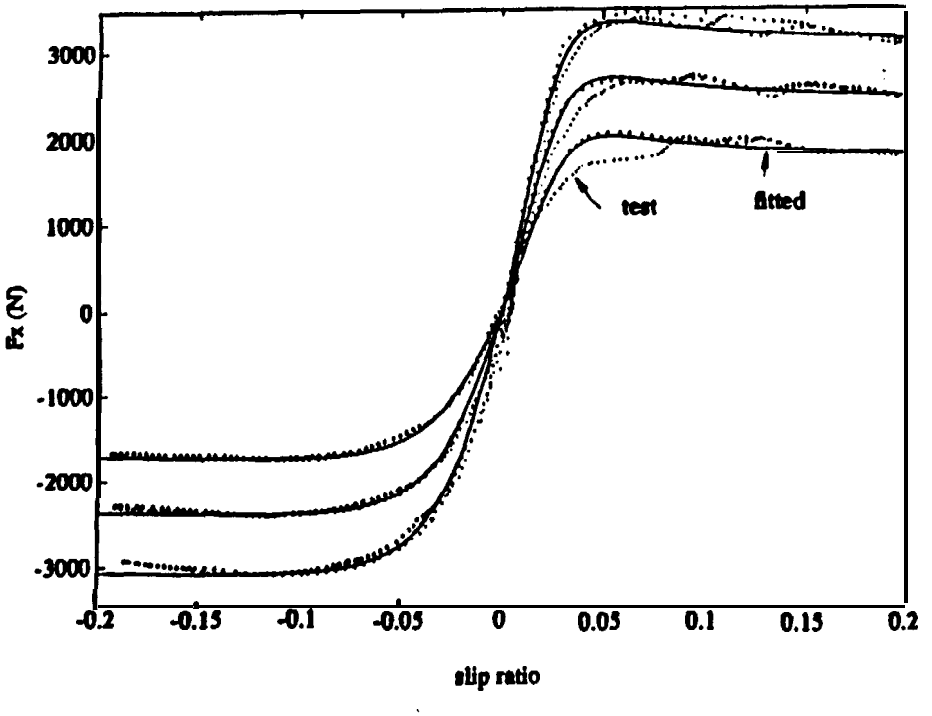

Figure 3.4 Longitudinal Tire Force Curve

4) The longitudinal and lateral forces can then be corrected with the following:

$$F_x = \frac{s^*}{\sigma^*} \times f_{x0}(\sigma^*, F_z) \tag{3.18}$$

$$F_y = \frac{\alpha^*}{\sigma^*} \times f_{y0}(\sigma^*, F_z) \tag{3.19}$$

It should be noted that the above correction method agrees with experimental results only when the correction factor, σ^*, is small (cl). The values of s_m and α_m are found to be:

$$s_m = 0.058 \quad (s > 0)$$
$$= -0.1 \quad (s < 0) \tag{3.20}$$

$$\alpha_m = 6.3 + \frac{F_z - 650}{3500} \tag{3.21}$$

3.25.2 Road surface conditions

The tire data used for the tire model development were obtained from tests that were performed under well-controlled laboratory conditions. What kind of corrections are needed in order to use the tire model to predict the force generated from the tire on a piece of road? The answer to this question is still open and relatively unknown. The reason is that many factors affect the tire force characteristics. Variations in temperature, load, tire slip speed ($r\omega - V$), camber angle, tire pressure, and road surface material all affect the tire force output in different ways [20, 21]. The simplification used in several theoretical models [22, 23] is to assume that the tire forces (longitudinal and lateral) are proportional to the friction coefficients (static and dynamic) between the tire and the road surface. Under this assumption, if one assumes that the friction coefficients drop to x% of their nominal values (regardless of whether it was caused by water, tire pressure variation, or some other reason), the tire forces generated are simply reduced by x% of their nominal values. Due to the lack of previous research results in this area, the above mentioned simplification is used. That is, Eqs. (3.17) and (3.18) are further modified to:

$$F_x = RC \times \frac{s^*}{\sigma^*} \times f_{x0}(\sigma^*, F_z) \tag{3.22}$$

$$F_y = RC \times \frac{\alpha^*}{\sigma^*} \times f_{y0}(\sigma^*, F_z) \tag{3.23}$$

where RC is the road condition correction factor, which is defined as the ratio between the true friction coefficient and the nominal friction coefficient.

3.3 Open Loop Experiments

The objective of the open loop tests is to obtain additional information on the steering system characteristics and on vehicle dynamic responses. The vehicle simulation model is fine tuned according to the test results to more accurately predict the response of the test vehicle.

The field tests were performed at the California Highway Patrol Academy Test Track in West Sacramento. Neither a reflective white line nor a magnetic reference system were available at the site, so no lateral deviation measurements were available. The vehicle's speed was estimated based on the speedometer.

3.3.1 Equipment Calibration Test

The accelerometer, yaw rate sensor and steering angle measurement used in the open loop experiments are described in sections 2.2.1, 2.2.2 and 2.2.4, respectively. A roll rate sensor was installed to calibrate the lateral acceleration measurement. However, the roll motions are not large enough to generate meaningful measurements. Therefore, the roll rate measurement is not used in this report. In the remainder of this section, the sensors will be short-handed as indicated in Figures 3.5 and 3.6.

yaw: yaw rate sensor
acc: lateral acceleration sensor
s 1: steering actuator position sensor
s2: steering wheel position sensor

A calibration test of the sensors was performed before the open loop field tests. The procedure of the calibration test is described as follows:

1) Move the actuator through the full stroke and measure the corresponding signal from the linear potentiometer (sl) with all four tires raised off the ground. This test provides the zero reference point for both the actuator command and sl sensor. Also, the scaling factor of sl is obtained.

2) On a flat road with the vehicle stationary, read the sensor outputs. This test determines the zero reference point for the yaw rate and lateral acceleration measurements.

3) On a straight road give a 0° steering command to the actuator and have the driver steer the steering wheel so that the vehicle moves as straight as possible. The vehicle speed is not important, however higher speeds are preferable. The zero point of s2 is obtained from this test.

4) Find a space where the vehicle can be safely driven in a circle. Give a 0° steering command to the actuator while the driver steers the steering wheel so that the vehicle travels in a circle at a constant speed. An estimation of the driver's steering angle should be recorded. The scaling factor of s2 is obtained from this test and the scaling factors of yaw and acc are verified.

By following these procedures, the characteristics of the sensors were calculated and listed in Table 3.2. The numbers in Table 3.2 relate to the physical quantities through the following equation:

$$\text{Physical quantity} = [\ \text{Voltage} + \text{Offset}\ ] \times \text{Scaling factor} \qquad (3.24)$$

and "Voltage" is the voltage signal read from the sensors or output to the actuator. The sl and s2 measurements have been calibrated to correspond with the ground wheel steering angle.

Table 3.2 Calibration Factors of the Sensors and the Hydraulic Actuator

Device	Offset (V)	Scaling factor
Actuator (deg)	-2.5	1.2
Accelerometer (g)	-2.48	-0.5
Rack (deg)	-4.92	0.718
Steering wheel (deg)	-4.86	7.8
Yaw rate (deg/sec)	0.42	-3

3.3.2 Field Tests

The field tests consisted of using two sets of steering commands: sinusoidal and step signals. Throughout the tests, the driver controlled the vehicle speed while not contributing

any steering input. The step input tests were performed at several vehicle speeds (20, 40 and 60 km/hr) and steering amplitudes (1.5° and 3°) for both right and left turns. Sinusoidal input tests were performed at selected vehicle speeds (20, 40, and 60 km/hr), steering angle amplitudes (1.5' and 3°) and frequencies (0.3, 0.5, 0.7 and 1 Hz). Each of these tests condtions were repeated three times.

3.3.3 Field Test Results

The test results were analyzed in both the frequency domain and time domain. The assumption was made that the overall vehicle automatic steering system on the test vehicle can be represented by the block diagram shown in Figure 3.5. Since the signals δ_d, s_1, s_1+s_2 and vehicle responses (acc and yaw) were recorded in the test, the problem of analyzing the whole system is decomposed into three subsystems: the actuator, the power steering system, and the vehicle dynamic system. These three sub-systems are analyzed further in sections 3.3.3.1 to 3.3.3.3, respectively. It should be noted that a fifth order Butterworth low-pass filter was used to condition the test signals before being used in the analysis. The cut-off frequency is 5 Hz for the acc and yaw measurements and 3 Hz for the sl and s2 signals.

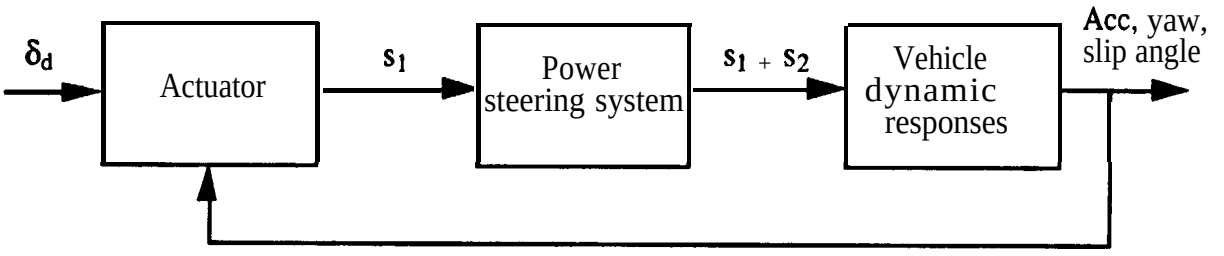

Figure 3.5 Steering System Block Diagram

333.1 Actuator characteristics

A hydraulic spool valve model was used to represent the hydraulic actuator on the test vehicle. It was observed from step input test results that the steering rate of the actuator decreases as the magnitude of the tire steering angle increases because the load (due to the self-aligning torque of the tires) on the actuator increases. The self-aligning torque is proportional to the tire slip angle, a, when a is small. In the step input tests, when the steering angle increases the tire slip angle also increases. The tire self-aligning torque helps the actuator when the actuator is steered to reduce the tire slip angle and resists the steering motion when the actuator moves to increase the tire slip angle. The above effect especially

appears in high frequency sinusoidal input tests. Due to this effect and the offset in the steering angle, the steering response of the hydraulic actuator is not symmetric in right and left turns. The actuator model is approximated by the following first order time lag system in the controller design process in order to use the preview-FSLQ control law.

$$\frac{\delta}{\delta_d} = \frac{0.85}{1 + 0.2\,s} \qquad (3.25)$$

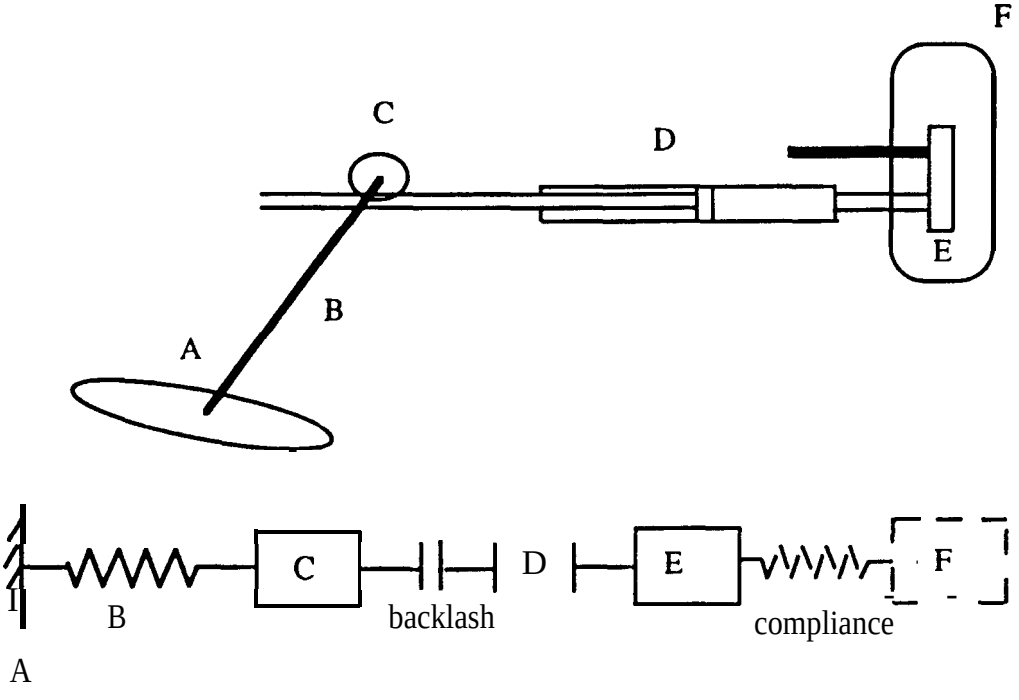

Figure 3.6 Steering System Schematic

3.3.3.2 Power steering system responses

The schematic diagram of the automatic steering system is shown in Figure 3.6. The detent fixes the steering wheel to the car body at point A, and it is assumed that the only element between point C (where s2 is installed) and point A is the compliance due to the torsion bar (element B). A comparison between the test signals of the actuator output, sl, and the true ground wheel steering angle, s1+s2, shows little phase difference. Therefore, the above assumption seems reasonable. In other words, the transfer function from the actuator output to the true ground wheel steering angle is approximated by a scaling factor. The scaling factors calculated from the test results are listed in Table 3.3. The numbers in Table 3.3 are calculated from the mean amplitudes of sl and s2 of each test run and averaged over results under the same test conditions. It should be noted that the backlash between point C

and actuator D and the compliance between point E and F have been neglected, and the measurement s1+s2 is assumed to represent the true ground wheel steering angle. The following equation is derived from Table 3.3 and is used in the simulation programs:

$$\text{Scaling Factor} = 0.89 - 0.006 \times V \tag{3.26}$$

where V is the vehicle forward speed in m/sec.

Table 3.3 Scaling Factors of the Power Steering System Response

freq(Hz) / V(km/hr)	0	0.3	0.5	0.7	1.0
20	0.88	0.87	0.87	0.87	0.82
40	0.90	0.82	0.82	0.82	0.79
60	0.89	0.81	0.80	0.80	0.77

3.33.3 Vehicle dynamic response

The vehicle dynamic response characteristics are analyzed in both the time domain using the complex model, and the frequency domain using the simplified model (Appendix E). In the time domain analysis, the test data (sl, acc and yaw) were fed to the vehicle complex model, and the tire cornering stiffness, Cs, was estimated by using the least square algorithm. The estimated Cs was then used to calculate the transfer functions $G_{\delta\dot{\varepsilon}}$ and $G_{\delta\dot{y}_s}$ from the simplified vehicle model. At a low vehicle speed (20 km/hr) the estimated cornering stiffness is approximately 42000 N/rad, which is 70% of the nominal value.

Therefore, it was concluded that the road condition scaling factor of 0.7 should be used. Figures 3.7 and 3.8 are the transfer function plots of $G_{\delta\dot{\varepsilon}}$ and $G_{\delta\dot{y}_s}$, respectively. The simplified (linear) vehicle model does not predict the vehicle response with good precision because the tire cornering capability is over-estimated.

3.3.3.4 *Open-loop response of the whole vehicle model*

Figures 3.9-3.11 show several simulated results combining the actuator, power steering system, and vehicle parameters obtained in the previous three sub-sections. Selected sinusoidal input signals are used as the open-loop commands to the steering actuator and

the results obtained from the field test are plotted for comparison. The following comments are made:

1) The actuator model predicts the ground steering angle with good accuracy at all vehicle, speeds and input frequencies.

2) The vehicle model simulates the vehicle responses (yaw and acceleration) satisfactorily at slow speeds (20 and 40 km/hr), and the difference between simulated and test results increase at higher speeds (60 km/hr).

3) Despite the fact described in 1), the vehicle model consistently overestimates the yaw-rate response and underestimates the lateral acceleration response.

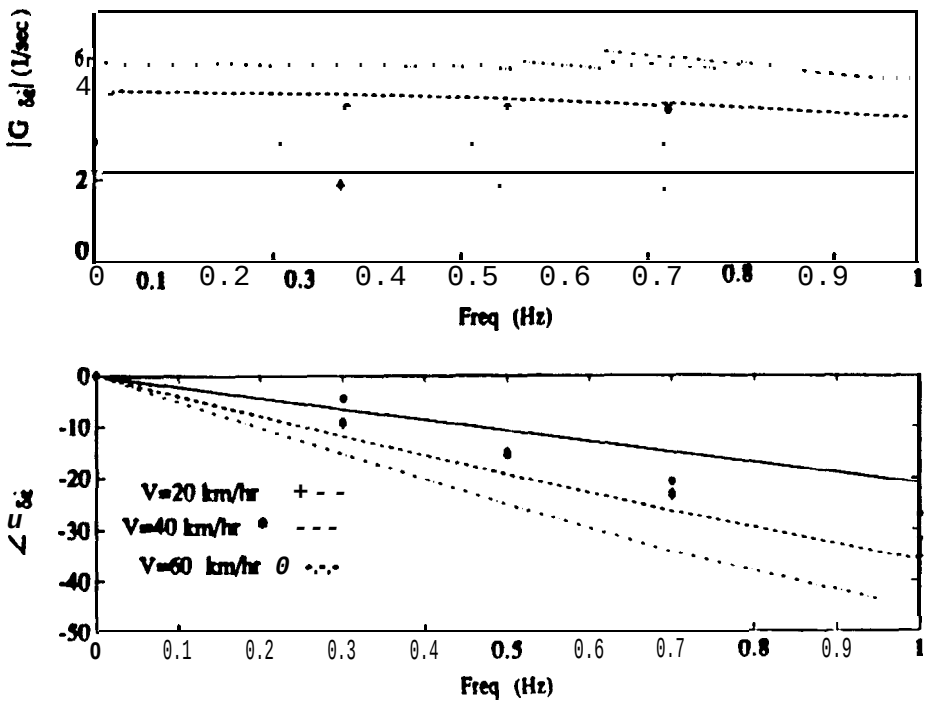

Figure 3.7 Simulated Vehicle Yaw Rate Transfer Function

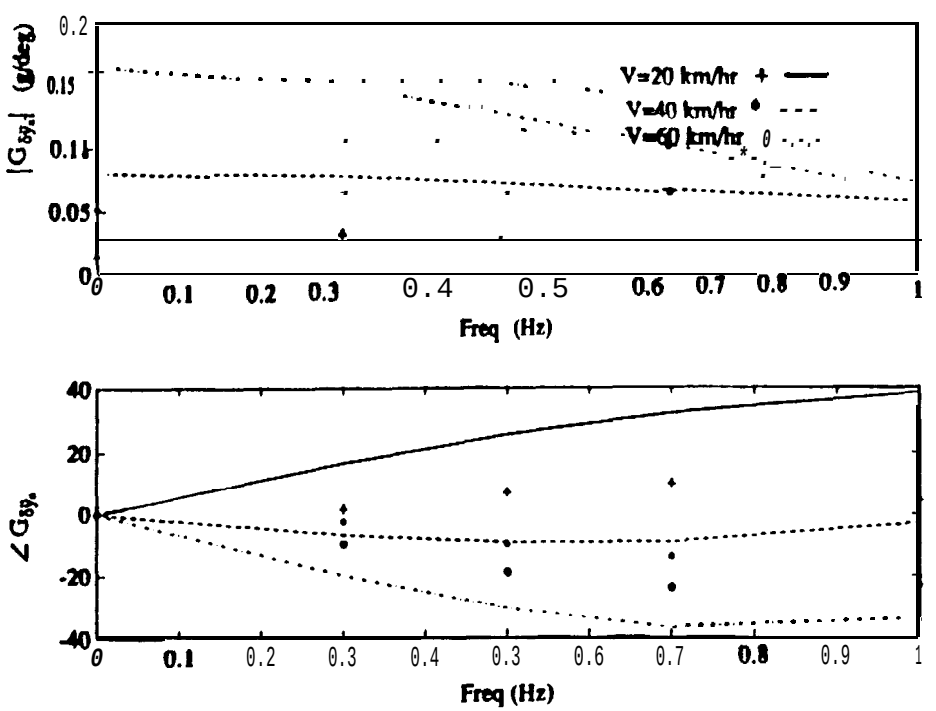

Figure 3.8 Simulated Vehicle Lateral Acceleration Transfer Function

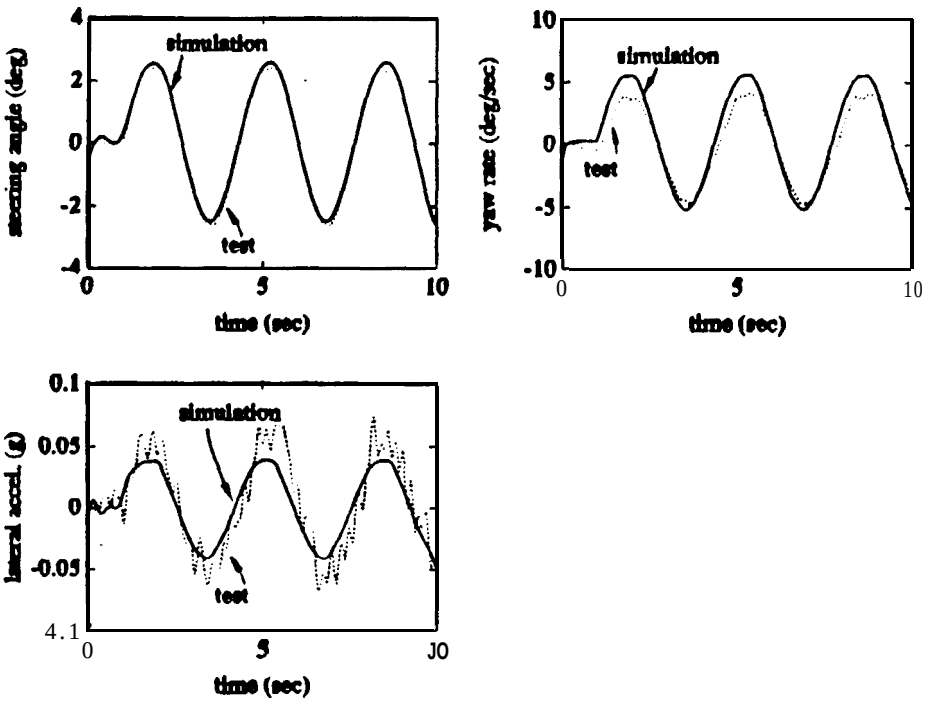

Figure 3.9 Open Loop Vehicle Simulation (0.3 Hz steering input, 20 km/hr)

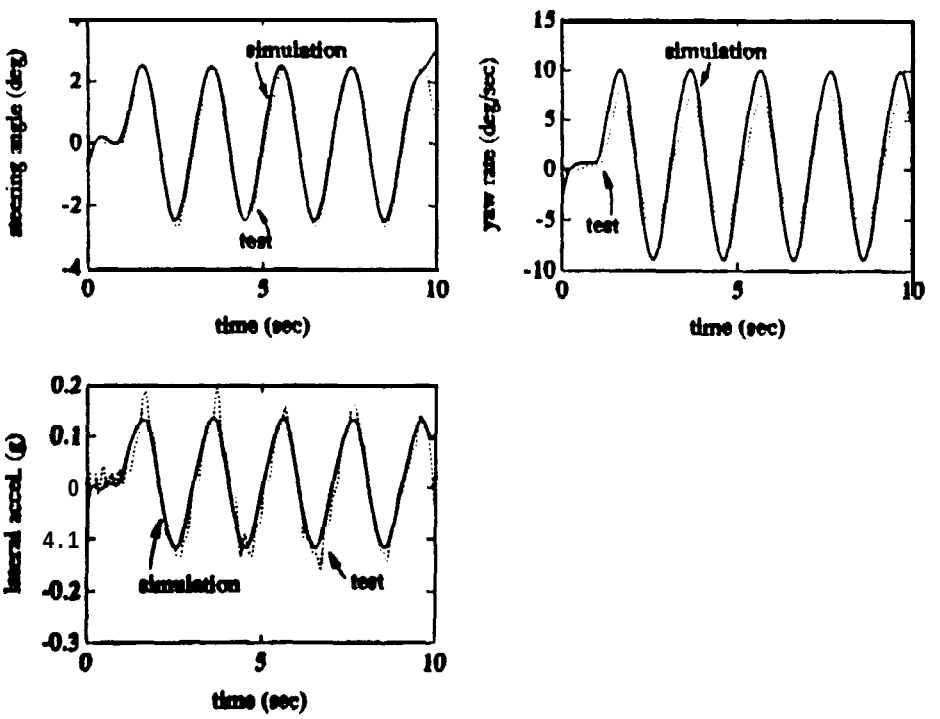

Figure 3.10 Open Loop Vehicle Simulation (0.5 Hz steering input, 60 km/hr)

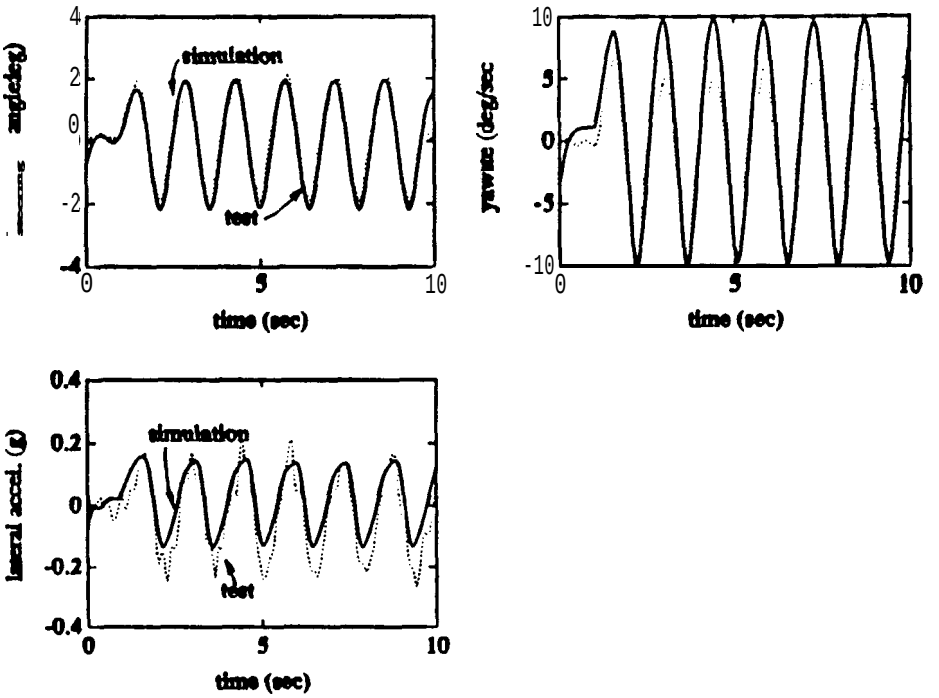

Figure 3.11 Open Loop Vehicle Simulation (0.7 Hz steering input, 60 km/hr)

4. CLOSED LOOP EXPERIMENTS

Results of the closed loop control experimental work are described in this section. The optimal preview control algorithm was evaluated and compared with a PID control algorithm. The vehicle test speeds were limited to 20-50 km/hr for test path #1, and 20-70 km/hr for test path #2 due to the limitations in the test track size. The maximum steady state lateral acceleration over paths 1 and 2 was approximately 0.26g and 0.20g, respectively, which is fairly high for non-emergency maneuvers.

The state variables required by the preview control algorithm were obtained by using a Luenberger observer. Error signals correct the observed state variables at each marker, and the observer works in the prediction mode (linear extrapolation) between markers where lateral position measurement is not available. The observer poles were placed to be slightly faster (-7.5) than the system closed loop poles (≈-5.5), and a small damping term was used to reduce the system sensitivity. The vehicle speed, which was obtained by counting the time ticks between markers, was updated only when a new marker was passed. All other measurements (yaw rate, acceleration, front wheel steering angle, and lateral position measurement from the video system) were obtained every 21 msec. The steering angle command to the front wheels was updated every 25 msec. The augmented state variables, which were computed by passing measurement outputs through appropriate filters, were integrated with a 3 msec step size.

The gain scheduling technique was used to tune the gains of the feedback and feedforward controllers according to vehicle speed. The cornering stiffness estimation, Cs. oscillated much more than expected. Therefore, a fixed Cs was used to calculate the controller gains. Linear interpolations were used to smooth the controller gains between the scheduling points. Key parameters used in the simulation and controller design procedures are listed in Table 4.1.

Table 4.1 Key Simulation Parameters

Symbol	Meaning	Value
m (kg)	mass	1573
I_z (kg-m^2)	moment of inertia (z)	2783
RC	road condition factor	0.6-0.7
V (km/hr)	vehicle speed	20-70
δ_{tol} (deg)	deadband of steering actuator	0.3
l_1 l_2 (m)	distances from c.g. to axles	1.034 1.491
d_s (m)	dist. c.g. to magnetometer	1.4
T_s (sec)	sampling time	0.025
D_m (m)	marker spacing	1.0
t_{la} (sec)	preview time	1.0
A_w	disturbance decay rate	0

4.1 Closed Loop Experimental Results

The closed loop test results using the FSLQ and PID control algorithms are presented in this section. The results of these experiments confirm that the preview action (which generates a steering command just before the vehicle reaches the curve) is necessary for the test vehicle to stay within the range of the magnetic sensing system ($\pm$50 cm). The test vehicle failed to follow the curve of test path #1 at 50 km/hr, even when the steady state feedforward controller was used. Tests under nominal conditions were first performed at selected vehicle speeds from 20 to 50 km/hr (20 to 70 km/hr) for test path #1 (#2). However, since the vehicle speed was controlled by a human driver, the target test speeds were only approximated.

Several non-ideal conditions were then tested at 40 km/hr over test path #1 to study the robustness of the control system: increased vehicle load, reduced tire pressure, missing

markers and misaligned markers. For safety reasons, the non-ideal tests were not performed on the second test path. To check repeatability, three test runs were performed for each test condition.

Simulations were performed to examine whether important features of the test vehicle were modeled in the simulation program. The measurements from the sensors were assumed to be contaminated by Gaussian white noise listed in Table 4.2, which was estimated from the sensor output data. The simulated noise in the lateral position measurement from the magnetic sensing system was only a good representation for the straight sections of the road. At the curved sections, a much larger error may arise because it is more difficult to install markers along an arc than along a straight line.

Table 4.2 Simulation Signal Noise

Signal	Standard Deviation
steering angle command	0.2°
steering angle measurement	0.2°
lateral acceleration	0.001 g
yaw rate	0.3°/sec
lateral tracking error	0.005 m
vehicle speed measurement	0.1 m/sec

Due to the limitations of the geometry of the test track and the range of the steering actuator, the actuator range had to be shifted to the right one degree to negotiate test path #1. In other words, the range of the actuator was set at -4" to 2° for test path #1 and -3° to 3° for test path #2.

4.1.1 Nominal Case (test path #1)

The test and simulation results of a 50 km/hr run over test path #1 under nominal conditions (two passengers and dry road surface) are shown in Figures 4.1-4.4. For this specific test the vehicle speed was actually 53 km/hr and the steady state lateral acceleration in the curved section was 0.29g. The maximum lateral deviation was kept under 16 cm for

the straight and curved sections by both the FSLQ and PID controllers. The simulations predict a faster response in the vehicle's lateral position and lateral acceleration than obtained in the tests.

The steering angle plots show that there is a time lag between the command (solid line) and true steering angle (dashed line). Also, due to the compliance of the vehicle steering system, the true steering angle will only reach approximately 90% of the command magnitude. The "chattering" of the steering command is much smaller at straight sections than at the curved section for the test result. Many factors contributed to the oscillation in the steering command in the curved section, and the marker misalignment may be the single most important factor. To improve the ride quality around curves, a low-cost technology needs to be developed to install markers on a path with a fixed radius of curvature.

The test and simulation results at 40 km/hr (with only one passenger) are presented in Figures 4.5-4.8 which will be used for comparison with the non-ideal test conditions. The maximum tracking error was less than 12 cm. Table 4.3 shows the magnitudes of peak tracking error on test path #1 under selected speeds.

Table 4.3 Peak Tracking Error on Test Path #1 Under Nominal Conditions

speed (km/hr)	PID+preview (cm)	FSLQ+preview (cm)	Lateral Acceleration (g)
20		-5 ~ +5	0.04
30	-5 ~ +5	-5 ~ +5	0.09
40	-10 ~ +10	-5 ~ +14	0.17
50	-16 ~ +13	-5 ~ +13	0.26

4.1.2 Nominal Case (test path #2)

The test and simulation results of a 60 km/hr run through test path #2 are shown in Figures 4.9-4.12. The peak tracking error is less than 15 cm. The tracking error and steering command signals oscillate due to the overshoot when entering or leaving the curves. The tracking errors of the nominal cases under various vehicle speeds over test path #2 are listed in Table 4.4 for reference.

Table 4.4 Peak Tracking Error on Test Path #2 Under Nominal Conditions

speed (km/hr)	PID+preview (cm)	FSLQ+preview (cm)
20	-5 ~ +8	-8 ~ +4
30	-8 ~ +8	-6 ~ +3
40	-8 ~ +8	-7 ~ +5
50	-12~ +10	-9 ~ +8
60	-10 ~ +12	-12 ~ +10
70		-12 ~ +10

4.1.3 Increased Load

To test the effect of increased vehicle load on the tracking performance, the load on the vehicle was increased by 2225 N (500 lb), which consisted of two extra passengers and 579 N (130 lb) of lead weight in the trunk. The control law was not adjusted to compensate for this change in vehicle mass. Figures 4.13-4.14 illustrate that the vehicle settles a little farther to the outside of the curve, and the lateral displacement response is slower than in the nominal case. These features were predicted by the simulation results (Figures 4.15-4.16).

4.1.4 Reduced Tire Pressure

In this test, the pressure of the two front tires was reduced from 248 kPa (36 psi) to 172 kPa (25 psi), a 30% reduction. Figures 4.17-4.18 show that the oscillation of lateral acceleration was reduced. This is probably due to the extra damping introduced by the soft tires. Reduced tire pressure also results in the reduction of tire cornering stiffness. Therefore, the steering angle needed to pass through the curve is increased. Also, both the steady state and peak tracking error were noticeably greater than in the nominal case, which were also captured in the simulation results (Figures 4.19-4.20). In the simulation program the true tire steering angle is assumed to reach 80% of the perceived value. In other words, an extra scaling factor of 0.8 is used to model the effect of a soft tire.

4.1.5 Missing Markers

In this test, two of the markers in the middle of the curved section of test path #1 were removed. The lateral tracking error measurement was not available at these two points. The missing markers also produced an error in the vehicle speed estimation. This erroneous vehicle speed measurement was used for approximately 0.7 seconds in the calculation of the control gains. The steering command (Figures 4.21-4.22) suddenly decreased near the missing markers because the erroneous vehicle speed information resulted in lower feedforward and feedback gains. Also, since two markers were missing, the preview control command continued two markers beyond the point where the curve actually ended. This results in a sudden change of approximately 13 cm in the lateral position. These responses were predicted by the simulation results (Figures 4.23-4.24).

4.1.6 Misaligned Markers

The test results using misaligned markers (twisted to inject a ± 1.5 cm rms random noise) arc shown in Figures 4.25-4.26. The steering command oscillated more frequently but the vehicle was able to follow test path #1 with an acceptable tracking error (<17 cm). The simulation results (with a 2.0 cm white noise in lateral position measurement rather than the 0.5 cm used for the nominal case) show a similar magnitude of oscillation in the lateral displacement response (Figures 4.27-4.28), which seems to support the hypothesis that the markers at curved sections were not aligned as well as those at straight sections. The steering command of the PID control algorithm becomes much noisier thdn in the nominal case, while that from the FSLQ control law oscillates only slightly more (see Table 4.5). The reason is that the measurement noise rejection capability was included in the FSLQ design procedure, but not in the PID controller.

Table 4.5 RMS Steering Command with Misaligned Markers

	Aligned Markers	Misaligned Markers
FSLQ	0.0172°	0.0216°
PID	0.0146”	0.0239’

4.1.7 Slippery Road

The performance of the control system was also tested on a rainy day. The effect was found to be similar to that of the reduced tire pressure, except that the steering angle is not

significantly increased (Figures 4.29-4.32). The transient overshoot in the lateral tracking error increased and more closely agreed with the simulated response than the comparison between the experimental and simulated responses for nominal conditions. This is probably due to the reduction in the dry friction, which is not included in the simulation. In the simulation, a smaller RC (0.6) is used to model the slippery surface.

4.2 Observations

The following are observations from the closed loop experiments, none of which were experienced during the simulation stage.

1) It was found from the experiments that it is very difficult to design the observer to estimate the state variables when vehicle speed is lower than 20 km/hr. The reason is that when the vehicle speed is zero, the vehicle becomes unobservable (in the control theory sense). When the vehicle speed is low, the observer gains become so large that the estimation blows up due to model uncertainties. In the experiments, the observer gains were designed based on the range of 25-55 km/hr. The PID control algorithm was used when the vehicle speed was low (<18 km/hr), even when the FSLQ control algorithm was tested, since the observer cannot be turned on until the vehicle speed is high enough (≥ 18 km/hr).

2) The-true zero point of the steering command has a significant influence on the tracking performance. Initially, there were some difficulties when trying to reduce the tracking error below 30 cm on test path #2. After lengthy analysis and repeated tests, it was found that the state estimations from the observer were biased, which was caused by a small offset in the steering angle measurement (0.2”). Furthermore, it was very difficult to calibrate the steering angle measurement with that precision. This problem was found during the tests on test path #2. It contributed to the fact that the tracking performance of the FSLQ controller is inferior to the PID controller on test path #1 since the steering angle measurement is used by the FSLQ controller (for the observer) but not by the PID controller.

3) Tests were performed with longer marker spacings but the results were not repeatable and are, therefore, not presented. The reason is thought to be that because the linear extrapolation method used to estimate the vehicle tracking error between markers was not accurate enough. The problem might be solved by using a quadratic extrapolation method.

4) The cornering stiffness estimation oscillates much more than expected. Therefore, the controller gains were scheduled only with respect to the vehicle speed. The cornering stiffness estimation scheme needs further tuning in the next stage of the experiments.

5) It was found in the experiments that preview action is necessary for good tracking performance with both PID and FSLQ control. The comparison between tht PID and FSLQ feedback control algorithms is made using the same preview action.

6) It was found that to make the PID simulation results more closely match the experimental results the derivative gains used in the simulations needed to be approximately 50% larger than the gains used in the experiments. The larger gains provided greater damping in the simulation.

The drawbacks of the FSLQ control algorithm compared with PID include the following: a more complicated control structure which requires a state observer, longer computation time, higher sensitivity to the steering angle measurement, and poorer performance at low vehicle speeds. However, FSLQ is superior to PID control in terms of better ride quality, as evaluated from the lateral acceleration measurement and the passengers' perception, less sensitivity to lateral position measurement noise, and greater ease in tuning the control feedback gains. The first two factors are included in the design process of the FSLQ control law, but not in the PID.

The FSLQ controller gains are easier to tune because the weighting factors of the performance index correspond to physical quantities like tracking error and steering angle. On the other hand, the PID gains must be tuned by trial and error based on experience and intuition.

It was observed from the experimental results that the preview action is necessary for good tracking performance, especially at higher speeds. The choice between FSLQ and PID feedback control algorithms involves personal preference. However, the preview control gains cannot be obtained without using the FSLQ (or LQ) control theory.

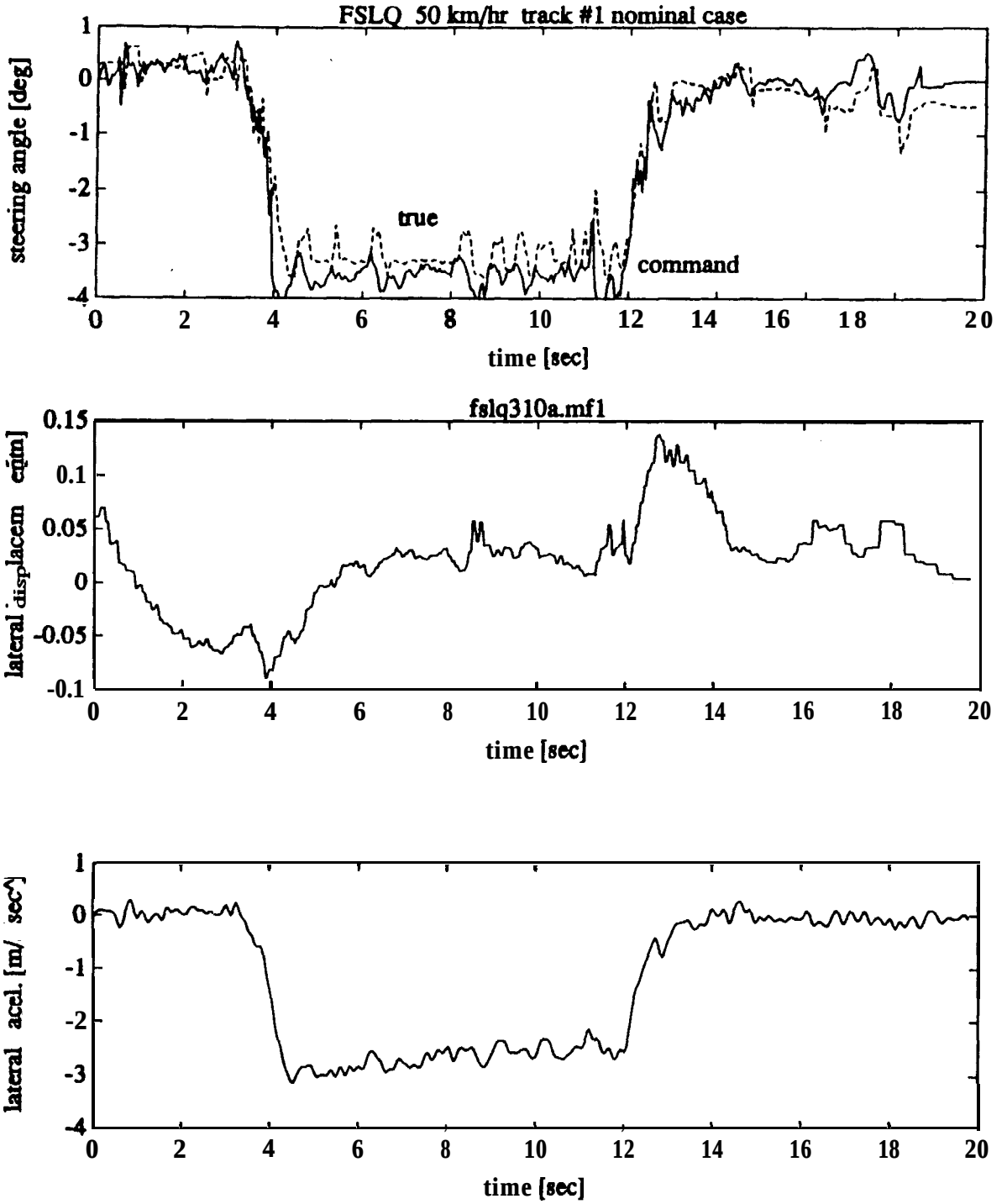

Figure 4.1 Nominal Case (test path #1) 50 km/hr - FSLQ test

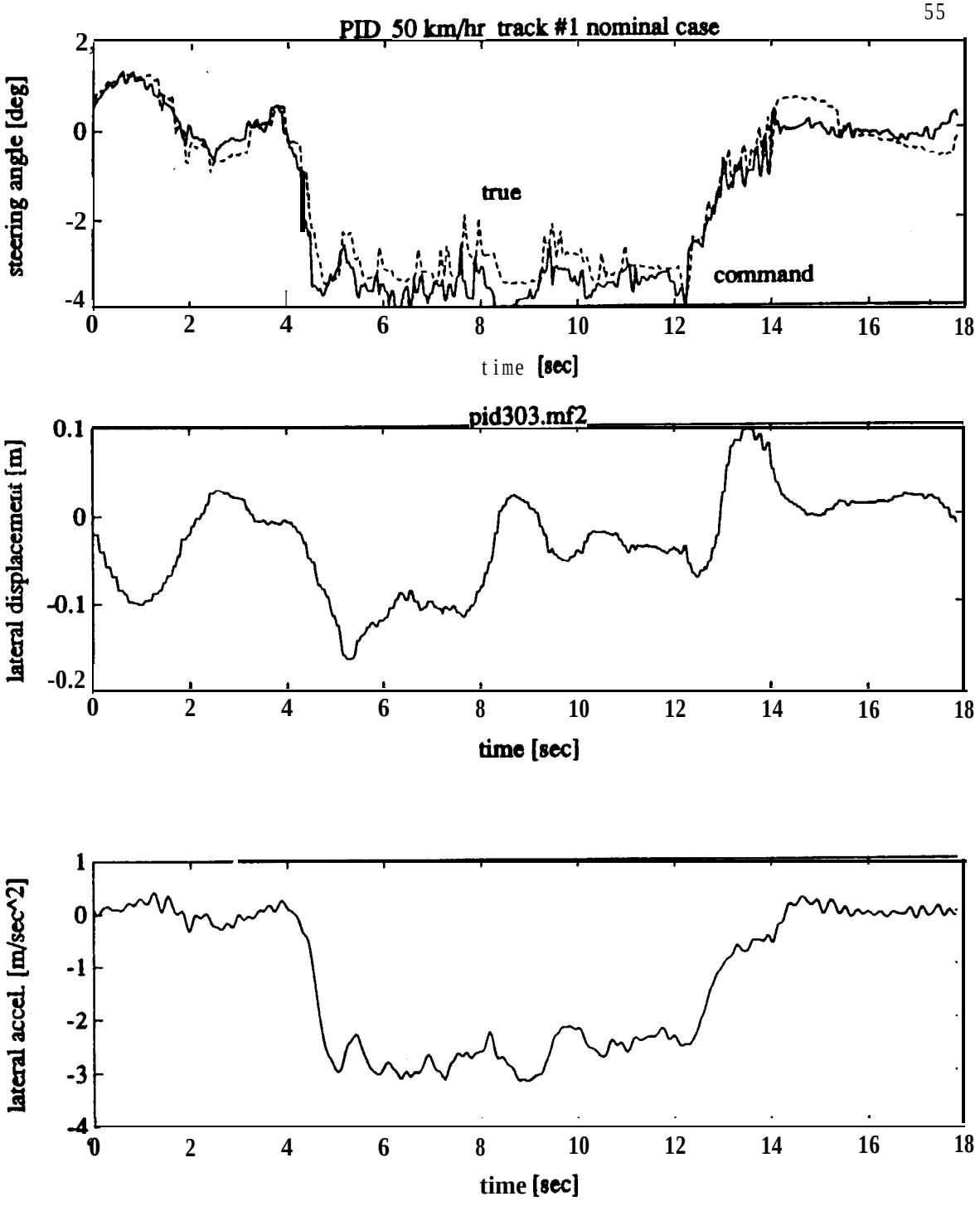

Figure 4.2 Nominal Case (test path #1) 50 km/hr - PID test

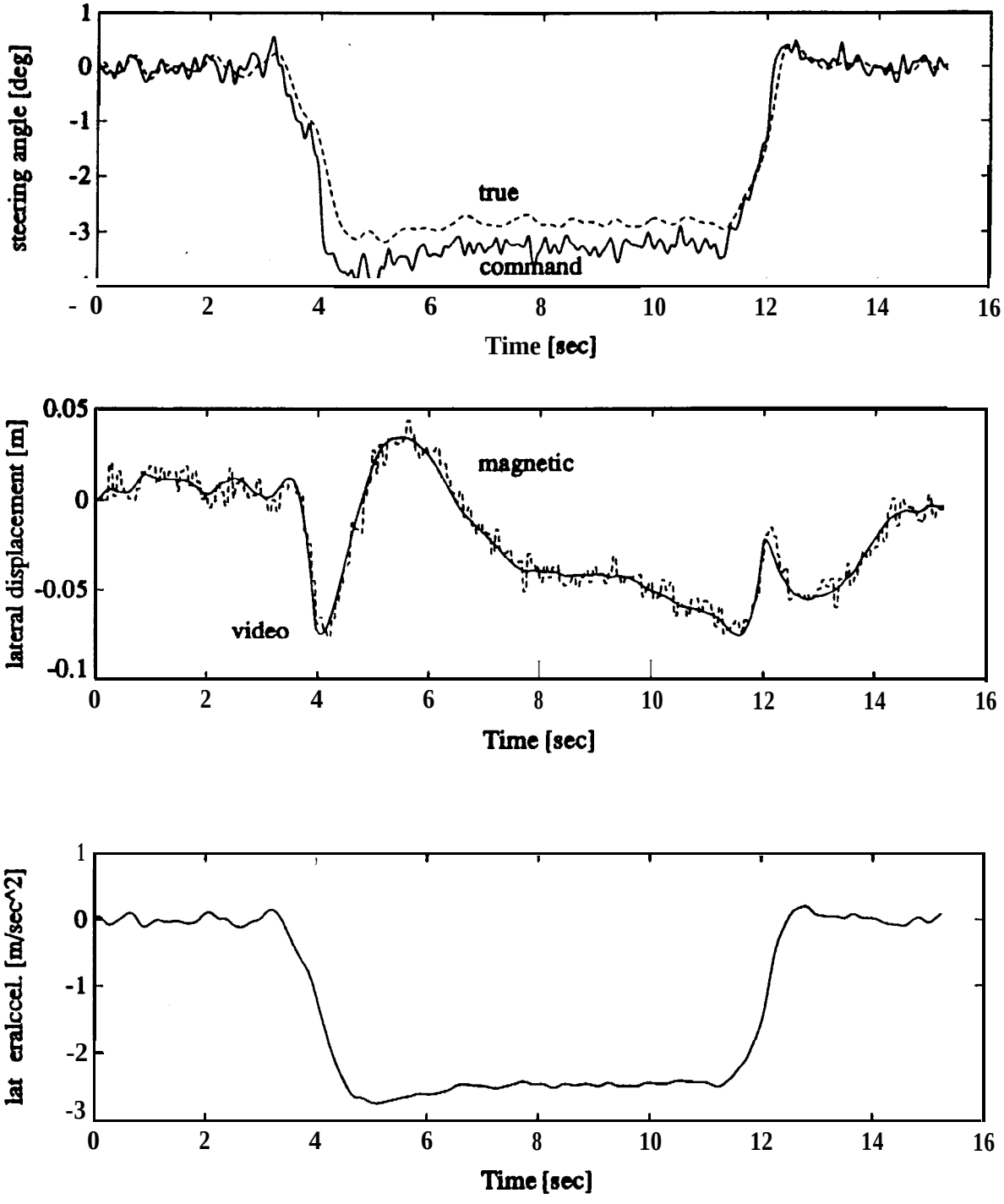

Figure 4.3 Nominal Case (test path #1) 50 km/hr - FSLQ simulation

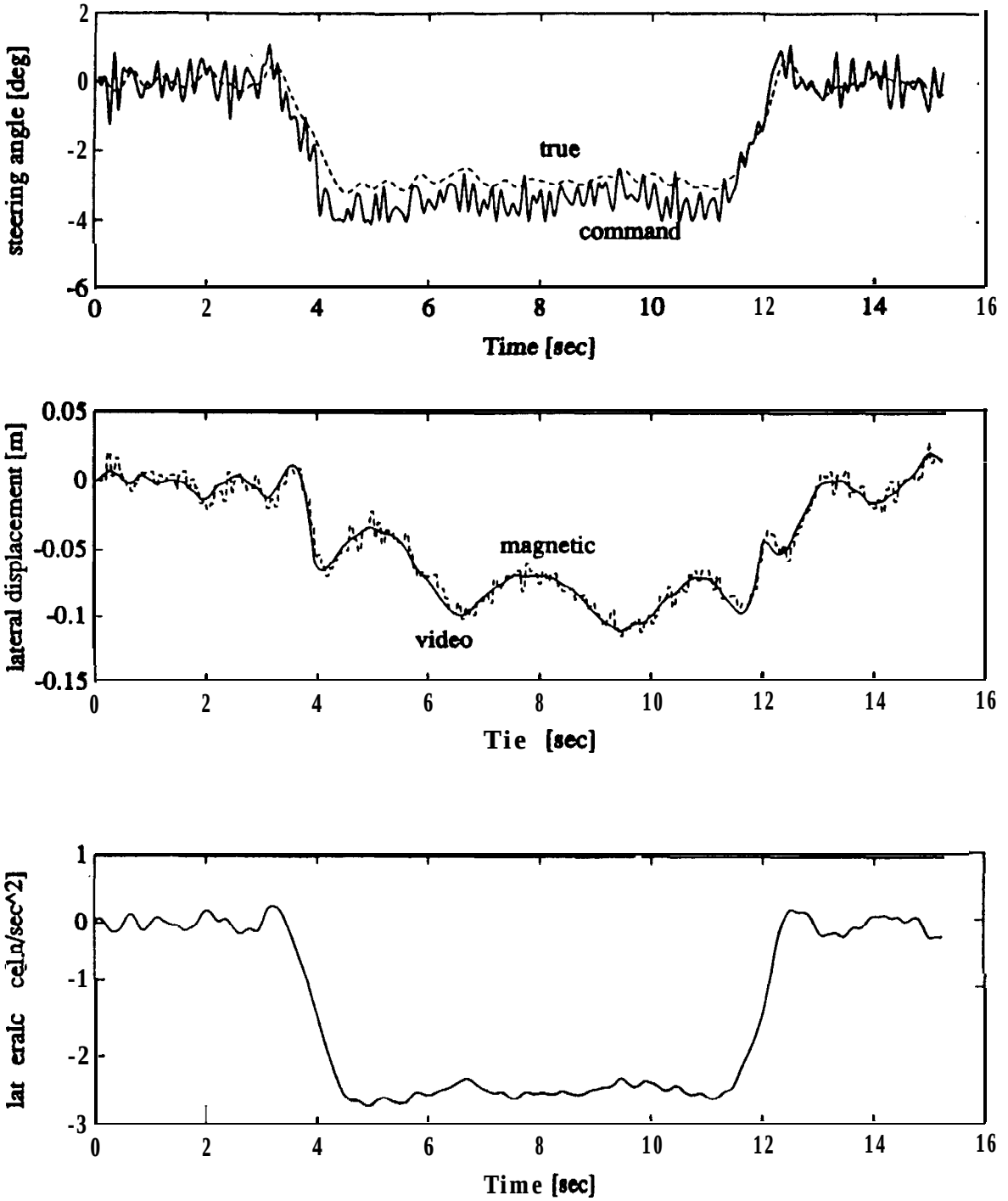

Figure 4.4 Nominal Case (test path #1) 50 km/hr - PID simulation

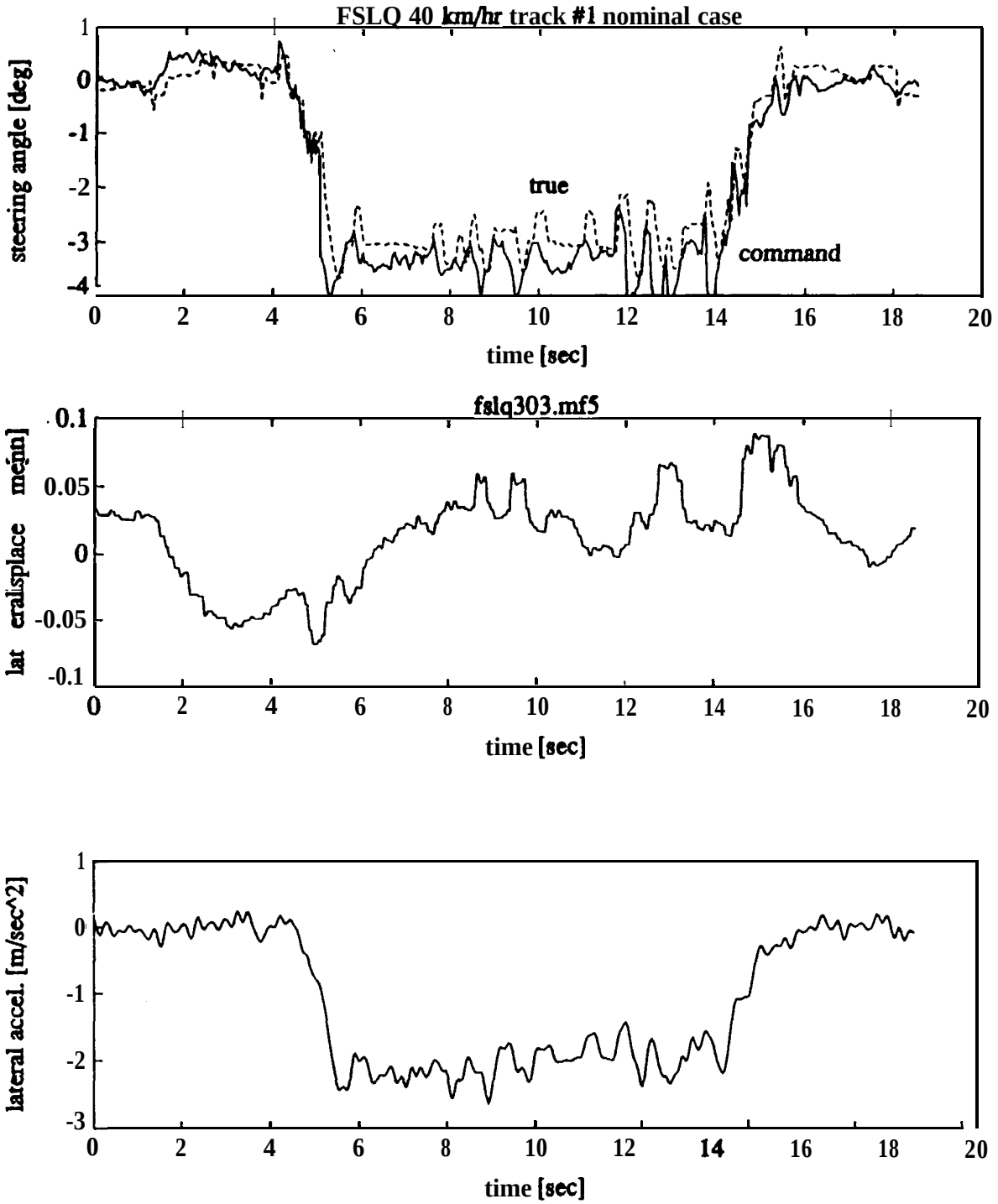

Figure 4.5 Nominal Case (test path #1) 40 km/hr - FSLQ test

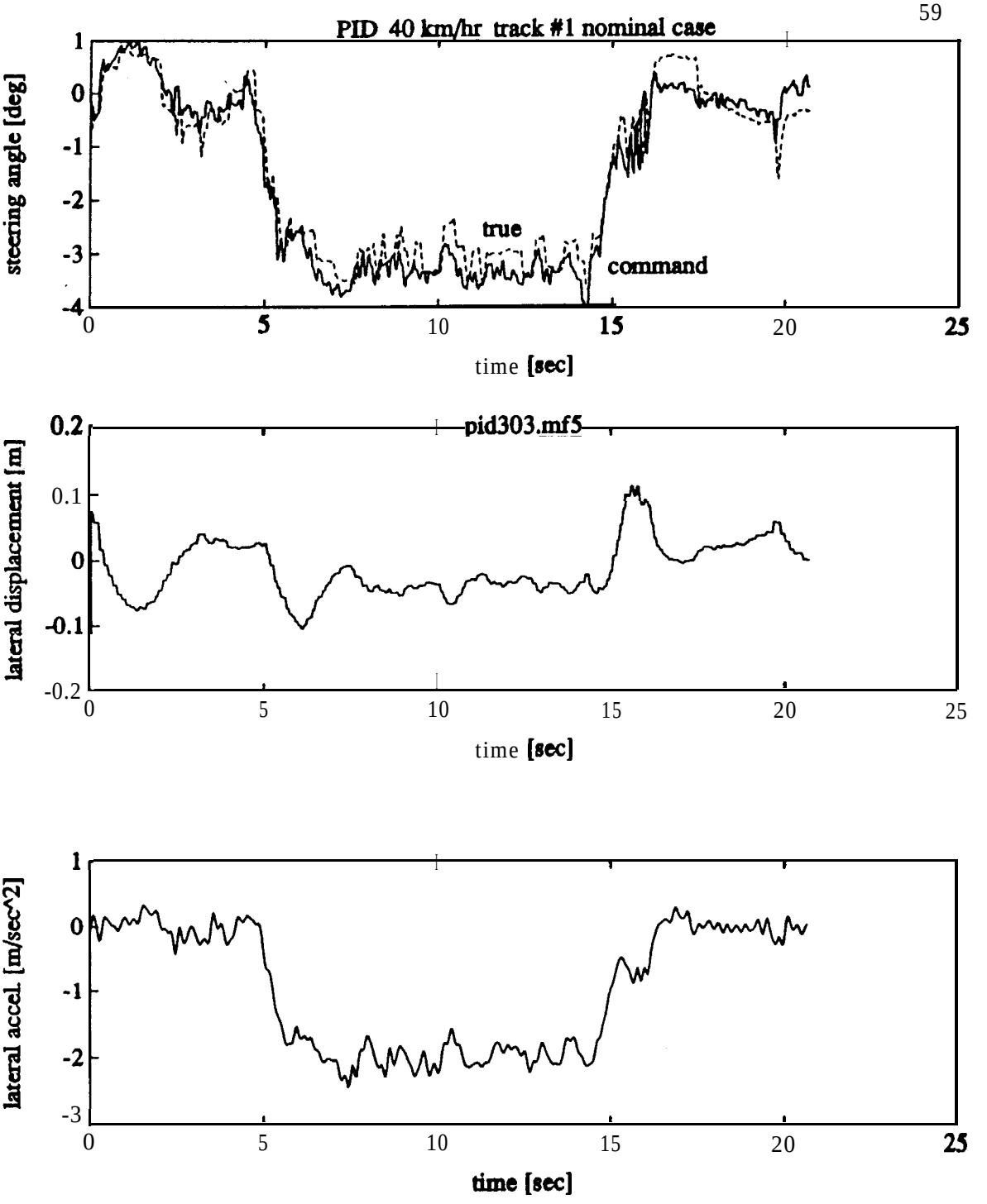

Figure 4.6 Nominal Case **(test** path **#1)** 40 **km/hr - PID** test

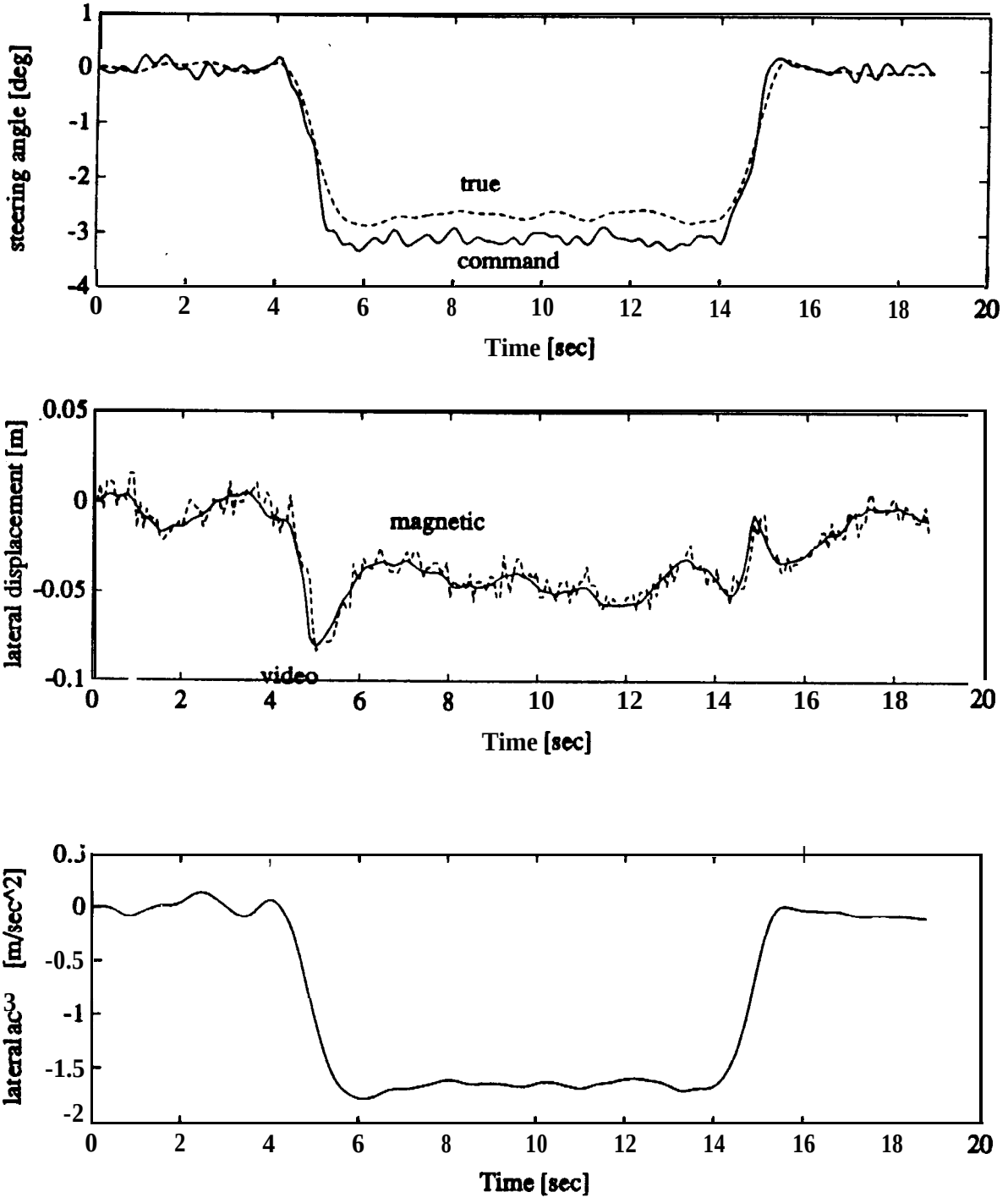

Figure 4.7 Nominal Case (test path #1) 40 km/hr - FSLQ simulation

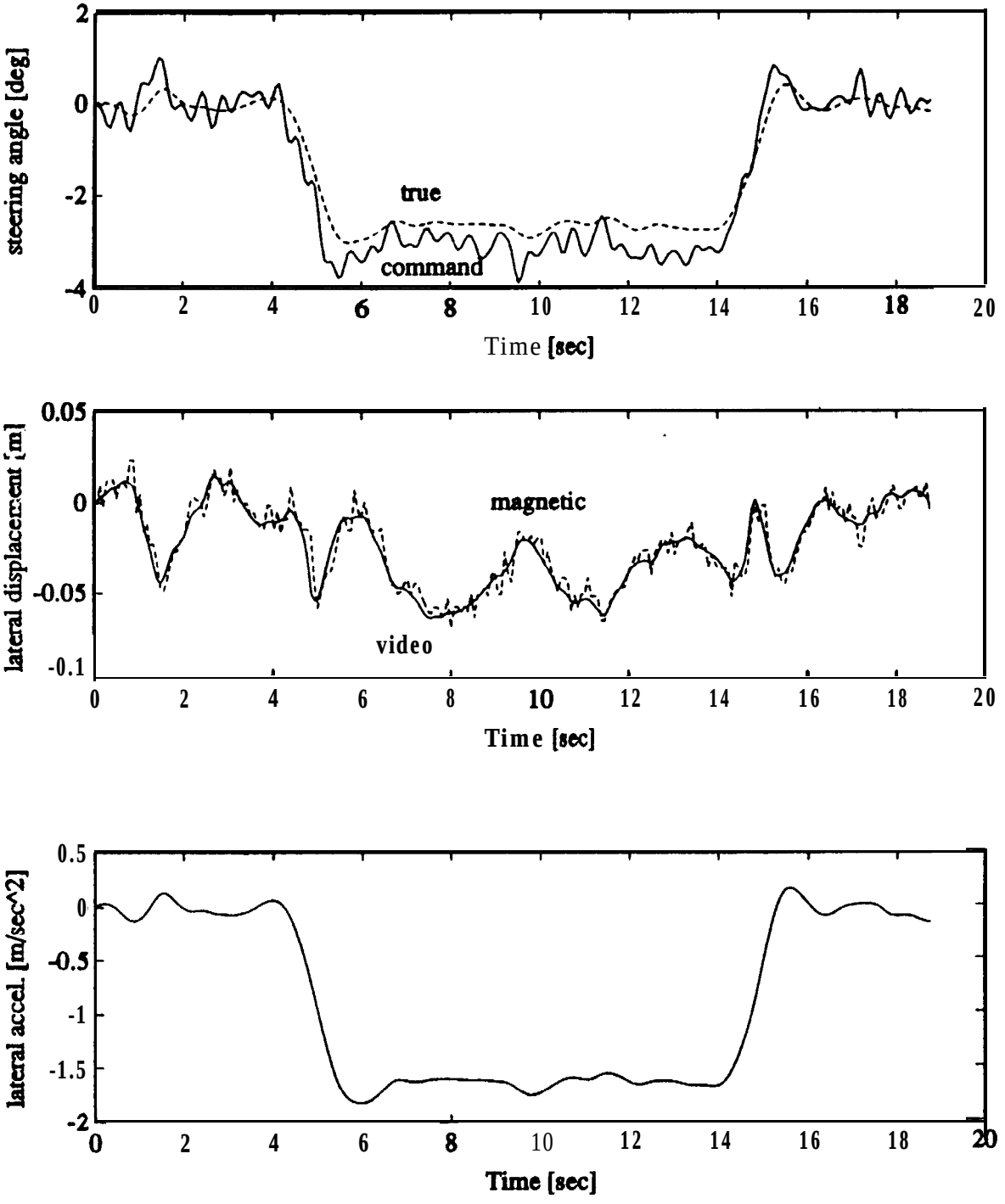

Figure 4.8 Nominal Case (test path #1) 40 km/hr - PID simulation

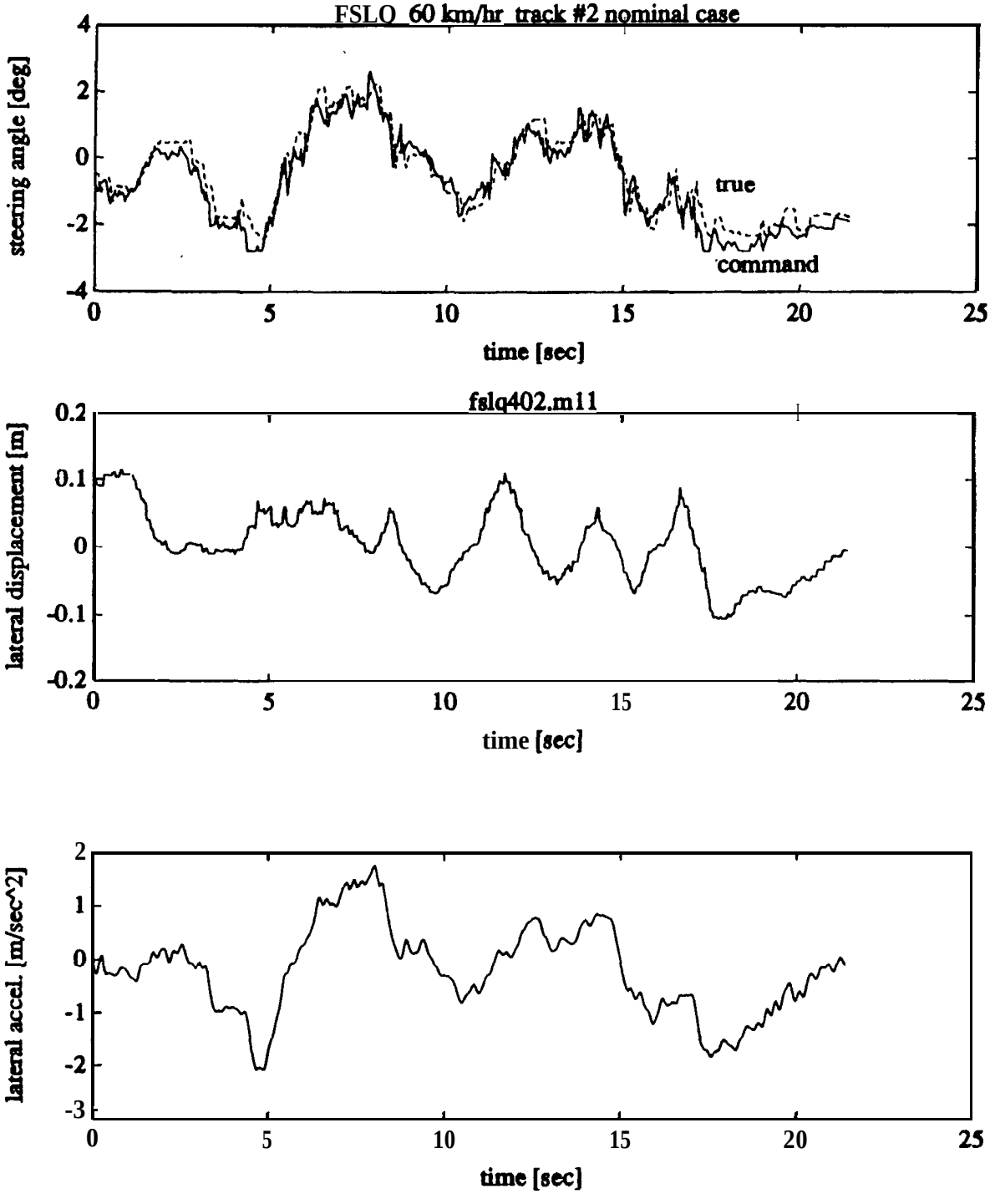

Figure 4.9 Nominal Case (test path #2) 60 km/hr - FSLQ test

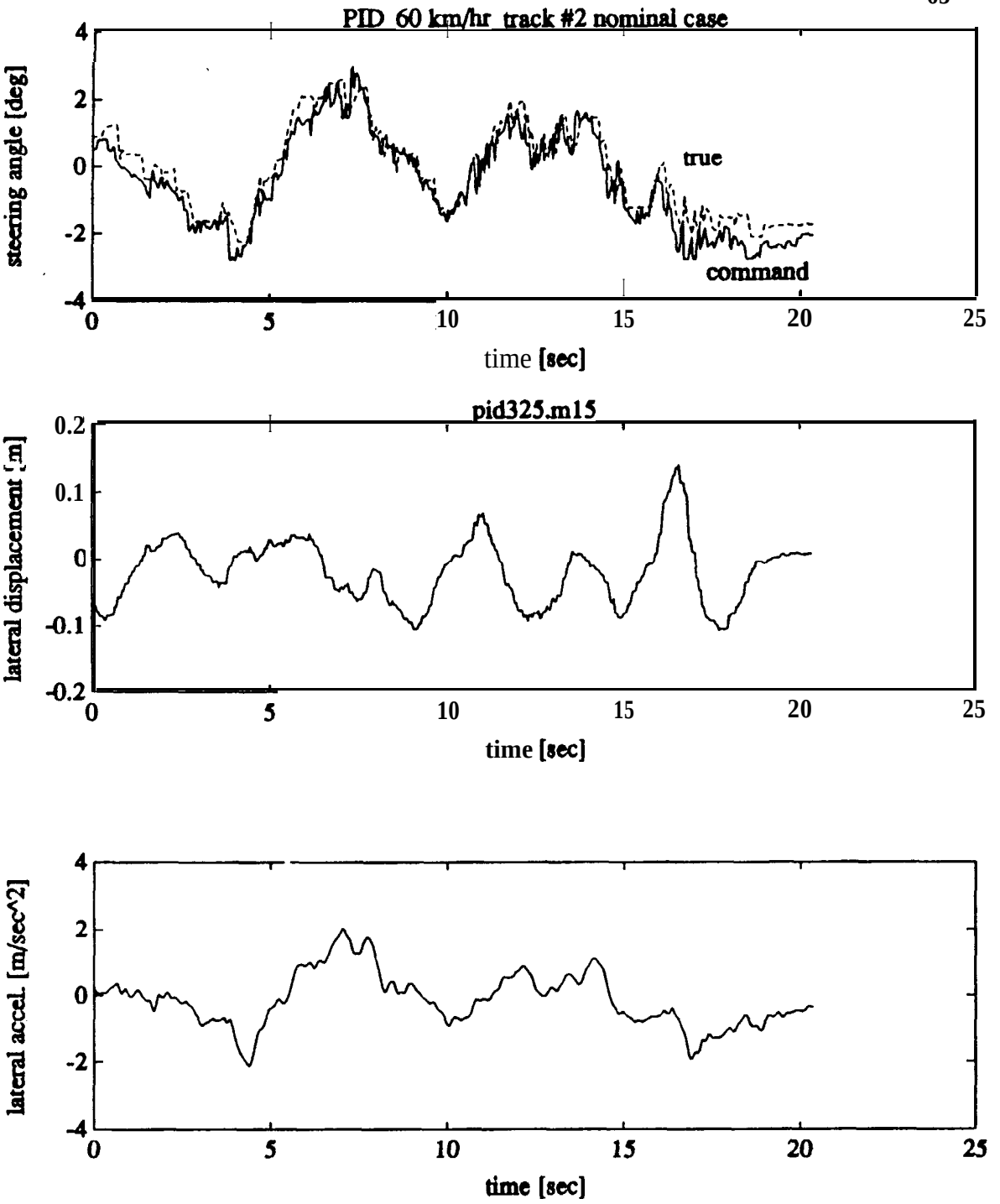

Figure 4.10 Nominal Case (test path #2) 60 km/hr - PID test

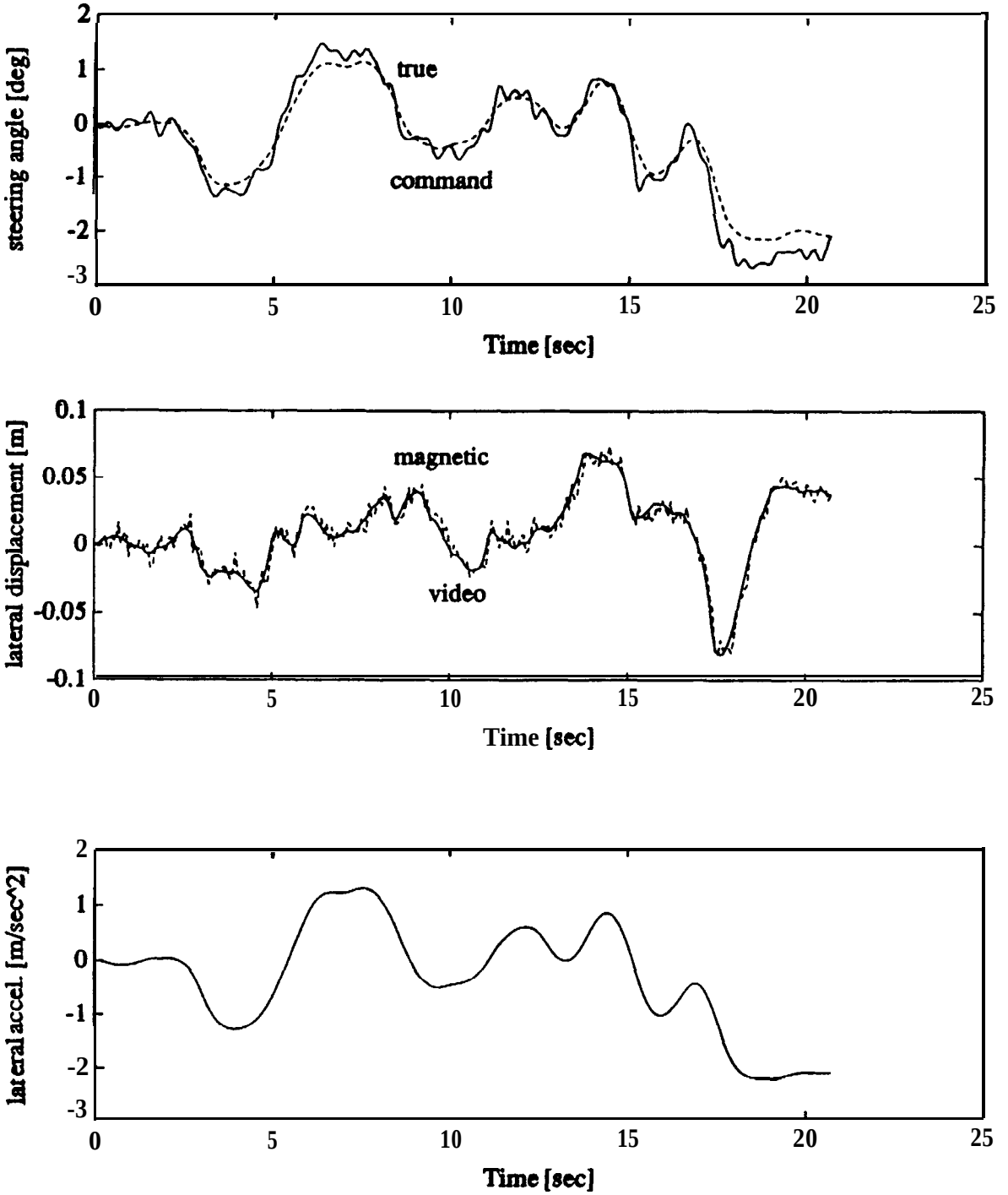

Figure 4.11 Nominal Case (test path #2) 60 km/hr - FSLQ simulation

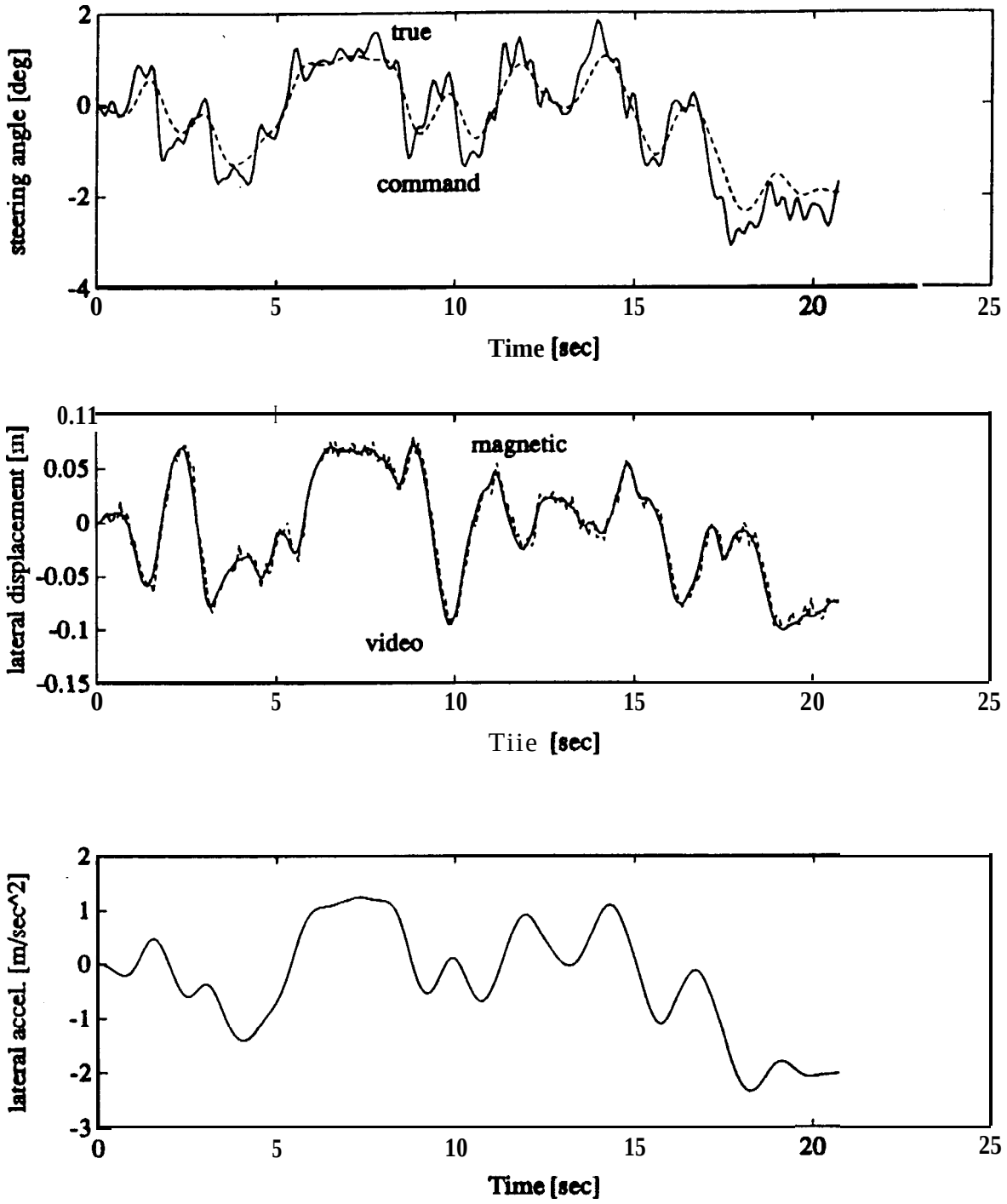

Figure 4.12 Nominal Case (test path #2) 60 km/hr - PID simulation

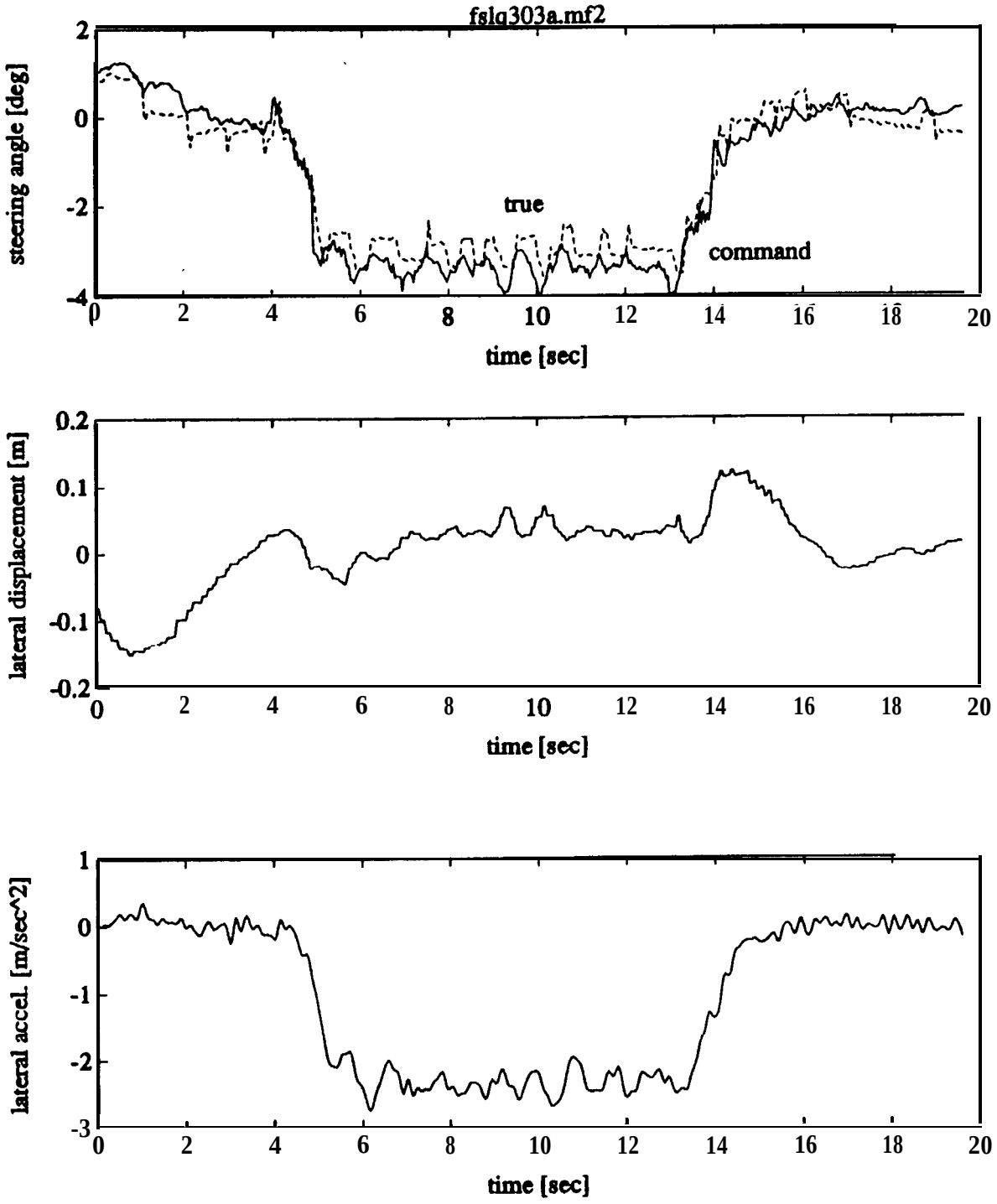

Figure 4.13 Increased Load (test path #1) 40 km/hr - FSLQ test

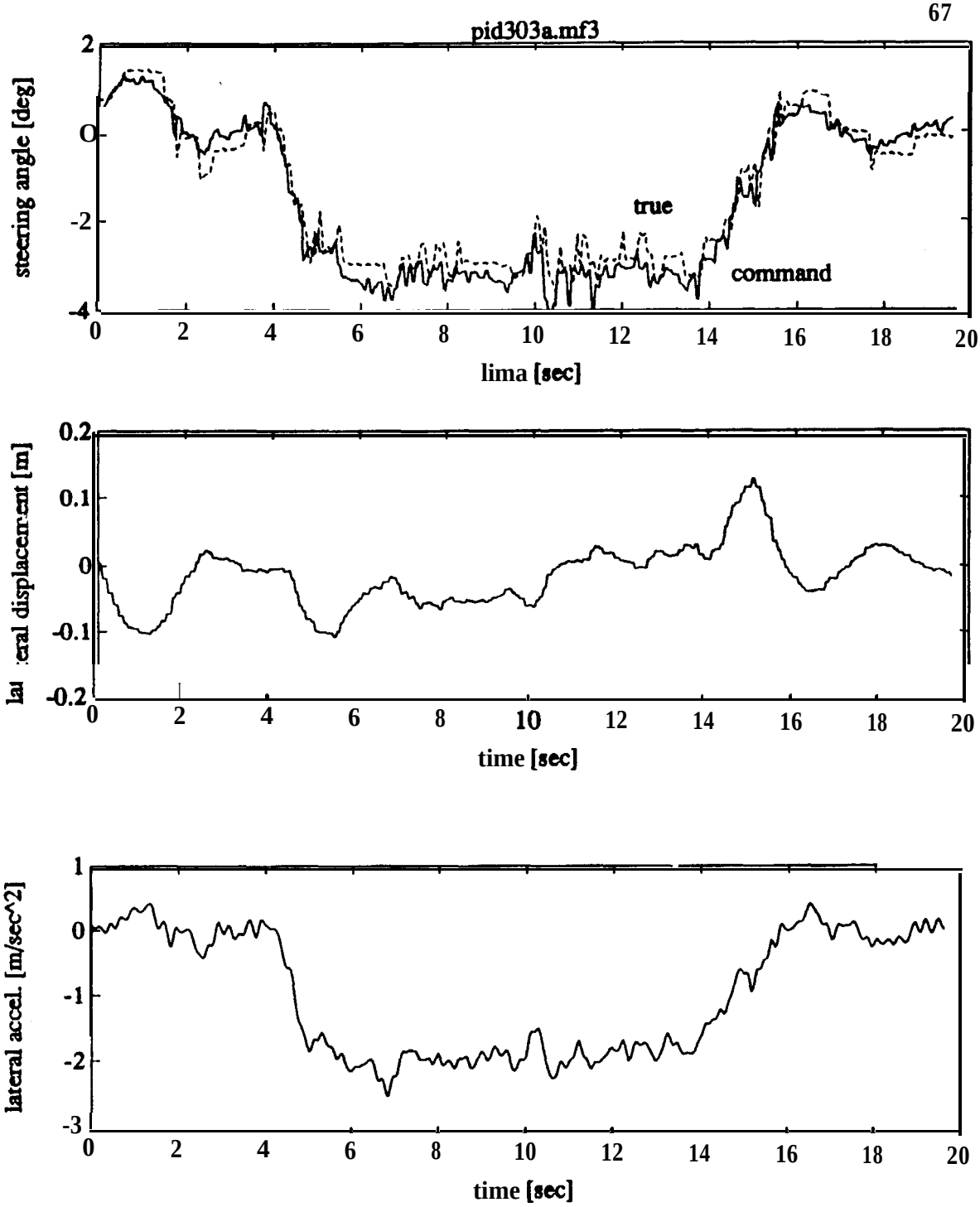

Figure 4.14 Increased Load (test path #1) 40 km/hr - PID test

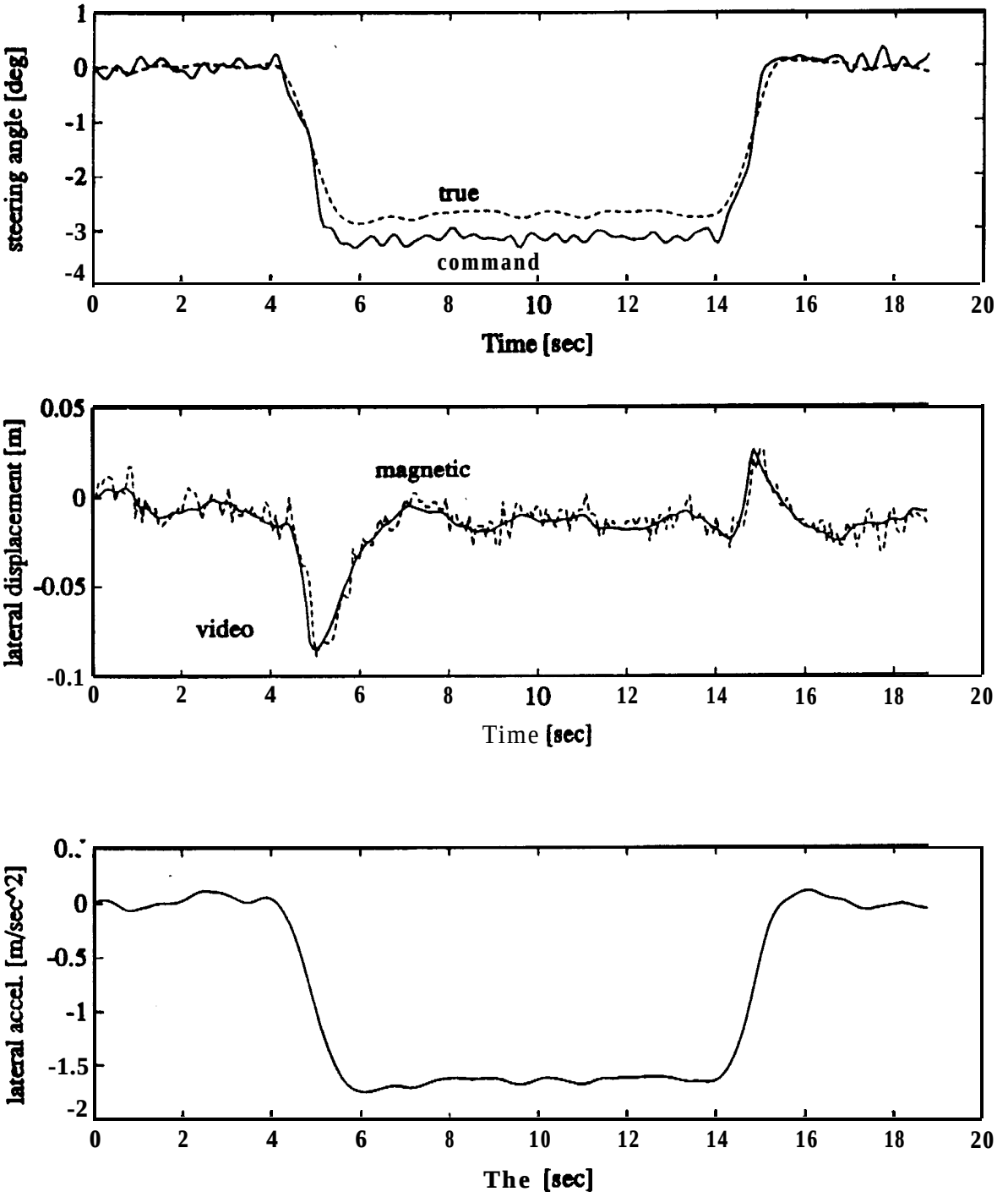

Figure 4.15 Increased Load (test path #1) 40 km/hr - FSLQ simulation

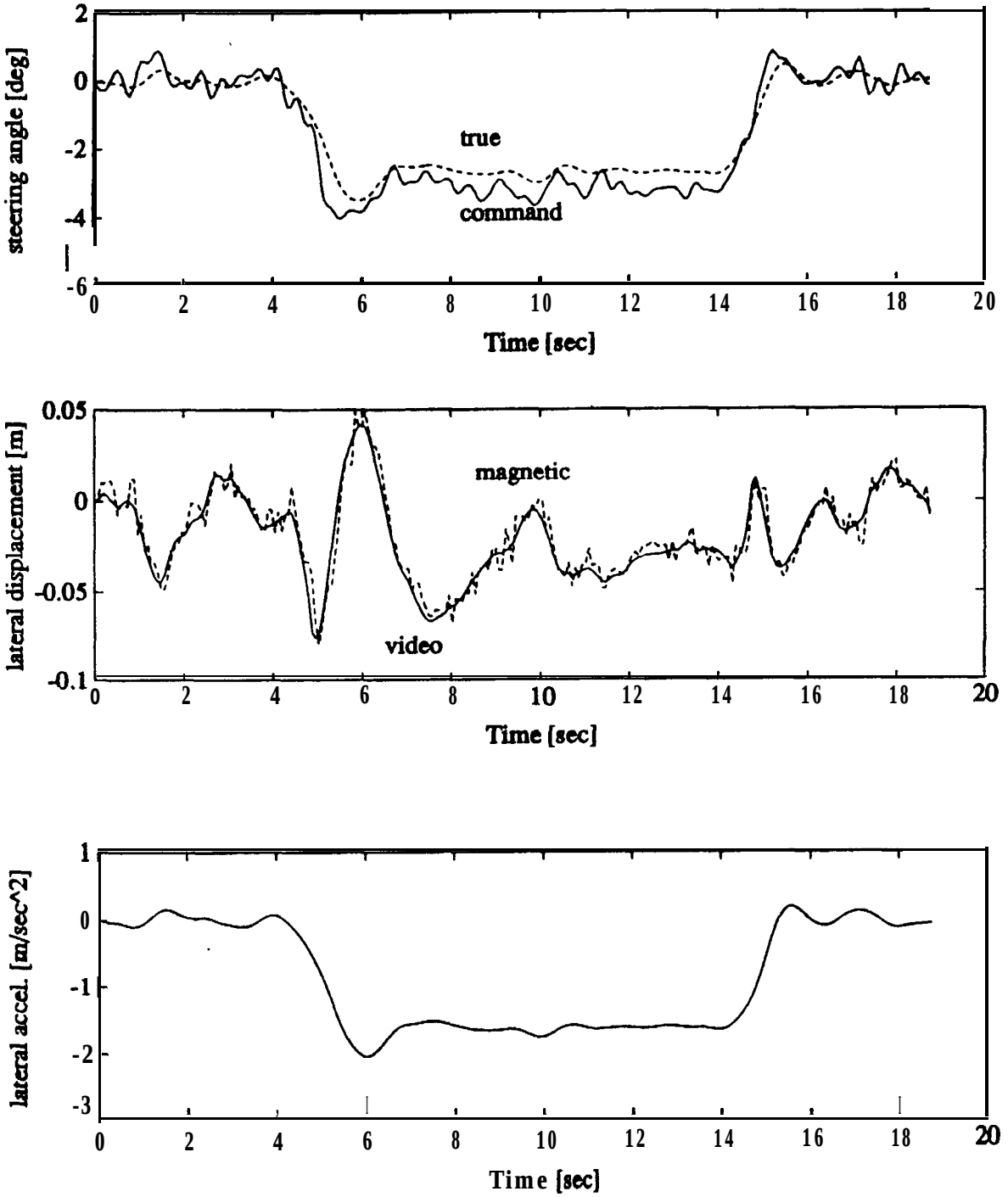

Figure 4.16 Increased Load (test path #1) 40 km/hr - PID simulation

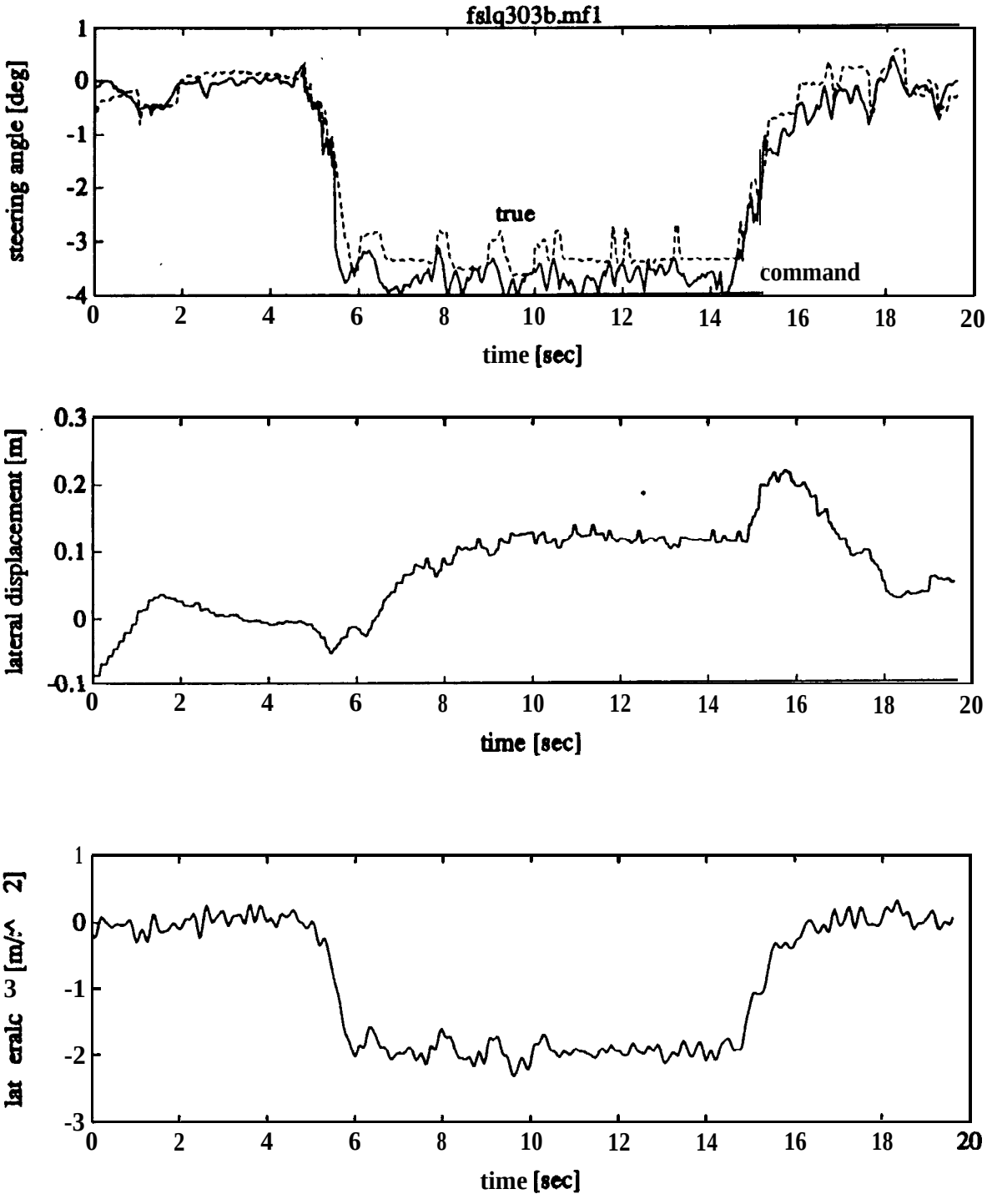

Figure 4.17 Reduced Tire Pressure (test path #1) 40 km/hr - FSLQ test

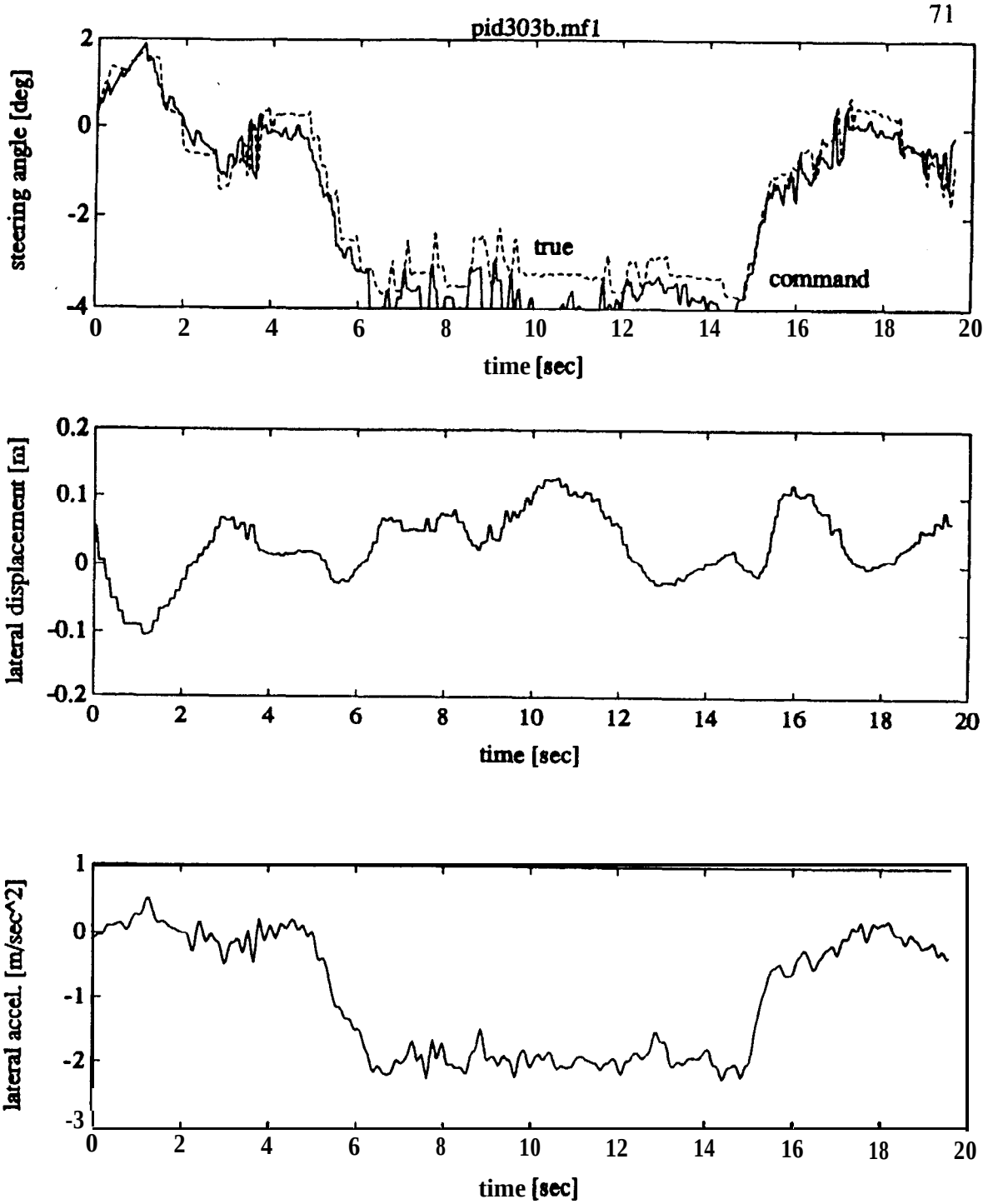

Figure 4.18 Reduced Tire Pressure (test path #1) 40 km/hr - PID test

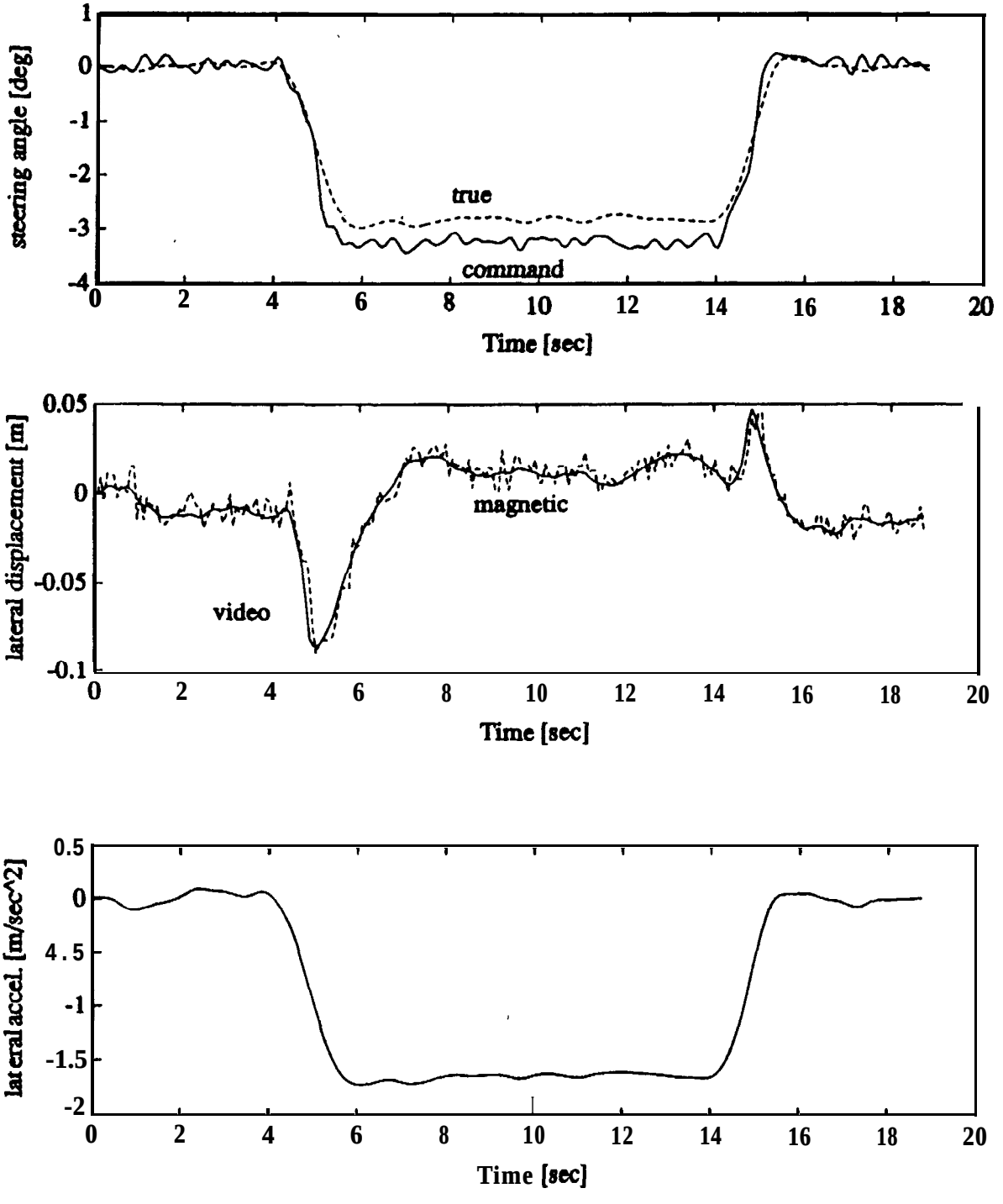

Figure 4.19 Reduced Tire Pressure (test path #1) 40 km/hr - FSLQ simulation

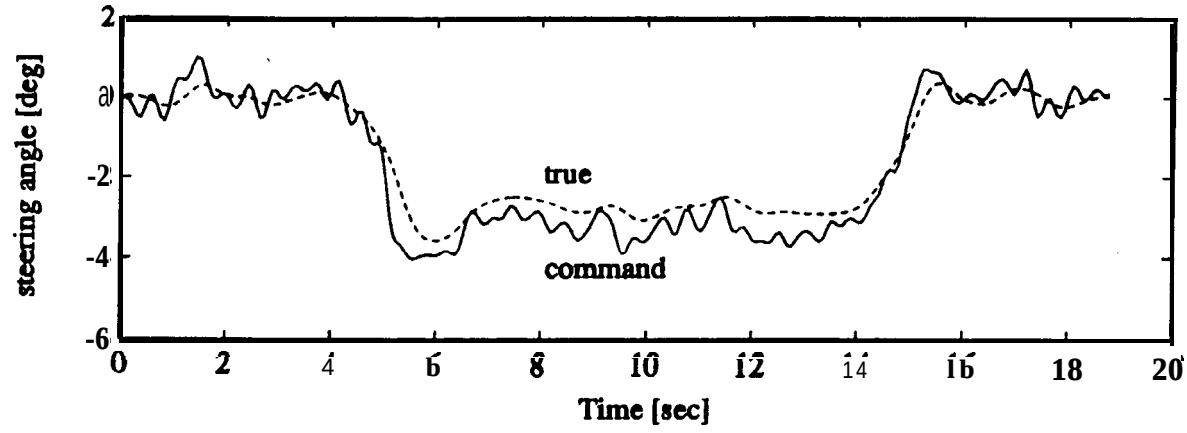

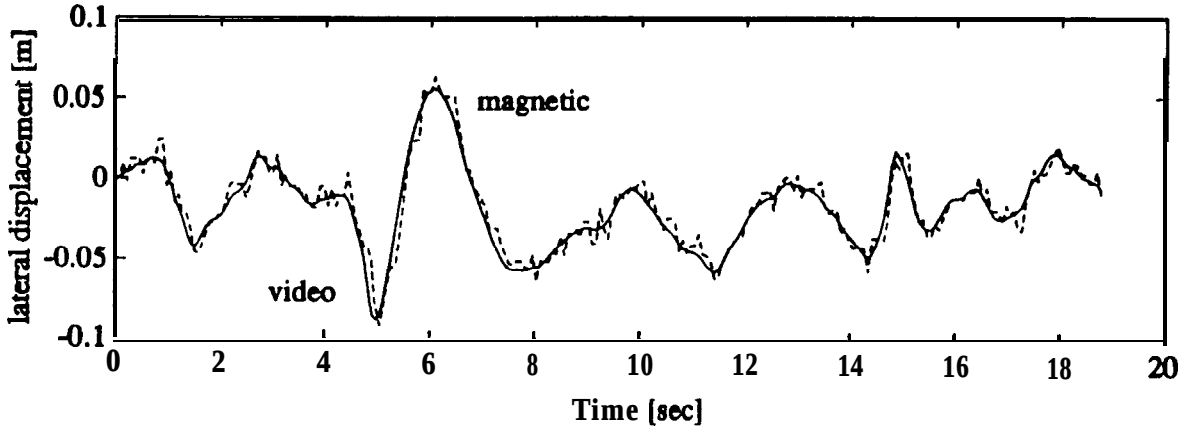

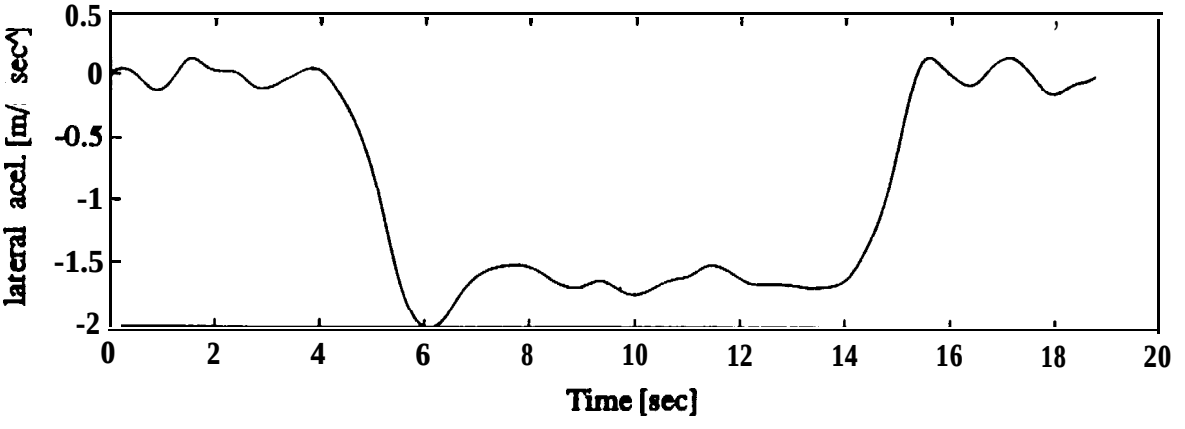

Figure 4.20 Reduced Tire Pressure (teet path #1) 40 km/hr - PID simulation

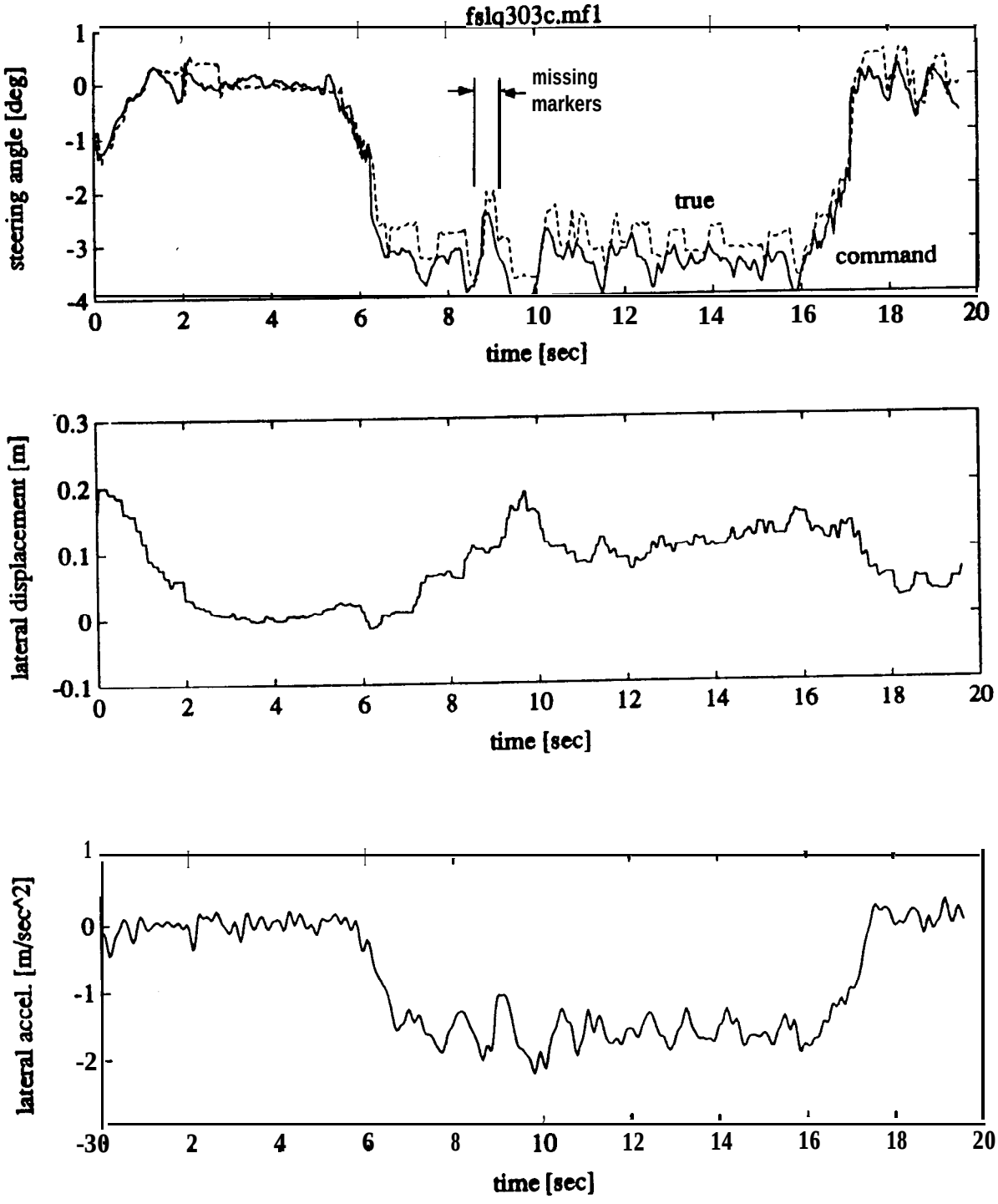

Figure 4.21 Missing Markers (test path #1) 40 km/hr - FSLQ test

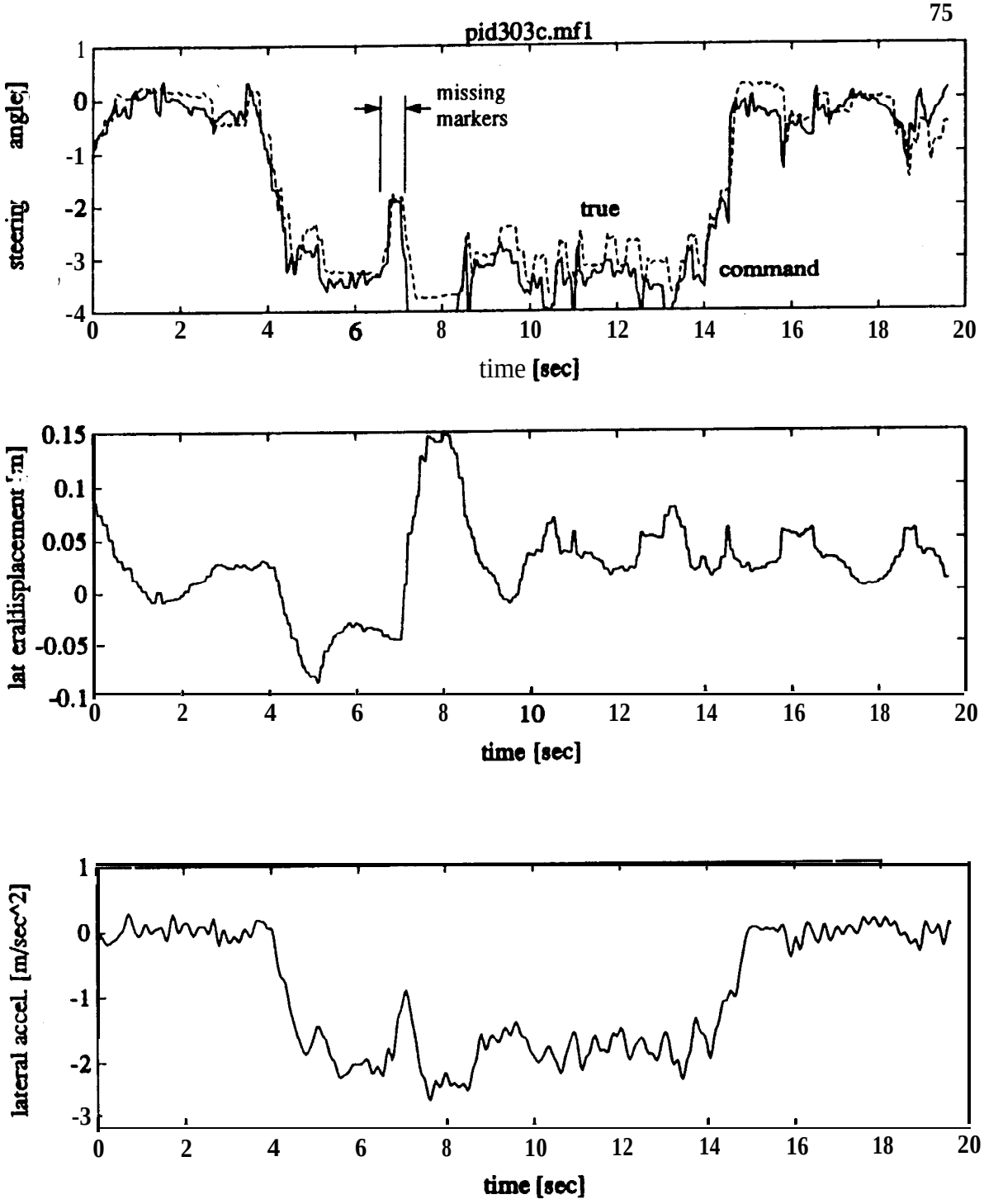

Figure 4.22 Missing Markers (teat path #1) 40 km/hr - PID test

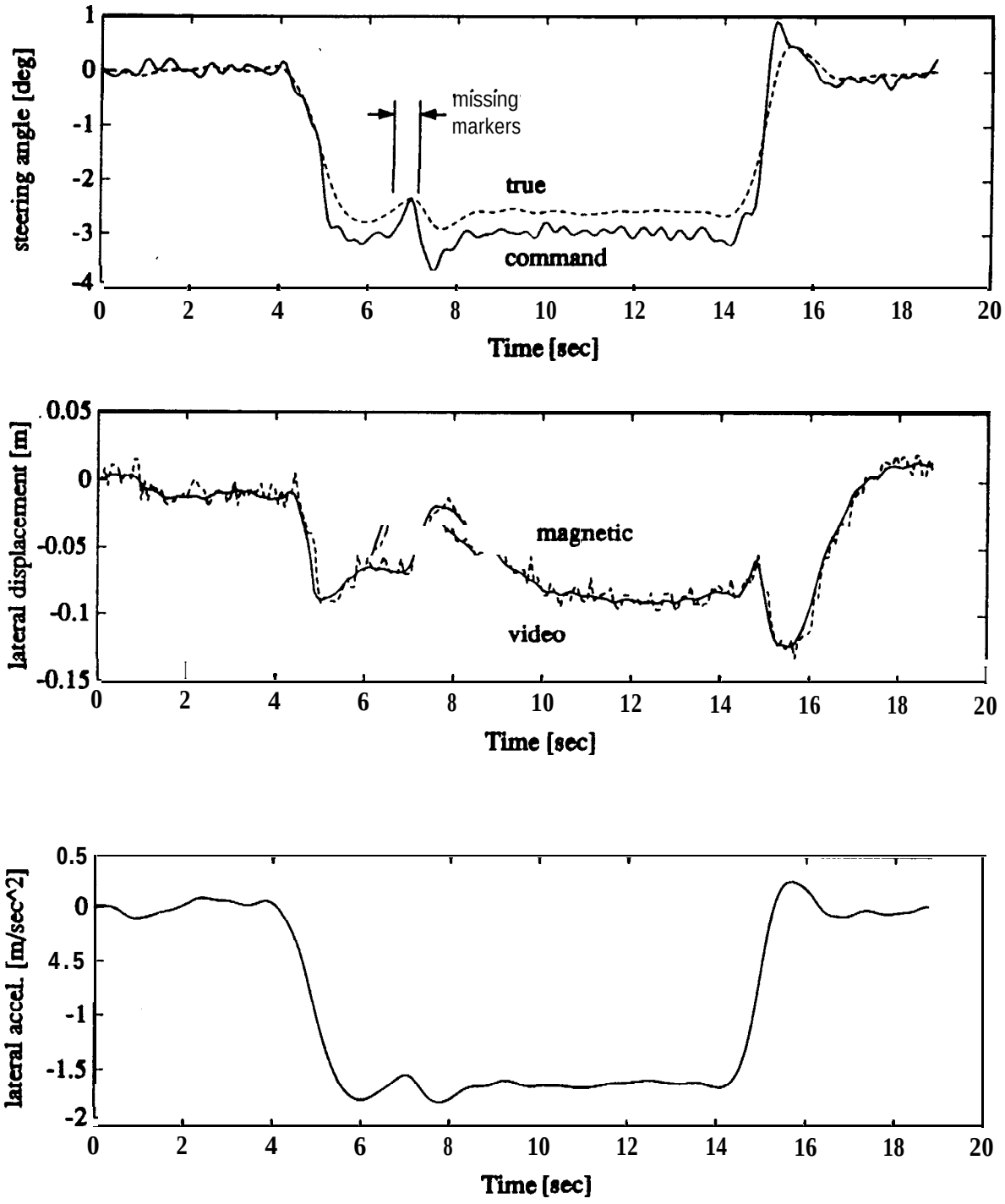

Figure 4.23 Missing Markers (test path #1) 40 km/hr - FSLQ simulation

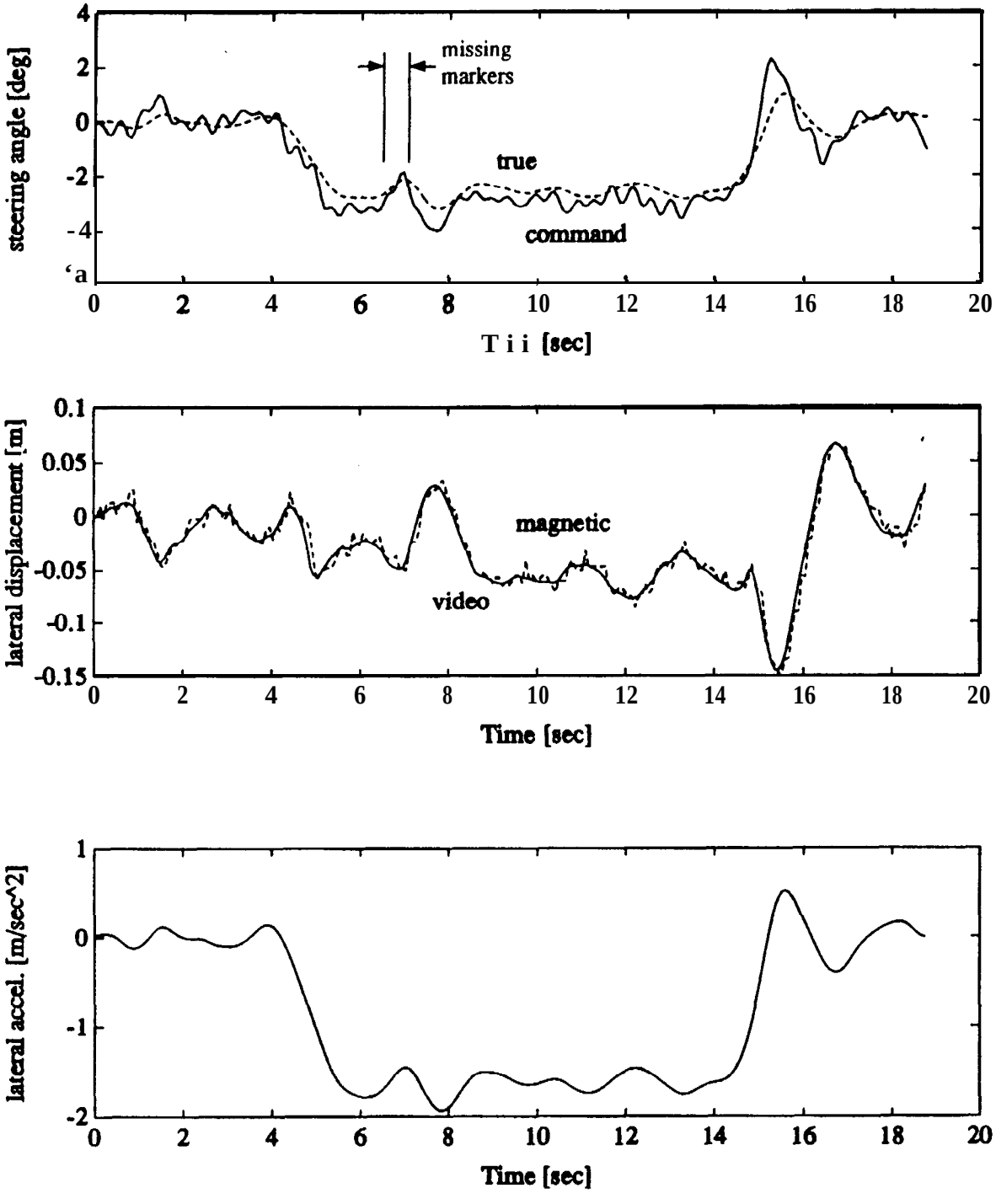

Figure 4.24 **Missing Markers (test path #1) 40 km/hr - PID simulation**

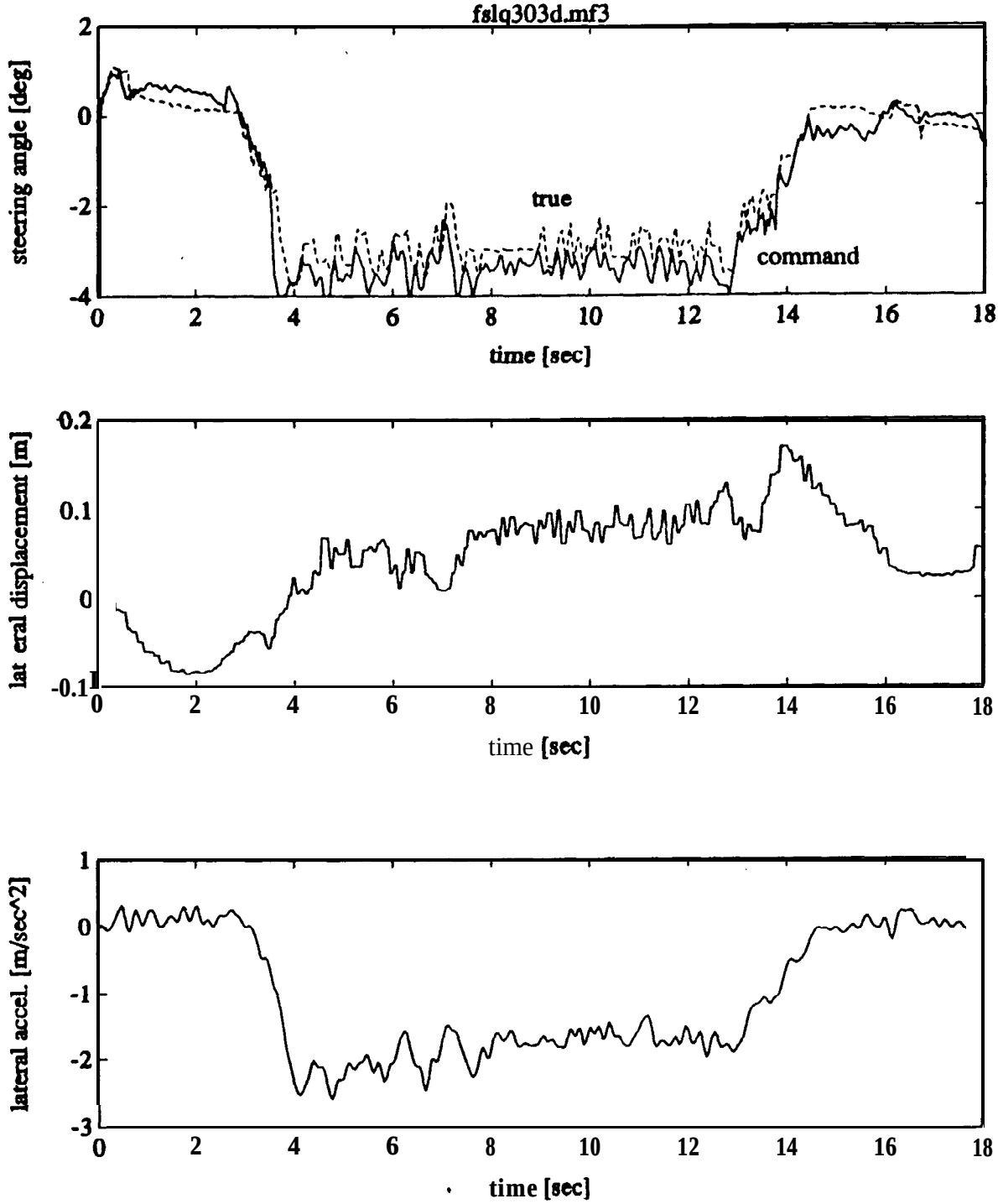

Figure 4.25 Perturbed Markers (test path #1) 40 km/hr - FSLQ test

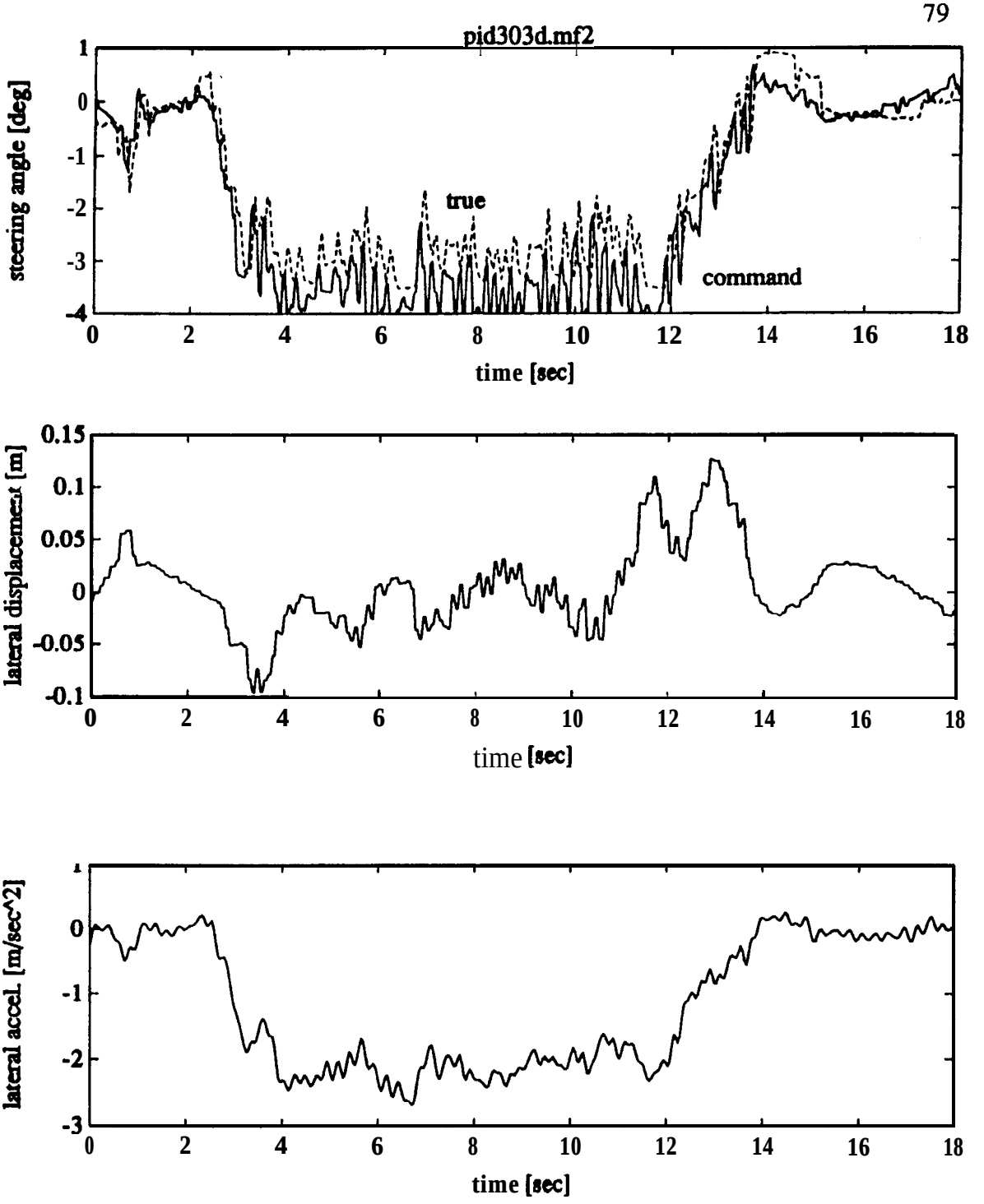

Figure 4.26 Perturbed Markers (test path #1) 40 km/hr - PID test

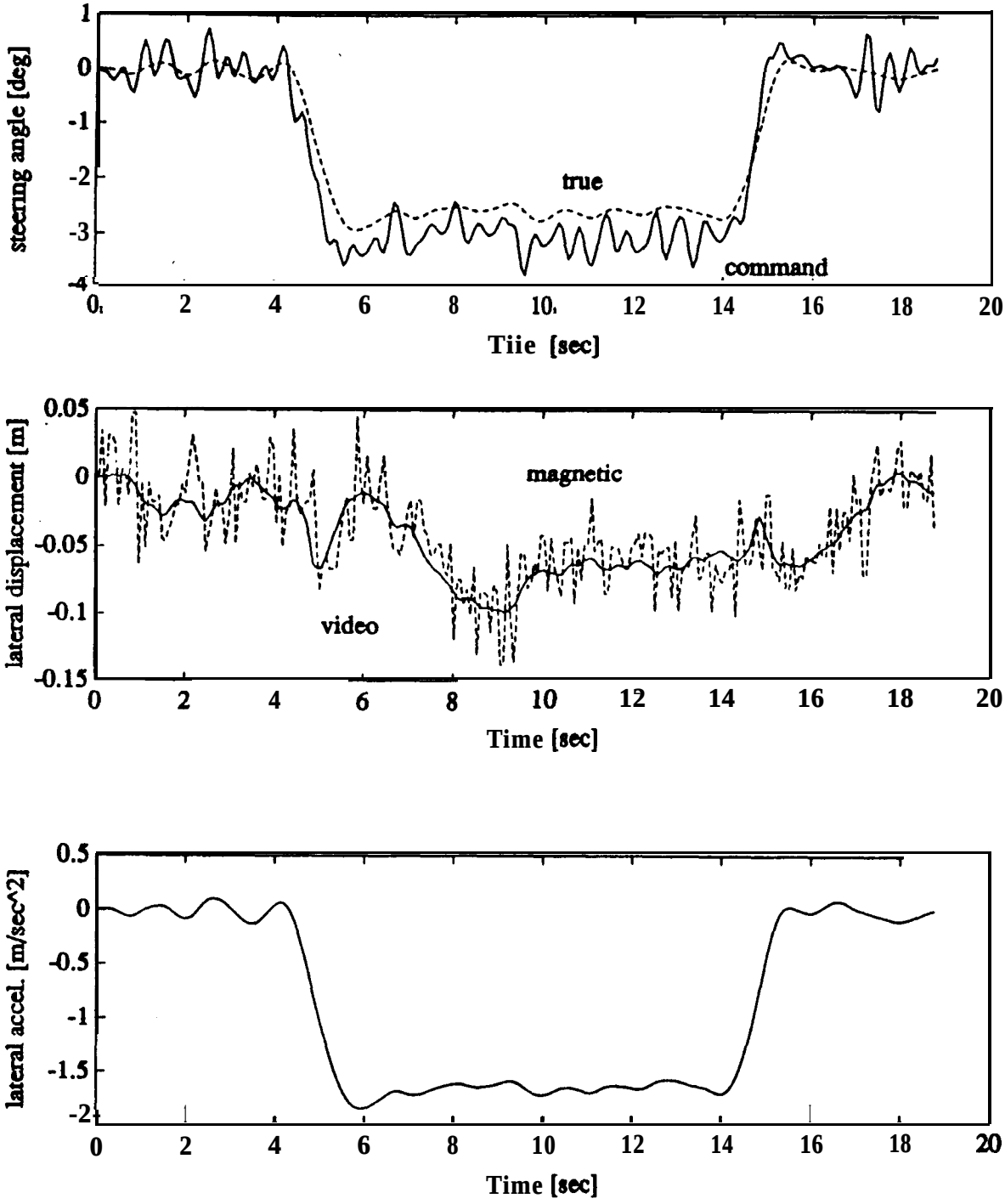

Figure 4.27 Perturbed Markers (test path #1) 40 km/hr - FSLQ simulation

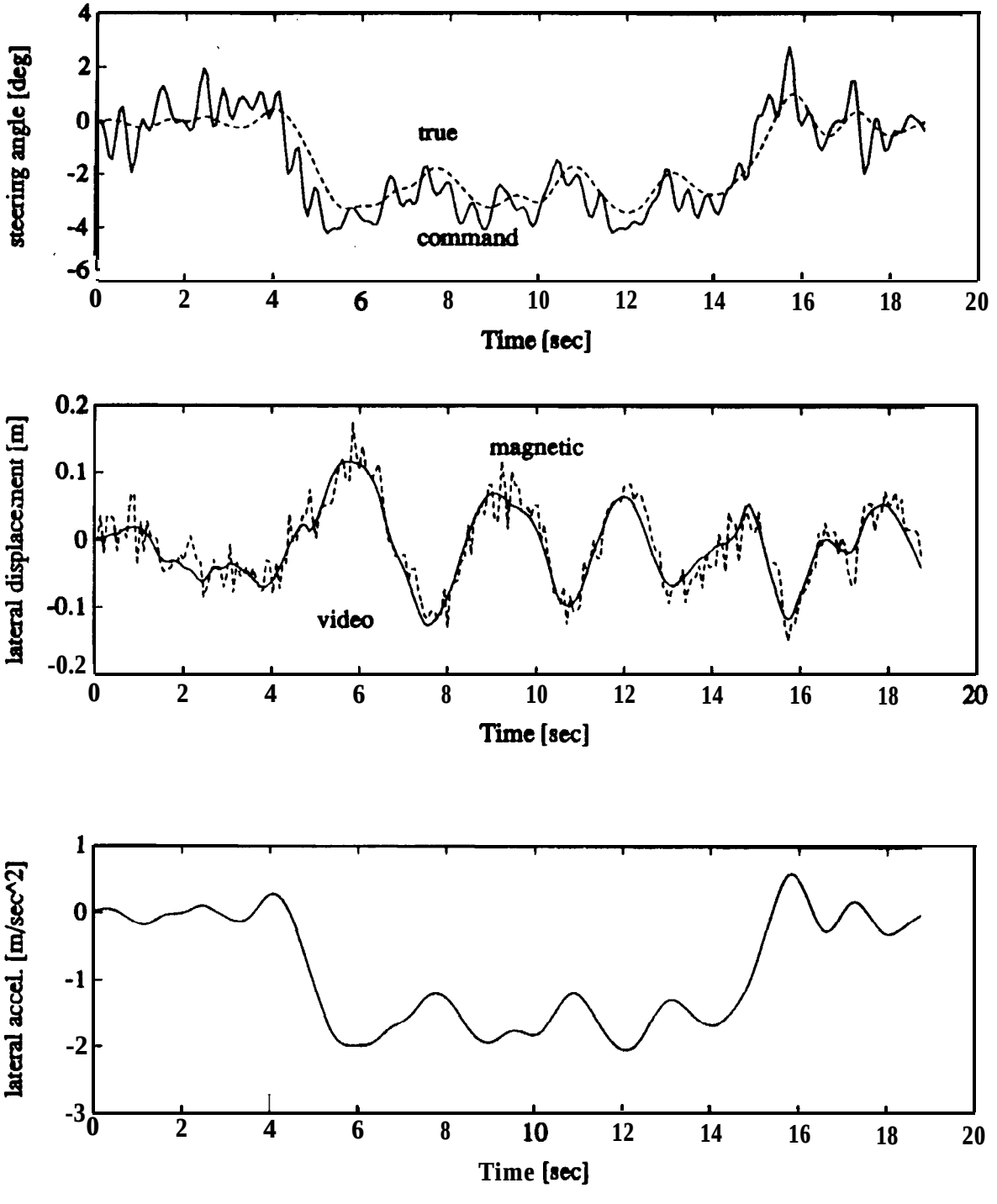

Figure 4.28 Perturbed Markers (test path #1) 40 km/hr - PID simulation

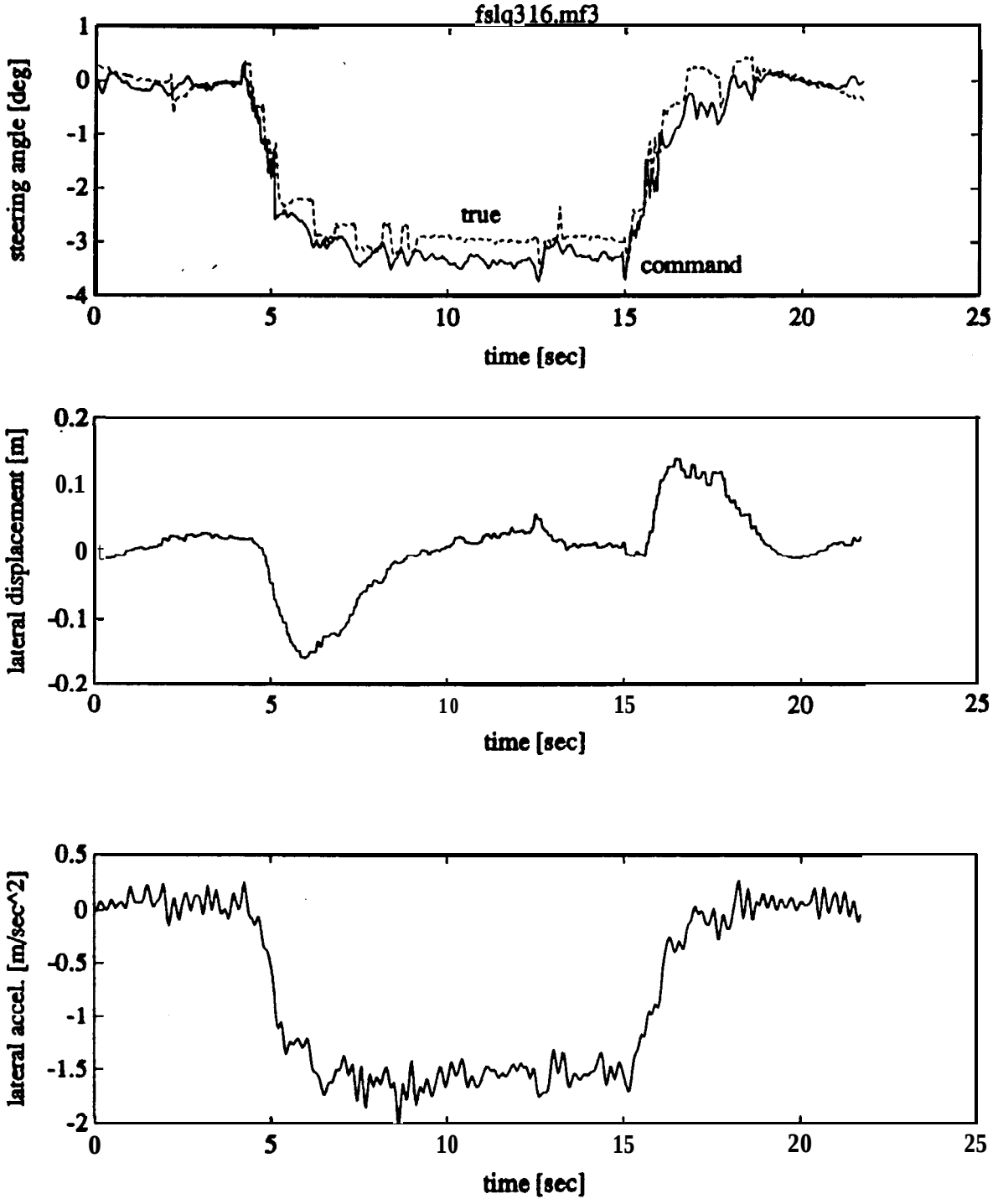

Figure 4.29 Slippery Road (test path #1) 40 km/hr - FSLQ test

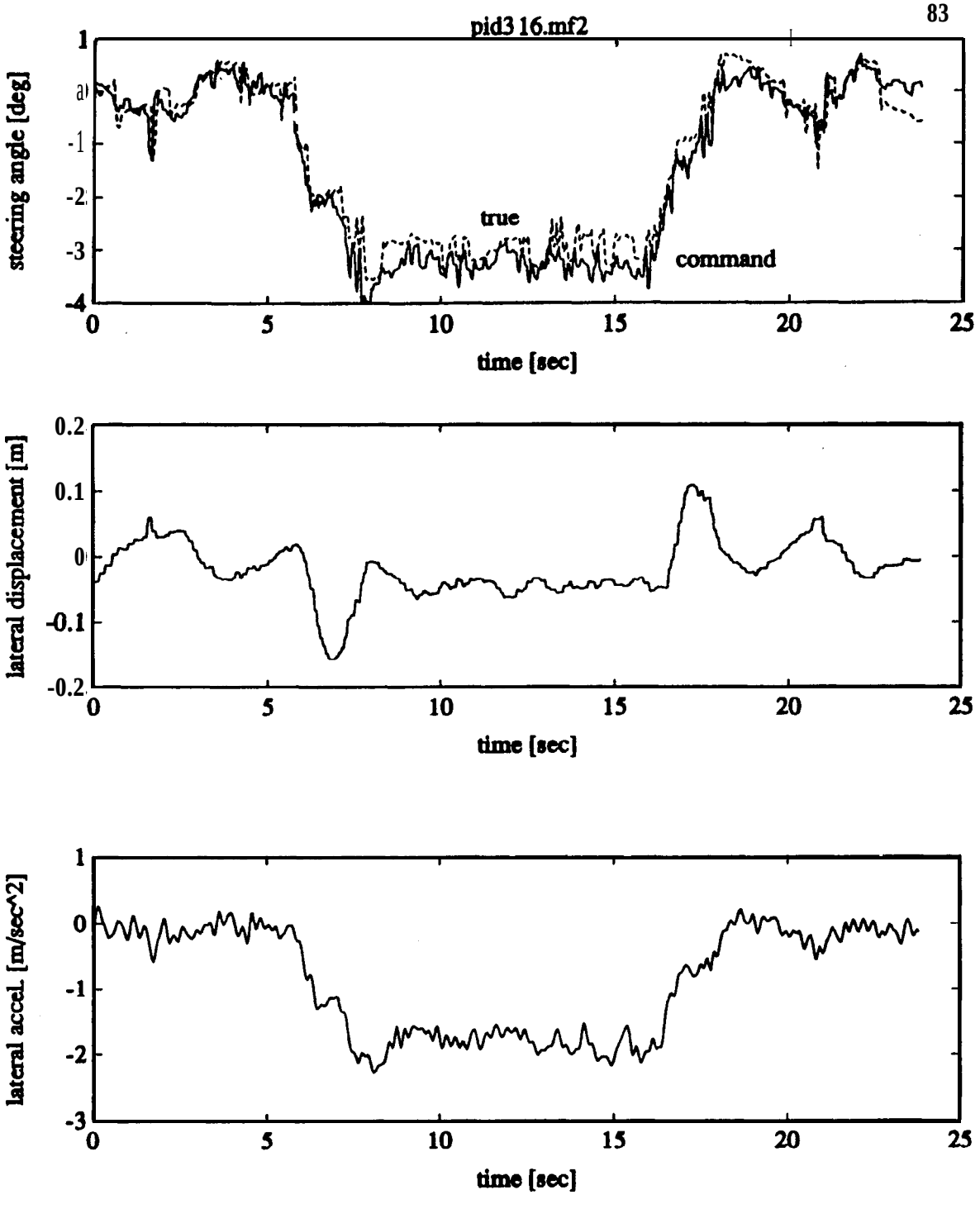

Figure 4.30 Slippery Road (test path #1) 40 km/hr - PID test

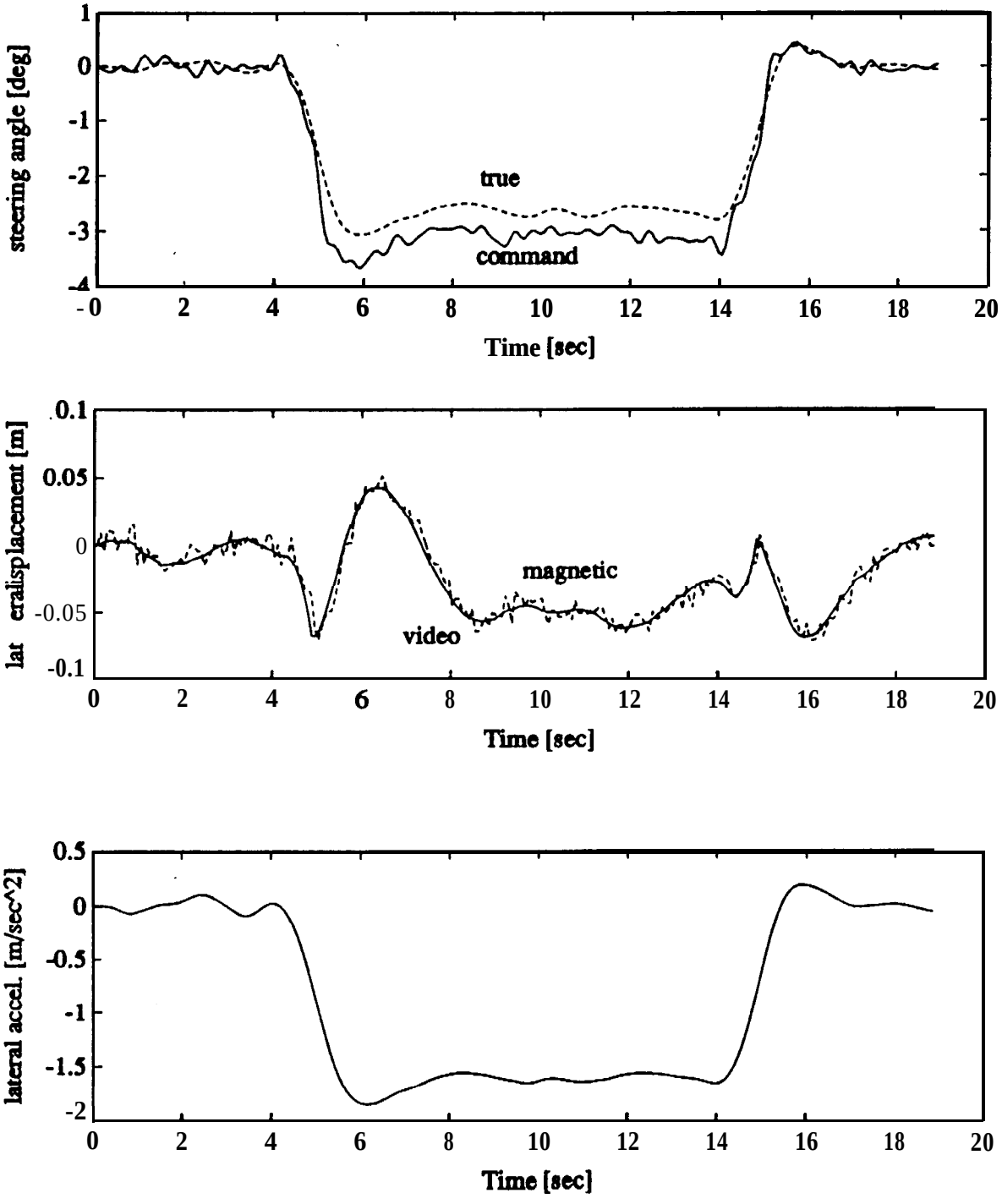

Figure 4.31 Slippery Road (test path #1) 40 km/hr - FSLQ eimulation

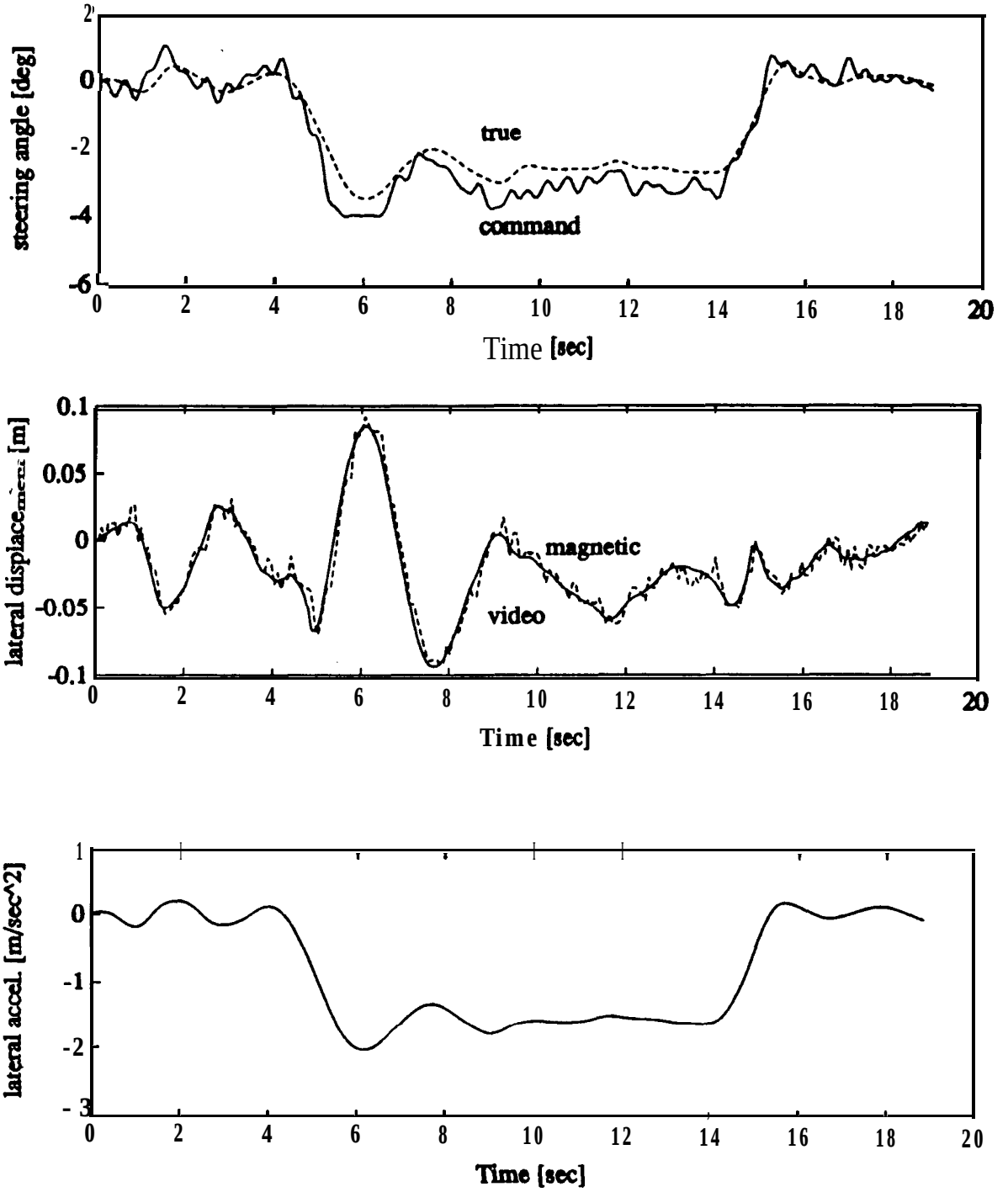

Figure 4.32 Slippery Road (test path #1) 40 km/hr - PID simulation

5. CONCLUSION

The PATH/IMRA project was based on in-depth investigations of vehicle lateral control technologies at both system and component levels. During the project, both open loop and closed loop experiments were conducted to evaluate the performance of the components and the integrated system. The following conclusions were made based on an extensive analysis of the test results.

1) The experimental results indicate that the PATH concept of a cooperative lateral control system using a discrete magnetic reference/sensing system can produce good control response. A system using this concept can acquire reliable and accurate vehicle state and road geometry information. By using the road geometry information, preview control logic can perform anticipatory steering maneuvers before curve sections, thus the maximum tracking error can be reduced and ride quality can be improved.

2) The experiments on the magnetic reference/sensing system indicate that the accuracy of the lateral measurement is good within the fine resolution region and adequate in the inferior resolution region. The system has been proven to be robust at different vehicle speeds up to 60 km/hr.

3) FSLQ and PID control tests results indicate that both control algorithms perform satisfactorily under the conditions tested. Comparing the two algorithms, it was concluded that the FSLQ control algorithm can provide better ride comfort than that achieved using the PID controller.

4) The steering actuator system with the series configuration was found to perform adequately under the conditions tested. The steering angle range of the actuator was a limitation, however the curve radii used in the tests were much smaller than would be found on an open highway, the intended target for the system.

5) The closed loop experiments show that the system performed satisfactorily under nominal and the tested non-ideal conditions at low vehicle speeds. The test vehicle can be controlled within ±20 cm on both straight and curved sections of test path #1 (with a radius of 74 m) at a speed of 50 km/hr. Tighter control was performed on the reverse curves in test path #2 at speeds up to 60 km/hr. Both test data and passenger

perception indicate that the ride quality was good even when the vehicle went through the 74 m radius curve at a speed of 50 km/hr.

6. RECOMMENDATIONS for FUTHER RESEARCH

Analysis of the conducted tests, test environments, and experimental results in this report also leads to the following recommendations:

1) Further experiments on the existing experimental system should be conducted in order to investigate the robustness of the system under other non-ideal conditions. Additional non-ideal conditions include: different road surface conditions, external forces such as wind gust, etc.

2) Several practicality issues regarding the magnetic reference/sensing system need to be investigated further. Interference effects related to metallic or magnetic materials close to the magnetic markers, rebar used in the construction of the road, and metallic bridge structures should be analyzed or tested. Enhanced signal processing for complicated maneuvers such as lane merging or diverging where more than one magnetic marker path appears within the sensing range needs to be investigated.

3) Other control algorithms which would provide more advanced features should be evaluated. In addition to tight tracking and good ride quality, these algorithms should not be sensitive to changes of vehicle parameters and tire/road conditions. A comprehensive safety logic should be included in the control algorithm in order to deal with emergency situations. As an advanced feature, learning or training functions would reduce the complexity of system tuning and allow the system to better adapt to different vehicles and environmental conditions.

As a specific recommendation, a fuzzy rule-based control algorithm can be investigated [26]. The central idea behind the use of a fuzzy rule-based controller is that it is a natural method of lateral control based on human-type decision making and learning. Different from the FSLQ and PID control algorithms, the fuzzy control algorithm is a highly non-linear controller which is designed based on the input and output relations of the plant. The advantages of such an algorithm include flexibility in the choice and utility of inputs and outputs, and on-line or off-line training capability. The intuitive nature of fuzzy inference rules not only allows the designer to make well justified control design decisions, but also allows the designer to incorporate an effective set of safety rules.

4) The tested actuator is designed for a driver assistance steering system. Based on the experimental results, specifications for an actuator for a fully automated lateral control system should be developed. The new actuator should be tested using a process similar to the one described in this report

‘5) As the system becomes more complex, the human’s role in the total system must be considered. Ultimately, the human may have a very minor role in the navigation and control of a vehicle. But prior to this final stage, the human driver will continue to be an important element and should be considered.

6) As a method of evaluating the performance of the lateral guidance system, it would be useful to determine how accurately a human driver can steer a vehicle.

In summary, further experimental study is needed in order to reach a comprehensive evaluation of the performance of the lateral control system tested. It is noteworthy to mention that alternative sensing, control and actuation technologies should also be evaluated, and selected technologies should be tested in order to determine the most promising system for vehicle lateral control.

REFERENCES

1. S. Shladover, et al, "Automatic Vehicle Control Developments in the PATH Program", ***IEEE Transactions on Vehicular Technology,*** Vol. 40, No. 1, February 1991, pp. 114-130.

2. R. Parsons, W-B. Zhang, "PATH Lateral Guidance System Requirements Definition", in ***Proceedings of First International Conference on Application of Advanced Technology in Transportation Engineering,*** ASCE, San Diego, CA, February 1990, pp. 275-280.

3. W-B. Zhang, R. Parsons, T. West, "An Intelligent Roadway Reference System for Vehicle Lateral Guidance/Control", in ***Proceedings of 1990 American Control Conference***, San Diego, California, May 1990, pp. 28 l-286.

4. H. Peng, M. Tomizuka, "Preview Control for Vehicle Lateral Guidance in Highway Automation", in ***Proceedings of 1991 American Control Conference,*** Boston, 1991, pp. 3090-3095.

5. T. Hessburg, H. Peng, M. Tomizuka, W. Zhang, E. Kamei, " An Experimental Study on Lateral Control of a Vehicle", in ***Proceedings of 1991 American Control Conference***, Boston, 199 1.

6. W-B. Zhang, et al, " A Full Scale Experimental Study of a Vehicle Lateral Control System", 71st TRB Annual Meeting, paper no. 920764, 1992.

7. H. Peng, et al, " A Theoretical and Experimental Study on Vehicle Lateral Control", to be presented at 1992 American Controls Conference.

8. A. Y. Lee, " A Preview Steering Autopilot Control Algorithm for Four-Wheel-Steering Passenger Vehicles," ***Advanced Automotive Technologies-1969,*** ASME, pp. 83-98.

9. Anonymous, ***Highway Design Manual,*** California Department of Transportation, fourth edition.

10. H. Sakai, "Theoretical and Experimental Studies on the Dynamical Properties of Tyres, Part 4: Investigations of the Influences of Running Conditions by Calculation and Experiment", ***Int. J. of Vehicle Design,*** Vol. 3, No. 3, 1982, pp. 333-375.

11. J. ***Y.*** Wong, ***Theory of Ground Vehicles,*** John Wiley & Sons, 1978.

12. N. Gupta, "Frequency-Shaped Cost Functionals: Extension of Linear-Quadratic-Gaussian Design Methods", ***J. of Guidance and Control,*** Vol 3, No. 6, Nov-Dee 1980, pp. 529-535.

13. B. D. 0. Anderson, J. B. Moore, ***Optimal Control -- Linear Quadratic Methods,*** Chapter 9, Prentice Hall, 1990.

14. H. Peng, M. Tomizuka, "Lateral Control of Front-Wheel-Steering Rubber-Tire Vehicles", Publication of PATH Project, ITS, UC Berkeley, UCB-ITS-PRR-90-5, July 1990.

15. D. G. Luenberger, "Observing the State of a Linear System", ***IEEE Trans. Mil. Electron.***, MIL-8, pp. 74-80, 1964.

16. M. G. Pottinger, "Tire Force and Moment in the Torqued State an Application of the Flat-Trac II Tire Testing Machine", Smithers Scientific Services, Inc.

17. E. Bakker, L. Nyborg, H. B. Pacejka, "Tyre Modelling for Use in Vehicle Dynamics Studies", SAE Technical paper 870421.

18. E. Bakker, H. B. Pacejka, L. Lidner, "A New Tire Model with an Application in Vehicle Dynamics Studies", SAE Technical paper 890087.

19. H. Sakai, "Theoretical and Experimental Studies on the Dynamical Properties of Tyres, Part 1: Review of Theories of Rubber Friction", ***International Journal of Vehicle Design,*** Vo1.2, No. 1, 1981, pp.78-110.

20. S. K. Clark, ***Mechanics of Pneumatic Tires,*** U.S. Government Printing Office, Washington, D.C. 20402, 1981.

21. H. Sakai, "Theoretical and Experimental Studies on the Dynamical Properties of Tyres, Part 4: Investigations of the Influences of Running Conditions by Calculation and Experiment", ***International Journal of Vehicle Design,*** Vo1.3, No. 3, 1982, pp.333-375.

22. P. F. Bohn, R. J. Keenan, "Improved Hybrid Computer Vehicle Handling Program", Applied Physics Laboratory, Johns Hopkins University, CP 049A, Oct., 1978.

23. B. Mitchell, R. Abrams, R. A. Scott, "Improvement of Mathematical Models for Simulation of Vehicle Handling", DOT HS-805-362 to DOT HS-805-368.

24. W. Rudin, ***Principles of Mathematical Analysis,*** McGraw-Hill, New York, 1976.

25. R. E. Bellman, ***Dynamic Programming,*** Princeton, Princeton University Press, 1957.

26. T. Hessburg, M. Tomizuka, "A Fuzzy Rule Based Controller for Automotive Vehicle Guidance", Fuzzy and Neural Systems, and Vehicle Applications '91, Japan, Nov. 1991.

APPENDIX

A. LIST of MEASUREMENT and COMPUTER EQUIPMENT

Lateral Control Computer

TMS320C30 DSP System Board	Spectrum	600-00545
32 channel Analog Input Board	Spectrum	600-00257
64kx32 RAM Upgrade	Spectrum	202-00189
Memory Expansion Board	spectrum	600-00906
Custom Signal Conditioning Board	Aisin Seiki	
Kontron IP Lite (PIC386DX-25MHz)	Kontron Electronics	
w/ 80387 math co-processor, 2MB RAM, 110MB HD		

Actuator Controller

Custom micro-computer	Aisin Seiki	

Sensors

Handheld Digital Magnetometer	MEDA	µMAG*
Angular Rate Sensor	Watson	ARS-C121-1A
Accelerometer	ICSensors	3110-001
Linear Potentiometer	cop al	JCL20
Rotary Potentiometer	cop al	Ml305
Smart Linear Sensor	Allen Bradley	2804-SLS2
w/ wide-angle, side-view lens 2804-NL2		
Power Inverter	Trace	612
Triple Output Power Supply	Hewlett-Packard	6236B

* The magnetometers have be customized to extend their range to +/- 3500 mGauss.

WA10 10:45

AN INTELLIGENT ROADWAY REFERENCE SYSTEM FOR VEHICLE LATERAL GUIDANCE/CONTROL

Wei-bin Zhang and Robert E. Parsons

Institute of Transportation Studies
University of California, Berkeley, CA 94720

Thomas west

California Department of Transportation
Sacramento, CA 94274-0001

ABSTRACT

An Intelligent Vehicle/Highway System (IVHS) may require a multifunctional roadway reference system. This roadway reference system should help the vehicle locate its lateral and longitudinal position, and provide other information required for vehicle control. This reference system is defined as an Intelligent Roadway Reference System (IRRS).

The California Program on Advanced Technology for the Highway (PATH) is developing an IRRS, consisting of roadway reference and vehicle sensing elements which can transmit necessary information for vehicle lateral guidance/control. The reference system, passive discrete markers that may code one or more bits of informatlon, is installed in the center of the traffic lane. An on-board sensing system acquires the informarion when the vehicle passes over the reference and determines the vehicle deviation and the upcoming road geometry. This sensing/reference system may also provide information for other IVHS functions.

1. Introduction

In order to develop an automated lateral control system, the roadway reference system is vital since it must provide the necessary information to the steering control mechanism for smooth and reliable maneuverlng. In studies conducted by the Program on Advanced Technology for the Highway (PATH), the sensing/reference system for vehicle lateral control has been researched intensively. This paper presents a concept for one possible roadway reference system designed for vehicle lateral control/guidance and its corresponding sensing and processing techniques.

In the past two decades, many efforts have been conducted to Investigate roadway or roadside reference systems for vehicular lateral control. Several systems have already been either developed or simulated. The baste operating principle for most existing systems is to acquire the vehicle's lateral deviation relative to the center of the traffic lane or roadside reference [1]-[3]. Technologies that have been investigated for this particular application include electromagnetic, magnetic, optical, radar, acoustic and video sensing techniques. Simulations or field tests have demonstrated that most systems using these techniques can obtain relatlvely accurate information for determining a vehicle's deviation. However recent studies have revealed that a lateral control system which uses only the vehicle's deviation information can only track the reference in a compensatory mode. Even approaches such as Kalman filtering are not adequate for predicting the future road geometry in a situation when the radius of the road curvature changes.

An assessment of vehicle lateral control technologies has indicated [3] that the sensing/reference system for automatic steering should possess an anticipatory capability for acquiring pertinent Ipformation on upcoming road geometry as well as the vehicle's lateral deviation and yaw angle (or yaw rate) in order to enable the lateral control system to smoothly guide the vehicle along the prescribed course. Once the vehicle lateral controller obtains the upcoming road geometry Information, It Is able to precalculate the steering response necessary to smoothly negotiate the upcoming curve, hence resulting in art anticipatory rather than compensatory maneuvering of the vehicle. Recent simulation results have shown that the tracking performance of a lateral control system Is improved when applying this concept (4). These studies suggest that a dual (or multl) functional sensing/reference system for vehicle lateral control (which can collect both the vehicle state information and road geometry information) should be developed.

PATH studies indicate the various approaches that might be applied for acquiring this information:

- A "smart" on-board sensing system that can objectively (or directly) 'perceive' the road geometry and the vehicle's state -- a 'direct sensing approach';

- An on-board sensing system that can "read" both the vehicle's state and road information by means of (or indirectly from) a specially designed roadway or roadside information system -- an "indirect sensing approach';

- A combination of the above two approaches.

The direct sensing approach is, functionally, very close to the human perception of the roadrvdy. A typical technique under investigation for this purpose is video sensing which utilizes video camera(s) to sense the image of the upco nin; road, frame by frame. The data is then processed nnd analyzed using an image processing technique. In the case of direct sensing, the sensing device or: the vehicle has to be intelligent in order to acquire and process adequate information in real time.

In the indirect sensing approach, road geometry information is abstracted by several characteristic parameters and then stored in a roadwny o: roadside information system. Both the vehicle state and road information can be interrogated via on-vehicle sensors or communication tools.

Advantages of the direct sensing approach are fairly obvious, since this system essentially replicates human driving perception. Theoretically, this system not only perceives upcoming road geometry, but detects objects in front of the vehicle. This would offer possibilities for a common sensing system for both lateral and longitudinal control. The disadvantage however is the extensive processing needed for extraction of the necessary information. Computer and image processing techniques have demonstrated some limitations in accessing the 3-D images in real time using a practical size computer. In addition, these techniques have not satisfactorily solved the problems of distortion related to shadows, weather and road conditions.

The indirect sensing approach provides a rarher easy means of acquiring the required road information as well as vehicle lateral position. Technically, the interrogation of roadway or roadside references for stored information is straightforward: only limited information is transmitted to the vehicle, thus the amount of data to be processed is minimized. Therefore, both the on-board sensors and roadway reference system can be reasonably simple and economical for large scale application.

After a review of existing lateral control technologies, PATH has proposed an Intelligent Roadway Reference system (IRRS), which would possess the necessary functions for providing the vehicle state and road geometry information, as well as potentially useful information which can be applied to other Intelligent Vehicle Highway System (IVHS) functions.

2. An IRRS Using Magnetic Discrete Markers

In order for the IRRS to provide lateral position measurements and road geometry information, the reference system will have to either create signals detectable by the on-board sensor or reflect a signal transmitted by an on-vehicle transmitter to the (on-board) sensor. In either case, the signal processor would then process the signals to extract the information.

A revtew of existing lateral control systems has suggested that a discrete reference system seems to be more appealing for information storage and transmitting. A discrete reference system consists of a series of discrete markers placed in the center of the traffic lane in order to define the desired path. Information would he coded in each marker. As the vehicle passes over the discrete markers, the on-beard sensor(s) can acquire both the road geometry information and the lateral deviation of the vehicle. It has been recognized that both the vehicle-borne equipment and the roadway installation for the discrete marker system might be significantly cheaper and easier to install than alternate technologies. As an important feature of the system, the discrete markers can be incorporated into existing highways without changing the present infrastructure. The system offers great flexibility: damage to a single marker may not influence the overall system, but only the immediate affected location. In addition, temporary markers could be easily installed to detour traffic around construction or maintenance zones or even accident areas [5].

The discrete marker system might be accomplished by means of optical sensing, magnetic sensing or other approaches capable of providing more information. Among these approaches, magnetic sensing appears to have some potential advantages. Although permanent magnetic markers are passive devices, they create magnetic fields. The magnetic field appears to be less influenced by environmental conditions than other reference systems. The life cycle of permanent magnets is several decades (which is comparable to the life cycle of highways), and they should not need any maintenance.

The vehicle-borne equipment for acquiring information from the IRRS using magnetic discrete markers is composed of a sensor(s), a computer, and an interface that links sensor to the computer. The schematic of an IRRS using discrete markers is given in Fig. 1. The current PATH research is focusing on the feasibility of an IRRS using magnetic markers for achieving reliable lateral position measurements and road geometry information transmission and acquisition.

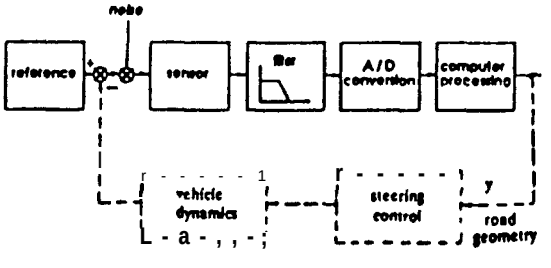

Figure 1. The system schematic

3. Information Processing for Vehicle Lateral Position Measurements

One sensing technique developed for acquiring signals from magnetic markers utilizes loop sensors [6]. However, it has been discovered that the amplitude of the sensed signal is proportional to the vehicle's speed, and trends to zero when the speed is very low. This causes problems in the signal processing. The sensing devices applied in our research are magnetometer-type sensors, which can acquire signals even at zero vehicle speed.

A substantial effort has been made to investigate approaches to overcome several interference problems in the lateral position measurement. The interference includes: the overlapping with the earth's magnetic field, high frequency magnetic noise generated by the vehicle engine system, and spontaneous vertical movements of the vehicle. The problem posed by the earth's field can be eliminated by measuring the magnetic field of the markers (defined as M-field) relative to the size of the earth's field. The vehicle magnetic noise can be reduced through a filtering process which incorporates a low-pass filter. Analysis shows that the vehicle vertical movements present the most critical issue. Fig. 2 shows the vertical component of the M-field measured from heights of 10cm to 30 cm. One can see that the M-field is very sensitive to the vertical displacement of the sensor. Studies have been conducted to develop an algorithm to overcome this problem.

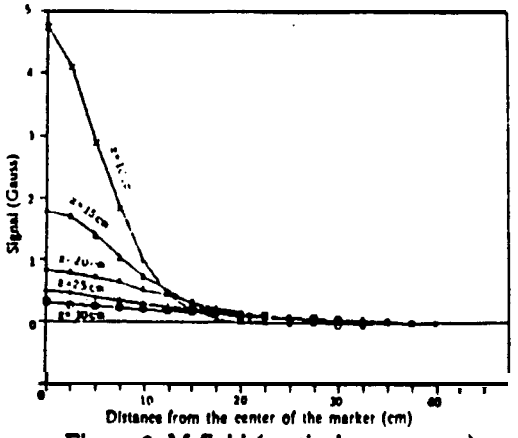

Figure 2. M-field (vertical component) measured with different sensor height

Lateral position measurements, y, using the M-field can be accomplished by deriving the relationship between the vehicle deviation and the magnetic field strength B, defined as

$$\gamma = f(B) \qquad (1)$$

Efforts have been conducted to mathematically describe the M-field using the theory of magnetic fields. Several models have been developed. The simplest approach is to refer to a magnetic marker as a magnetic dipole, then the M-field B at an observation point P(x, y, z) is

$$B = \frac{\mu M}{4\pi r^5}(3xz\,a_x + 3yz\,a_y + (2z^2 - x^2 - y^2)a_z) \qquad (2)$$

where $r = \sqrt{x^2+y^2+z^2}$
μ is the permeability of free space
M is the magnetic moment

Equation (2) represents the M-field by its three components, B_x, B_y, B_z, therefore, the Equation can be expressed as

$$B = (B_x, B_y, B_z) \qquad (3)$$

where B_x and B_y are oriented tangent to and normal to the road center line respectively, while B_z is perpendicular to the road surface. Analysis has been focusing on the M-field at x = 0, where only two nonzero components exist, defined as the horizontal component $B_h(y, z) = B_y(0, y, z)$ and vertical component $B_v(y, z) = B_z(0, y, z)$. Let $s = B|_{x=0}$, then the M-field strength at x = 0 is

$$s = (B_h(y, z), B_v(y, z)) \qquad (4)$$

and expression (1) can be rewritten as

$$\gamma = f(s) \qquad (5)$$

Fig. 3 gives both the test data and the analytical predictions of the magnetic field components. It was found that the analysis result has slight deviations from the test data. These deviations would cause errors if the vehicle position processing were dependent on (2). Furthermore, a study has shown that major simplifications should be introduced to derive a relationship between y and s, where y is specified not to relate to the height of the sensor, but the simplification could result in significant errors.

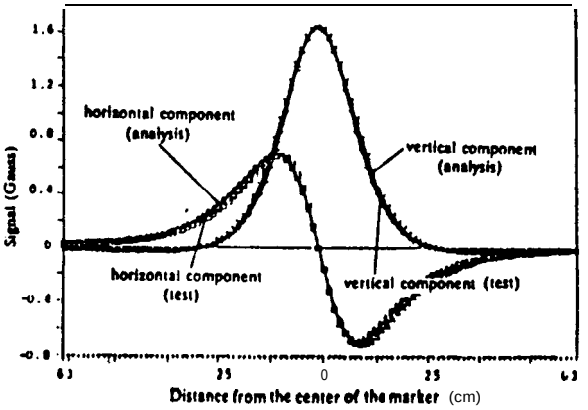

Figure 3. Analytical and empirical results of the M-field

In order to derive (5), the properties of an input-output relationship of the function f are analyzed. Let S be a

signal set, $S=\{s \mid s=(B_h(y,z), B_v(y,z))\}$, and Y be a deviation sef $Y=\{y \mid (-y_{max}<y<y_{max})\}$. The function f can be interpreted 8s a rule which specifies a deviation y for each signal element s, that is, f maps $s \in S$ to a corresponding deviation $y \in Y$, written as

$$f: \quad S \rightarrow Y \qquad (6)$$

The mapping relationship *given* in (6) implies that any signal measurement s must have a unique deviation value $y \in Y$. *A* sensor that is located in the M-field, when $x=0$ and $y=y_i$, 'will require only one signal measurement $s_i=f(y_i)$ $(s_i \in S)$. However, the signal s_i my not be unique because of variations in the vertical displacement of the vehicle, which cause the sensor height to change. These variations in s are bounded *because of tbe* limits of the vehicle suspension travel, therefore the signal s is within a certain range. If a signal subset S_i c S could be defined, which includes all the possible signal measurements $s_i \in S_i$, then a map f_i could be given as

$$f_i: \text{ if } s_i \in S_i \text{ then } y = y_i$$

The function f_i denotes the transformation from s_i to y_i. Fig. 4 illustrates this mapping relationship from $s_i \in S_i$ to $y_i \in Y$. If the vehicle deviation value is digitized as $y=\{y_1, y_2, \ldots y_n \mid y_1=-y_{max}, y_n=y_{max}\}$, function f can be specified by a set of rules $f=\{f_i\}$. Clearly, this approach provides an alternative algorithm for solving the problem by defining the signal subsets St.

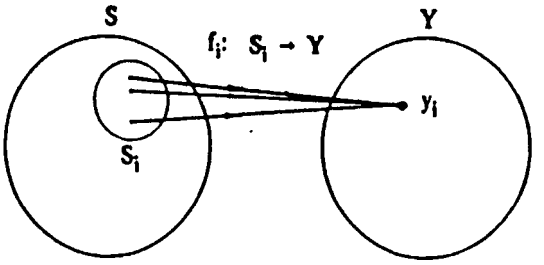

Figure 4. Tbe function f_i maps a signal subset St of S to a deviation y_i of Y

The signal subset S_i can be specified by defining the domain of the subset. Suppose that a plane specified by $B_h(yi, z)$ and $B_v(y_i, z)$ exists, then all the signal measurements s_i will constitute a curve on the plane when the height of the sensor varies from 8 cm to 20 cm (the allowable vertical displacement), This curve is called the 8 curve and is given by

$$B_v(y_i, z) = g(B_h(y_i, z)) \qquad (7)$$

An optimal fit of the s curve can be found by a regression of samples of the measurements which gives

$$\hat{B}_v = g'(a_1, a_2 \ldots a_k; B_h)$$

Conveniently, the s curve has very good linearity (Fig.5 gives several s curves in the B_h-B_v plane). Thus, S_i can be defined as

$$S_i=\{s_i \mid s_i \text{ is defined by } \hat{B}_v(y_i, z) = a; B_h(y_i, z) + b_i\}$$

where a_i and b_i can be calculated directly from the empirical data by regression.

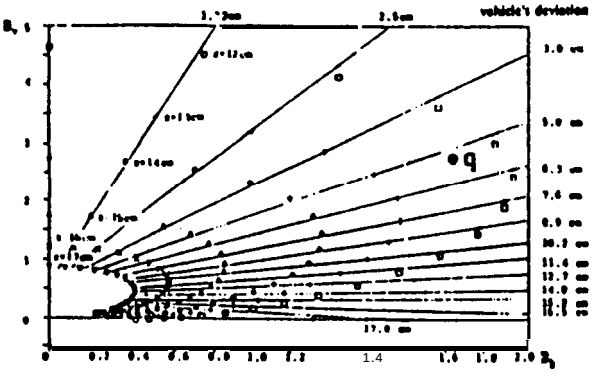

Figure 5. Transfer relationship for M-field/deviation conversion

After obtaining the signal subsets, a set of rules (f_i }, which cover the complete sensing range, can be defined. The rule f_i is rewritten as

$$f_i: \quad \text{when } B_h = B_{hi}, \text{ if } \hat{B}_{vi+1} < B_v < \hat{B}_{vi} \text{ then } y_{i+1} < y < y_i \; (i=1,2,\ldots n) \qquad (8)$$

By applying these rules, an algorithm can be constructed which finds each acquired signal s_i its belonging subset S_i, and then transforms it to a lateral deviation value. For instance, when $s=(B_{hq}, B_{vq})$ is acquired, based on B_{hq} the algorithm calculates $\hat{B}_v(y_i, z)$ sequentially from $i=1$ until a result $\hat{B}_v(5cm,z) < B_{vq} < \hat{B}_v(6.3cm,z)$ is reached. This indicates that the vehicle's deviation is in a range between 5 cm and 6.3 cm. A more detailed estimate can be obtained by interpolation.

In field tests, a series of 2.5 cm diameter and 10 cm long ceramic magnetic bars were buried vertically in the center of the test track. Each magnetic bar provides a 20 cm radius M-field (measured at 12 cm above the road surface). Both simulations and full-scale tests demonstrated that the algorithm is able to reliably read the vehicle deviation independent of variations in the sensor height. The accuracy of the reading is adequate, and the speed of the data processing is extremely fast, such that no problems were encounted in tests at speeds up to 135 km/h (85 mph). Fig. 6 illustrates a test result using the above described algorithm. In the Figure 6, (a) shows both the vertical and horizontal components acquired by the sensor from the test track, and (b) gives the vehicle lateral deviation information calculated using equation (8).

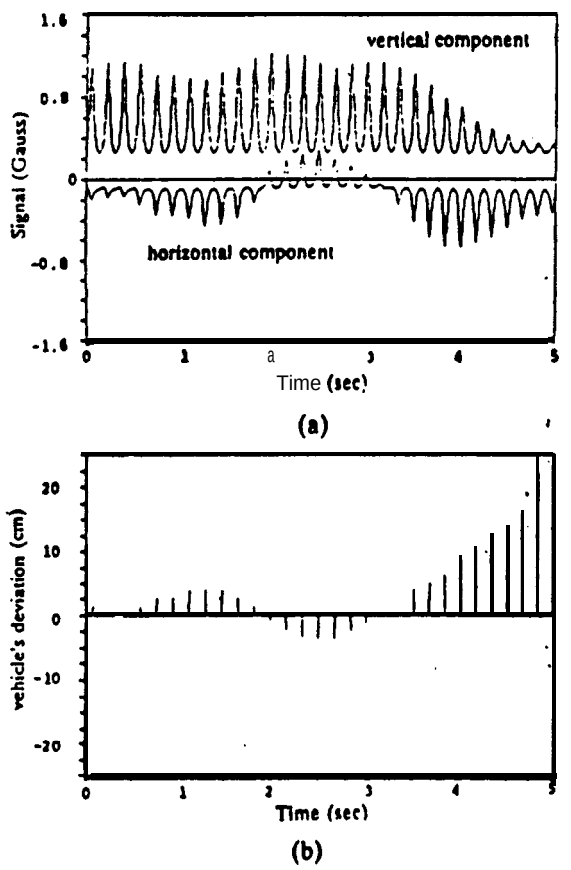

Figure 6. Input/output of the discrete sensing/reference system

4. Road Geometry Information Transmission and Acquisition

The road geometry information required for a preview lateral control system includes characteristics of both horizontal and vertical curves, with the emphasis on the former. The horizontal curves may be composed of both circular curves and spiral sections.

Generally, road curves can be represented by several characteristic parameters. A circular curve is characterized by its radius of curvature, while a spiral curve can be specified by a "transition parameter" which gives the relationship between the radius of curvature and the distance into the spiral section. Several parameters such as the length, direction and superelevation of the curvature are applied to all types *of* horizontal curves.

In the IRRS, the characteristic parameters of the road curves are coded in a binary system, using a series of magnetic markers. The natural magnetic poles are used to represent the two different binary codes (0, 1). By strategically alternating the magnetic poles successively, the road geometry information can be stored in the reference system. A vehicle that passes over the IRRS is able to predict the upcoming curve by collecting the curvature information through the electro-magnetic sensing system while at the same time acquiring the vehicle's lateral position relative to the marker's position at the lane center. Since the curvature information is given directly by the characteristic parameters, the information processing is much simpler than it would be for a vision system. The reliability of the information can be controlled by using error checking or correction codes, and multiple repetitions of the information.

The amount *of* information provided by the IRRS depends on the required precision of the information. For example, 8 bits *of* information can represent 1275 meters radius if the precision is 5 meters, while representing only 255 meters radius for 1 meter precision. Given the precision E, the capacity of the information for k magnetic markers is:

$$I(k) = 2^k \bullet E$$

Assuming that the road geometry Information includes two pieces of data with required magnitudes I, and I, and standard errors Et and E_2, preceded by m_h bits of header codes and m_c blts of correction codes, the number of bits (or discrete markers) needed for representing this information is

$$M_\Sigma = m_h + m_c + \sum_{i=1}^{k} \log_2\left(\frac{I_i}{E_i}\right) \qquad (9)$$

Equation (9) can be used to determine the longitudinal space needed for transmitting road geometry information by

$$D = d \cdot (M_\Sigma - 1)$$

where d is the distance between magnetic markers.

The required precision for different road information may vary. In comparision to the lateral deviation acquisition, the lateral control system will not (in a general sense) require very precise road geometry information because the lateral controller will possess both preview and feedback control functions. Possible minor errors generated by the preview control procedure, which is based on relatively imprecise road geometry information, can be corrected by feedback control laws. However, studies indicate that even if a very strict error requirement is given, road geometry information can stiH be stored in a reasonable amount of binary code. As a case example, for the curve at station 200 (radius 1097 meters, length 709 meters) on Interstate 280 In San Francisco, less than 50 bits of binary code are required if the desired precisions for both radius and length are 1 meter, where 11 bits are used for representing radius, 10 bits are used for representing length and 25 bits are applied for headers and correction codes. If the spacing between markers is 1 meter, less than SO meters are needed to transmit this road information. This implies that the sensing system on the vehicle is able to acquire this road geometry

message in less than 2 seconds at a speed of 90km/h.

The algorithm for data acquisition and processing of road geometry information must recognize an J store the binary codes provided by the N/S poles of the magnetic markers, and then translate them into the road geometry information This algorithm appears to be simple, however major efforts have to be conducted to develop a standard format in order to simplify the representation of road geometry Information and to design a proper checking or correction coding scheme for Improving the reliability of this information system.

5. Concluding Remarks

In recent PATH studies on lateral 'control/guidance systems, the concept of the IRRS has been developed. A practical algorithm for deriving vehicle lateral deviation measurements from the M-field of buried permanent magnets has been designed and tested. The approaches for preview road Information transmission are currently under investigation. Experiments were conducted to look into the effectiveness of the IRRS, showing that environmental conditions (e.g. water, ice, snow. etc.) have minimal interference on the system. The simplicity, low maintenance, low cost, all weather capability and expected reliability of the IRRS indicate that this system offers potential advantages in real world application.

We have also explored the possibility for IRRS functional expansions. Initial studies indicate that an IRRS possesses the capabilities for storing information such as absolute longitudinal vehicle position, lane recognition, speed limit, traffic sign information, etc.. The vehicle sensing system will also be able to acquire information regarding a vehicle's speed through the IRRS. The information provided by the IRRS will be beneficial for most of the functions of IVHS. For example, the road geometry and vehicle speed information can improve the performance of longitudinal control. Through the assistance of a communication link, the lane recognition information will enable the lateral control system to accomplish more complex maneuvers such as changing lanes, or merging onto or diverging from the highway. The vehicle speed, longitudinal position and lane recognition information will also be key inputs for navigation or motorist information system and for the central traffic control system. Therefore, an IRRS could be a single multi-functional roadway reference system for IVHS.

PATH researchers are currently conducting further in-depth studies on IRRS using discrete magnetic markers to investigate an approach for representing road geometry information. These studies will attempt to design the information coding and decoding protocol which would provide adequate efficiency and reliability. Issues related to the reliability and safety of the IRRS system are also under investigation.

Acknowledgment

The research reported herein is a part of the Program on Advanced Technology for the Highway (PATH), prepared under the sponsorship of the State of California, Business, Transportation and Housing Agency, Deprrtmcnt of Transportation, and the U.S. Department of Transportation, Federal Highway Adm nistration. The authors also wish to thank Dr. Steven Shladover who helped rev ise this paper.

Reference

[1] B. M. Dobrotin, "Fully Automated Urban Traffic System", Report DOT-TST-78-3, pp.A1-A20,1977

(2) R. Fenton, 'Technology for Individual Vehicle Control", Proceedings of Technology Options for Highway Transportation Operation, UCB & CALTRANS, Berkeley, UCB-ITS-P-87-1, Oct. 1986

[3] R. Parsons, W-B. Zhang, "Program on Advanced Technology for the Highway - Lateral Guidance System Requirements Definition", ASCE 1st International Conference on Applications of Advanced Technologies in Transportation Engineering, San Diego, pp.257-280, Feb. 1989

[4] A. Y. Lee, "A Preview Steering Autopilot Control Algorithm for Four-Wheel-Steering Passenger Vehicles", Advanced Automotive Technologies, ASME, DSC-Vol.13, pp 83-98, 1989

[5] A. Johnston, et al, 'Automated Vehicle Guidance Using Discrete Reference Markers", IEEE Trans. Veh. Tech., Vol. VT-28 No.1, Feb, 1979

[6] R. Mahrt, "Principle of Automatic Guidance of Vehicles on a Lane by Means of Permanent Magnetic Nails and On Board Computer Control", 22st Annual Conference of Vehicle Technology Group, IEEE, Washington DC, pp. 115.0-115.2 1970

C. INDEPENDENT MEASUREMENT SYSTEM

C.1 Purpose

The independent measurement system performed the role of verifying the calibration of the magnetic reference/sensing system for vehicle-in-motion conditions. The independent measurement system also functioned to provide a method for evaluating the performance of the total vehicle control system. The independent measurement system monitors the same lateral position deviation that the magnetic reference/sensing system does. But the magnetic reference/sensing system is part of the vehicle control system, and thus should not be used to evaluate its own performance.

C.2 General Description

The independent measurement system used is Allen-Bradley's 2804-SLS2 Smart Linear Sensor (SLS), which consists of a line scan video camera with a built in microprocessor, a power supply unit and supporting software. Two SLS are used for the vehicle lateral control test. One is mounted at the front of the test vehicle, the other is mounted at the rear, to measure vehicle's lateral displacement and vehicle yaw angle relative to the white line on the road.

During the test, each video camera senses the two edges of the white tape on the road and produces two output current signals (Output A and B). The output currents are proportional to the positions of the tape edges in the Field-of-View (FOV) of the video camera. The input-output relation is as follows:

$$\text{Analog output current (A or B)} = \frac{\text{position (A or B)}}{\text{FOV}} \times 16 + 4 \ [\text{mA}] \qquad \text{(C.1)}$$

A 120 Ohm resistor at each channel is used to transform the current output to voltage output (0.48 V - 2.4 V). These voltage signals are then sent into the control computer through the A/D converter for further processing (see section 4) to obtain the lateral displacement of the video camera relative to the white tape on the road.

Before the vehicle control testing phase, the system is calibrated using a stationary target. The following system parameters were obtained through calibration:

- Input: Lateral displacement 0 -- full range of FOV

- Output: voltage = 0.48V - 2.4V
- Theoretical Camera FOV [m] = 0.5 176 x (Camera height [m]) - 0.0313
- Actual FOV: Front camera = 0.644 [m]; Rear camera = 0.704 [m] (nominal)
- Minimum sampling period: 20 ms updating time (1-D spatial measurement only)
. Measuring error due to 1" vertical displacement: less than 3%

The actual FOV was determined from static testing rather than from the theoretical equation.

Inside each SLS camera is a twelve setting DIP switch which is used to set the system configuration for various operating modes and adjust system operating parameters. At present, the spatial 1-D measurement mode was chosen to provide the fastest processing speed of 20 ms cycle time. All these operating parameters can also be downloaded from PC through a RS-232 cable connected to the J3 terminal at the rear of the camera.

C.3 Verification of the Independent Measurement System

Static calibration tests showed that the independent measurement system can provide accurate lateral displacement measurement of a stationary target with uniform light intensity. To find the system measurement performance in the actual test environment, the window washer system on the car was modified to direct a steam of water onto the road directly below the camera.

The verification test procedure is summarized as follows:

1) The test vehicle was driven at low speed with a slowly oscillating steering input. A small stream of water was sprayed on the testing track as the vehicle moved. The vehicle was driven at a low vehicle speed to reduce the lateral movement caused by car body motions, and to avoid any uncertainty due to the lateral momentum of the water jet sprayed out of the nozzle.

2) The lateral distance of the water trail relative to the white tape edge was measured manually at discrete magnetic marker positions.

3) The corresponding lateral displacements from the independent measurement system at discrete marker positions were obtained from the sampled video data and magnetic signals. The peaks in the magnetic signal were used to mark the corresponding video measurement points at each marker position.

4) The error between the water trail and video measurements was used to evaluate the performance of the independent measurement system.

The measurement results for three test runs are shown in Figures C.l-C.3. The standard deviations for the first two tests are 0.0033 m and 0.0037 m. The standard deviation for the third test is 0.0117 m. This larger error is likely due to measurement error of the water trail displacement.

C.4 Independent Measurement System Offset

After successful development of the magnetic sensing system, the independent measurement system was used to verify its performance. The test vehicle was driven by the test driver at different speeds along the test path. Both video and magnetic data were collected. The stored video data was the position of the white tape in the Field of View of the two cameras. The following formula was used to convert this video data into vehicle lateral displacement relative to the test track center:

$$\text{y-front (video)} = \frac{\text{FOV}}{2} - \text{indep\_y 1} - (\text{offset1} - \text{offset2}) \qquad \text{(C.2)}$$

where

offset 1 = offset between camera center and center of the horizontal magnetic sensor
offset2 = offset between center of magnets and white tape on the track

For the present setup, the above converting formula becomes:

$$\text{y-front} = 0.322 - \text{indep\_y 1} - 0.045 \qquad \text{(C.3)}$$

offset1 = 0.158 m
offset2 = 0.113 m

C.5 Camera Signal Filtering

The signal processing sequence of the camera output signal in the control computer is described below. No other filtering was performed.

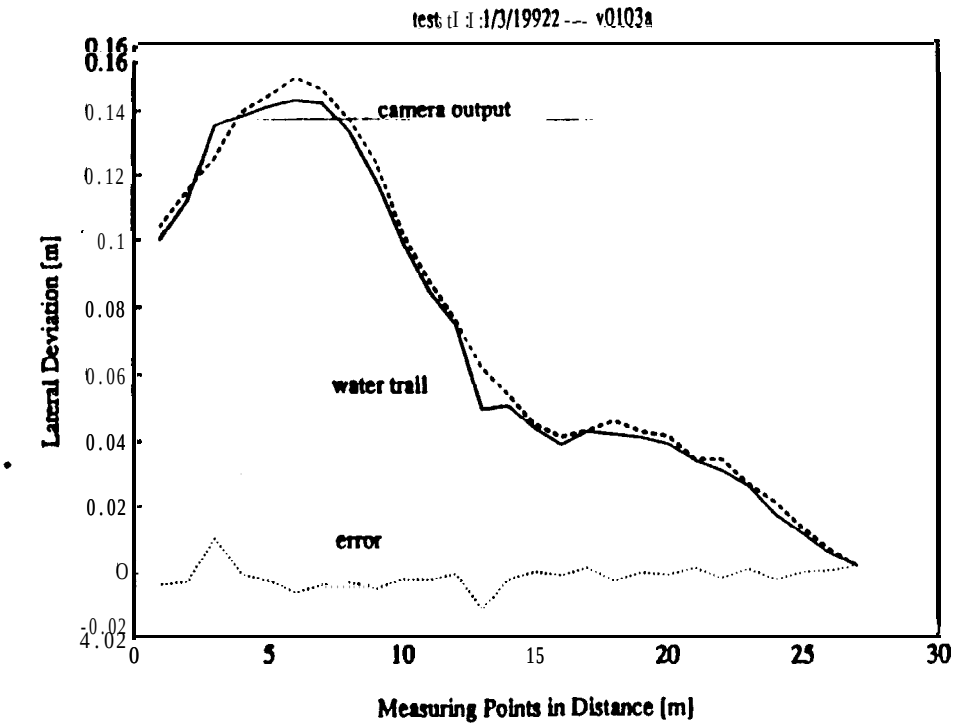

Figure C. 1 Independent Measurement System Verification, test 1

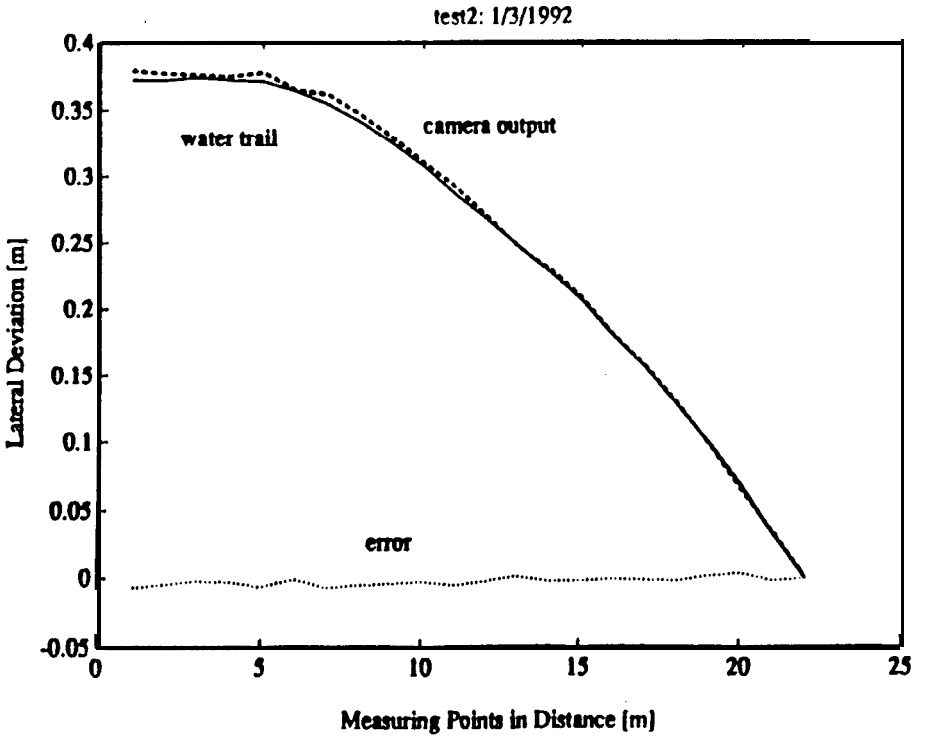

Figure C.2 Independent Measurement System Verification, test 2

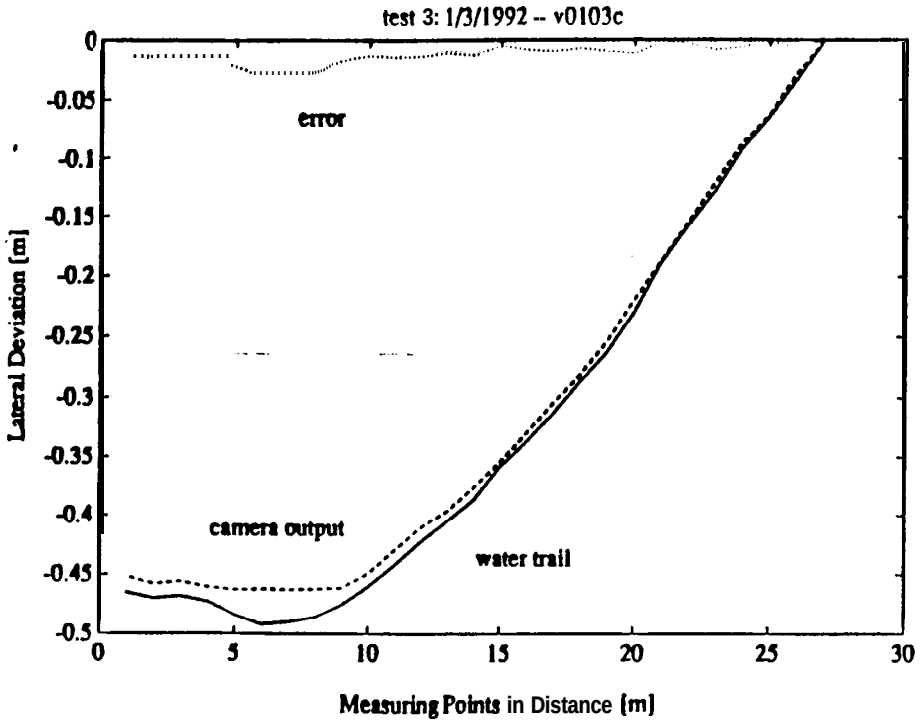

Figure C.3 Independent Measurement System Verification, test 3

1) The signal entering the computer is a voltage signal proportional to the position of the tape edge (left edge: dark to light transition, right edge: light to dark transition) in the field of view. OV = line is on the right edge of the field of view. 9.6V = line is on the left edge of the field of view.

2) 0.48 V is subtracted from the voltage signal so that OV is at the center of the field of view.

3) The width of the tape is calculated by taking the difference of the left and right edge positions. If the calculated width is outside a specified range, the difference between the current right and left edge positions is compared with the measurements from the previous sample. The edge measurement that changed the least between successive samples is used to calculate the tape center position. This calculation is based on the width of the tape specified by the manufacturer.

4) If the calculated width of the tape is within the specified limits, the tape center position is calculated by averaging the positions of the left edge and right edge.

5) This new tape center position is compared with the measurement from the previous sample. If it is larger than a specified tolerance, the old tape center position is retained and the new one is ignored.

D. STEERING ANGLE MEASUREMENT CALIBRATION

The task of calibrating the steering angle measurement and command signal was not an easy one. Absolute measurement of the steering angle is not as important with PID control as with FSLQ since PID uses steering angle difference while FSLQ uses the actual steering angle measurement.

D.1 System Set Up

From the sensor, the steering angle signal goes into the signal conditioning board for filtering and adding a gain and offset factor to make the signal fit within the range of the A/D board which is limited to a ± 2.5 V range. The signal conditioning board was configured with the expectation that the A/D board would accept signals in the 0 to 5 V range, so the offset was set to -2.5 V. This offset shifted the steering angle measurement signal sent to the A/D board to be between -2.5 V and 0.5 V.

The range of the D/A channel on the DSP system board is ± 3 V. Potentiometers on the actuator control box are used to make the full range of the actuator stroke match the 0 to 3 V command signal from the control computer.

D.2 Measurement Procedure

Two methods were attempted to find the true 0" steering angle position. The first method did not seem to be satisfactory.

D.2.1 Method 1

The vehicle was manually driven along a straight line at a low speed. The steering column detent was not engaged. The potentiometer on the actuator interface display box was used to position the actuator near its center position. The camera data was used to evaluate the straightness of the path.

The measurement and command offset factors from this test were programmed into the control code in the volts to radian and radian to volts conversion equations. The factors must also consider the signal conditioning board gain. Vehicle tests using these factors showed the vehicle always running to the left of the markers (negative side). This indicated that the measured $0°$ steering angle position was not accurate. This shift was more noticeable in the FSLQ tests as compared to the PID tests.

D.2.2 Method 2

Using the correction factors obtained from Method 1 still seemed to produce a biased lateral deviation result. To improve the tracking accuracy of the vehicle, the steering angle measurement and command offset factors in the program were adjusted until the lateral deviation test results were fairly symmetric about 0 for tests using test path #2.

D.3 Actuator Position Measurement

The signal range of the potentiometer that measures the position of the actuator is between 0 and 3 V. The tire steering angle range that this signal corresponds to is 6". Therefore, the voltage to radians conversion factor is as follows:

$$\text{actuator sensor conversion factor} = \frac{6^\circ \times \pi \text{ rad}}{180^\circ \times 3 \text{ V}} = 0.03497 \frac{\text{rad}}{\text{V}} \qquad \text{(D.1)}$$

D.4 Steering Wheel Measurement

The signal range of the potentiometer that measures the rotation of the steering wheel is between 0 and 5 V. A -2.5 V offset in the signal conditioning board shifts this signal to between -2.5 V and +2.5 V. The steering wheel is assumed to be able to rotate 3 full rotations, stop to stop. This corresponds to a tire steering angle sweep of 64.8".

$$\text{steering ratio} = \frac{1080 \text{ (steering wheel)}}{64.8 \text{ (tire)}} = 16.67 \qquad \text{(D.2)}$$

$$\text{steering wheel conversion factor} = \frac{3 \text{ rot.} \times 2\pi}{16.67 \times 5 \text{ V}} = 0.2262 \frac{\text{rad}}{\text{V}} \qquad \text{(D.3)}$$

E. LATERAL CONTROL PROGRAM TECHNICAL REFERENCE

E.1 Hardware Description

The measurement/control system is shown in Figure E.1.

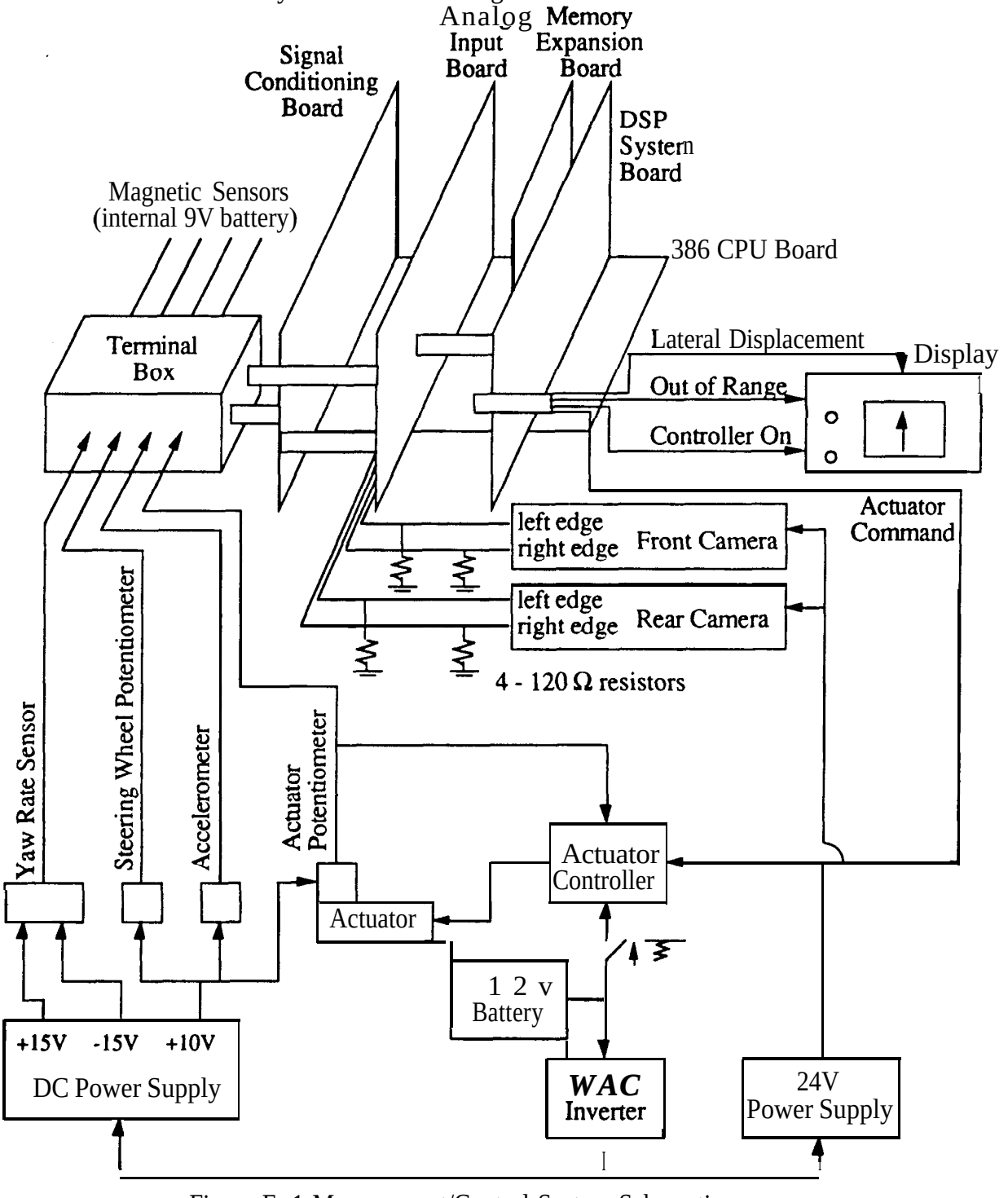

Figure E. 1 Measurement/Control System Schematic

E.1.1 TMS320C30 Digital Signal Processor

The controller computer used for the vehicle lateral control is SPECTRUM Signal Processing Inc.'s TMS320C30 DSP board. The TMS320C30 is a high-performance CMOS 32-bit floating-point digital signal processor, whose innovative architecture and 60-ns cycle time allows it to run at a performance rate of up to 33 MFLOPS. The powerful performance of the device can also be attributed to its large on-chip memories, concurrent DMA controller, instruction cache, and hardware-intensive design. The TMS320C30 can perform parallel multiply and ALU operations on integer or floating-point data in a single cycle.

The key features of the TMS320C30 are listed below:

- 60-ns single cycle instruction execution time, which results in 33.3 MFLOPS and 16.7 MIPS (million instruction per second)
- One 4Kx32-bit single-cycle dual-access on-chip ROM block
- Two 1Kx32-bit single-cycle dual-access on-chip RAM blocks
- 64x32-bit instruction cache
- 32-bit instruction and data words, 24-bit addresses
- 40/32-bit floating-point/integer multiplier and ALU
- 32-bit barrel shifter
- Eight extended-precision registers (accumulator)
- Two address generators with eight auxiliary registers and two auxiliary register arithmetic units
- On-chip DMA controller for concurrent I/O and CPU operation
- Two- and three-operand instructions
- Parallel ALU and multiplier instructions in a single cycle
- Block repeat capability
- Zero-overhead loops with single-cycle branch
- Condition calls and returns
- Interlocked instructions for multiprocessing support
- Two external interface ports
- Two serial ports to support 8/16/24/32-bit transfers
- Two 32-bit timers
- Two general-purpose external flags, four external interrupts

This DSP board is installed in the PC bus (a full-size AT slot). The memory expansion board and the 32 channel analog input board occupy another two PC slots (XT size). A DSPLINK cable is used to connect the main board with its daughter board. The communication between the host PC and DSP is accomplished through a PC I/O address (290 hex). The interface library is provided to allow the user to write high-level language PC programs to control the DSP board and to pass data back and forth between the program running on the TMS320C30 and the PC.

The main support software for programming the DSP are:

1) TI C Compiler/Linker (Directory: C30TOOLS)
2) TI Assembler/Linker (Directory: C30TOOLS)
3) Interface Library (Directory: C30TOOLS)
4) SDS30 Monitor (Directory: LSIC30)
5) SPOX API (Directory: SPOX) -- not used at present

E.12 Analog Interfaces of TMS320C30

The analog interface includes two A/D channels and two D/A channels on the DSP system board, and 32 A/D channels on the analog input board.

The A/D and D/A channels on the DSP system board are accessed via a 15 pin D connector at the system board's "end-plate". They are 16-bit A/D channels with an input signal range of ±3V. The connector is shown in Figure E.2.

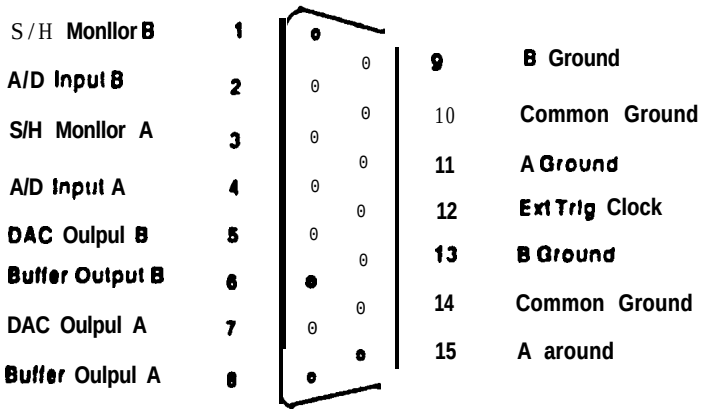

Figure E.2 DSP Analog Interface Connector

The assignment of these two A/D and two D/A ports are as follows:

- A/D input A and B are not used at present.
- D/A output A: Steering actuator control.
- D/A output B: Display meter control.

The 32 A/D channels on the analog input board are accessed via a 37 pin D connector. They are 12-bit A/D channels with an input signal range of ±2.5V. The connectors are shown in Figure E.3. For the present test, only channel 0 - 13 are used. Their assignments are listed as follows:

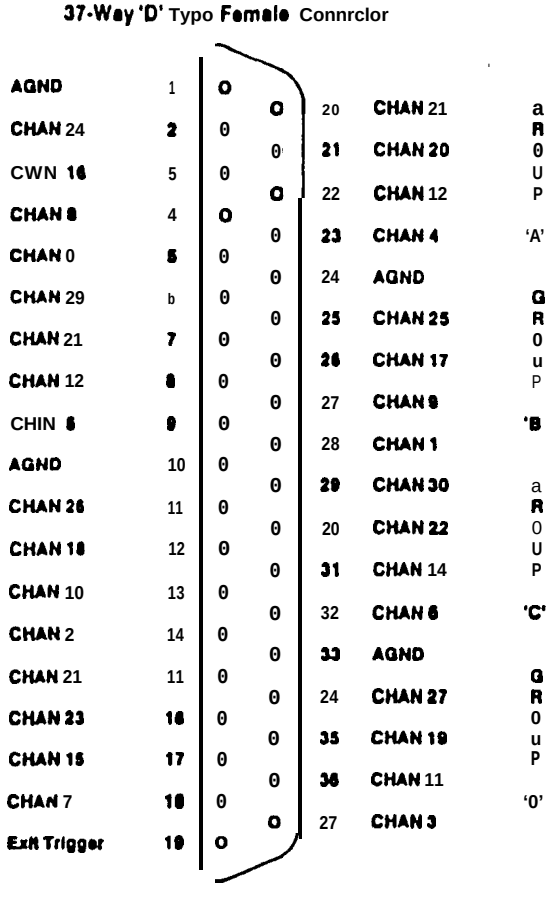

Figure E.3 37-way D Connector for Analog Input Board

- Channel 0: Center vertical magnetic sensor (pin 5)
- Channel 1: Left vertical magnetic sensor (pin 28)

- Channel 2: Right vertical magnetic sensor (pin 13)
- Channel 3: Horizontal magnetic sensor (pin 37)
- Channel 4: Lateral acceleration (pin 23)
- Channel 5: Longitudinal acceleration (pin 9) -- not used
- Channel 6: Vehicle speed from speedometer (32) -- not used
- Channel 7: Yaw rate (pin 18)
- Channel 8: Steering actuator potentiometer (pin 4)
- Channel 9: Steering wheel potentiometer (pin 27)
- Channel 10: Front video camera analog A (pin 13)
- Channel 11: Front video camera analog B (pin 36)
- Channel 12: Rear video camera analog A (pin 22)
- Channel 13: Rear video camera analog B (pin 8)

E.1.3 Serial Interfaces of TMS320C30

The serial port of the DSP board is accessed via a 15 pin D connector on the "end-plate" of the system board, as shown in Figure E.4. The assignment of pins are as follows:

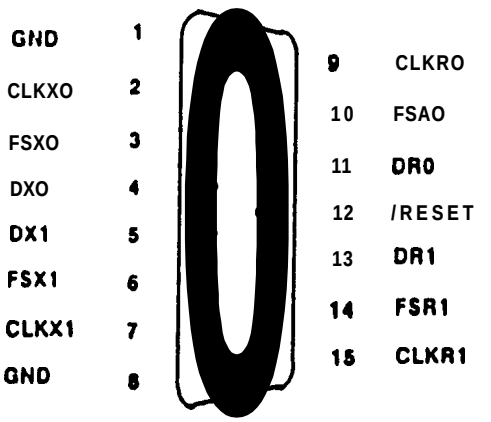

Figure E.4 DSP Serial Interface Connector

- CLKXO: Controller state: On -- Controller is working (pin 2)
- CLKRO: Magnet marker out of range warning (pin 9)
- CLKXl : Front camera trigger (pin 7)
- CLKR1: Rear camera trigger (pin 15)

E.1.4 Signal Conditioning Board

The purpose of the signal conditioning board is to filter the sensor signals and provide a gain and offset factor to make the signal fit within the range of the analog input board.

- Channel 1 - 2: Not used at present.
- Channel 3: Steering actuator potentiometer (pin 3)
  Offset: -2.5 V
  Gain: 1
  Cut off frequency: < 5 Hz
- Channel 4: Steering wheel potentiometer (pin 4)
  Offset: -2.5 V
  Gain: 1
  Cut off frequency: < 5 Hz
- Channel 5: Longitudinal accelerometer (pin 5) -- not used
- Channel 6: Lateral accelerometer (pin 6)
  Offset: -2.5 V
  Gain: 1
  Cut off frequency: < 2 Hz
- Channel 7: Speed sensor (pin 7) -- not used
- Channel 8: Yaw rate senor (pin 8)
  Offset: 0 V
  Gain: 0.5
  Cut off frequency: < 4 Hz

The input signals enter through a 15-pin D connector. The output signals are sent out through a 25-pin D connector, which goes directly to the 37-pin D connector of the analog input board.

E.1.5 Vehicle Control System Wiring

Different types of connectors (size and sex) and wire colors were chosen when connecting the sensors to the computer to avoid misconnections.

1) Magnetic sensors: The four magnetic sensor output signals are first connected to the terminal box and then are connected directly into the analog input board via a 9-pin D connector.

2) The lateral accelerometer, yaw rate sensor, and steering wheel and steering actuator potentiometers are also connected to the corresponding junctions of the terminal box. All these signals are then sent to the signal conditioning board via a 15-pin male D connector.

3) Four analog signals from the two video cameras are sent to the analog input board via a 15-pin D connector.

4) The steering actuator command, the lateral displacement display meter signal, and the signals for the two LED warning lights are connected using single wires, labeled to avoid confusion.

E.2 Control Software

E.2.1 General Description

The vehicle lateral control software consists of PC-resident programs and a DSP-resident program, which are described below.

E.2.1 .I PC-resident programs

The following programs are run on the host PC to download the executive control code and the input data to the DSP board, and to upload test data stored in the DSP memory after the test. They are:

- **pc_con.c**: A C program used to download the control task code **dsp_con.out** and other input data to the DSP board. It also serves to start and to terminate the execution of the DSP board. The program creates a temporary file to pass the data saving flags to the uploading program. The program flow chart is shown in Figure E.5.

- **upload.c**: A C program used to upload test data stored in the DSP memory to the PC hard disk. The program flow chart is given in Figure E.6. Two files are created to store integer and floating-point data separately, **dsp_con.dd1** and **dsp_con.dd2**, respectively. The data are stored in ASCII format and can be directly viewed and edited. Two extra files (**dsp_con.dm1** and **dsp_con.dm2**) can be created to store integer and floating-point data in binary format. Binary

format files are more compact and can be processed faster and more conveniently by MATLAB.

E.2.12 DSP-resident program

dsp_con.c is the main program for executing vehicle lateral control. The program flow chart is shown in Figure E.7. Each individual function module is described below.

- initialize@ This module is used to: i) assign the program variables with proper initial values and load the gains (which are downloaded by the host PC from disk tiles) into a data array, ii) calibrate the analog input board and set up the interrupt and timer.

- **getmarker()**: The magnetic sensing system module calculates the vehicle's lateral position relative to the road center (magnets). The flow chart for getmarker() is shown in Figure E.8.

- **curvature()**: Uses information from "**getmarker()**" to obtain road geometry parameters such as the upcoming curve's starting position, ending position, curvature, superelevation, etc. for either feedforward or preview control. The flow chart for **curvature()** is shown in Figure E.9.

- **display()**: Converts the vehicle's lateral displacement into a voltage signal and sends it through D/A channel 1 to the display meter to provide the vehicle's lateral position to the test vehicle driver.

- **safechecker()**: Checks the vehicle's lateral position relative to the center of the road. If the out-of-range flag is set or the lateral displacement is greater than 0.4 m, the computer sends a warning signal to the test vehicle driver by turning on one of the LEDs in the display panel.

- **speed_estimator()**: Estimates the vehicle's speed based on the magnetic peak signals. The speed is updated at every new marker encountered. The speed will not be available at the start of the test until the vehicle passes over three magnets. The flow chart for **speed_estimator()** is shown in Figure E. 10.

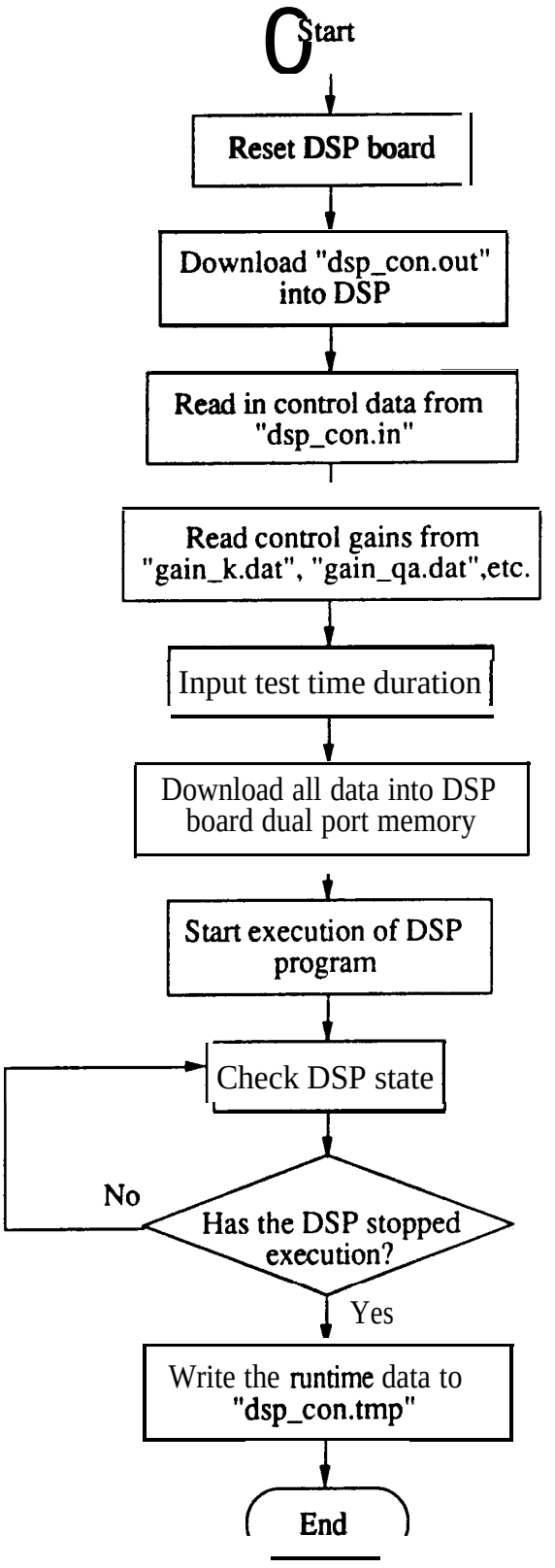

Figure E.5 Flow Chart for pc_con.c

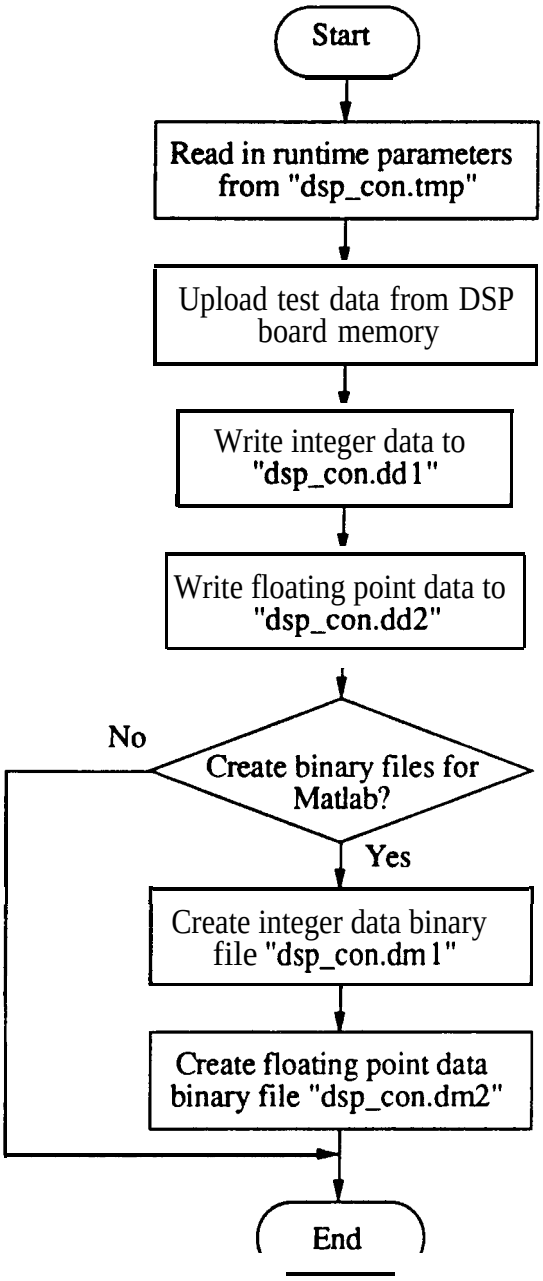

Figure E.6 Flow Chart for **upload.c**

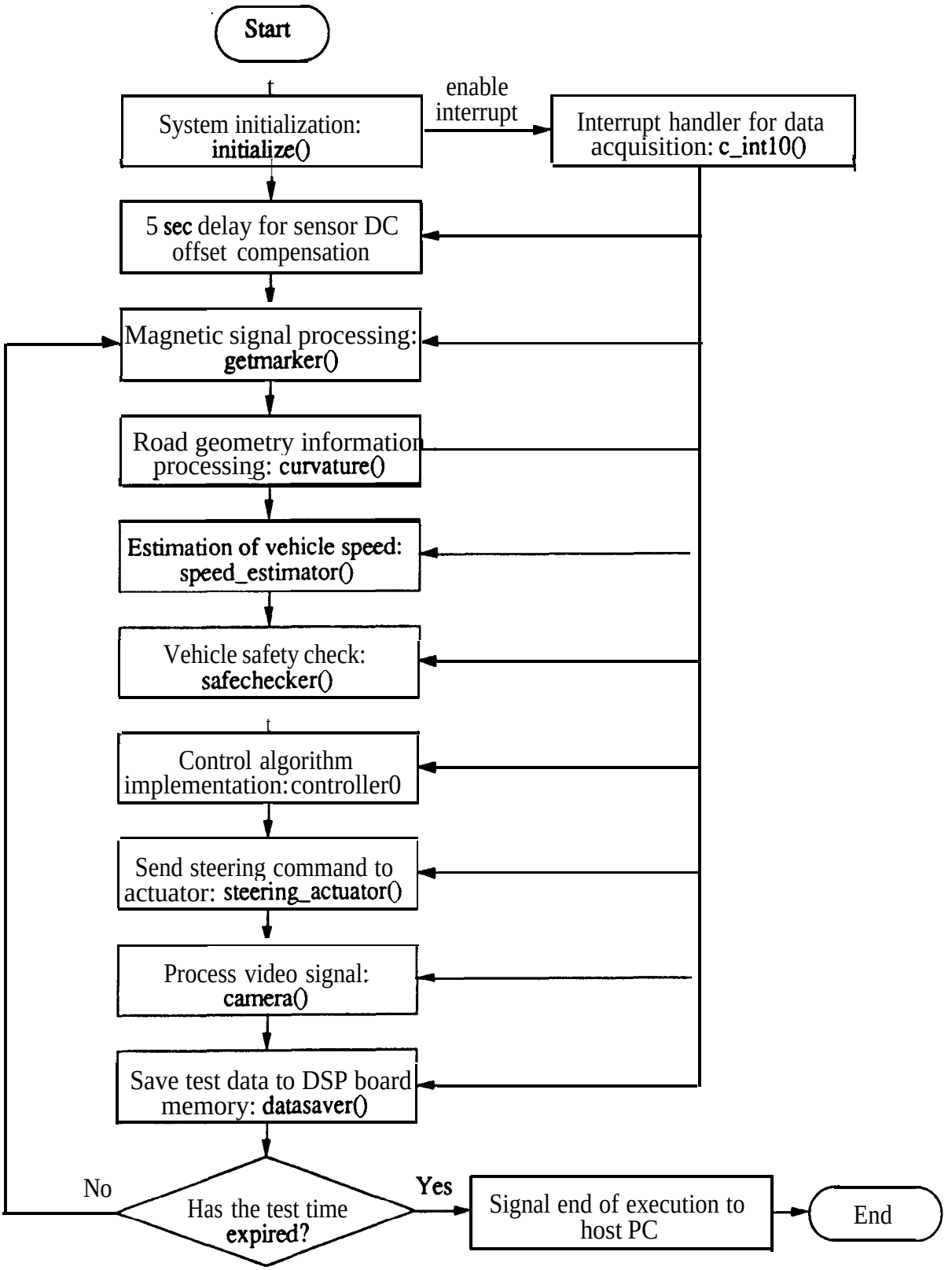

Figure E.7 Flow Chart for **dsp_con.c**

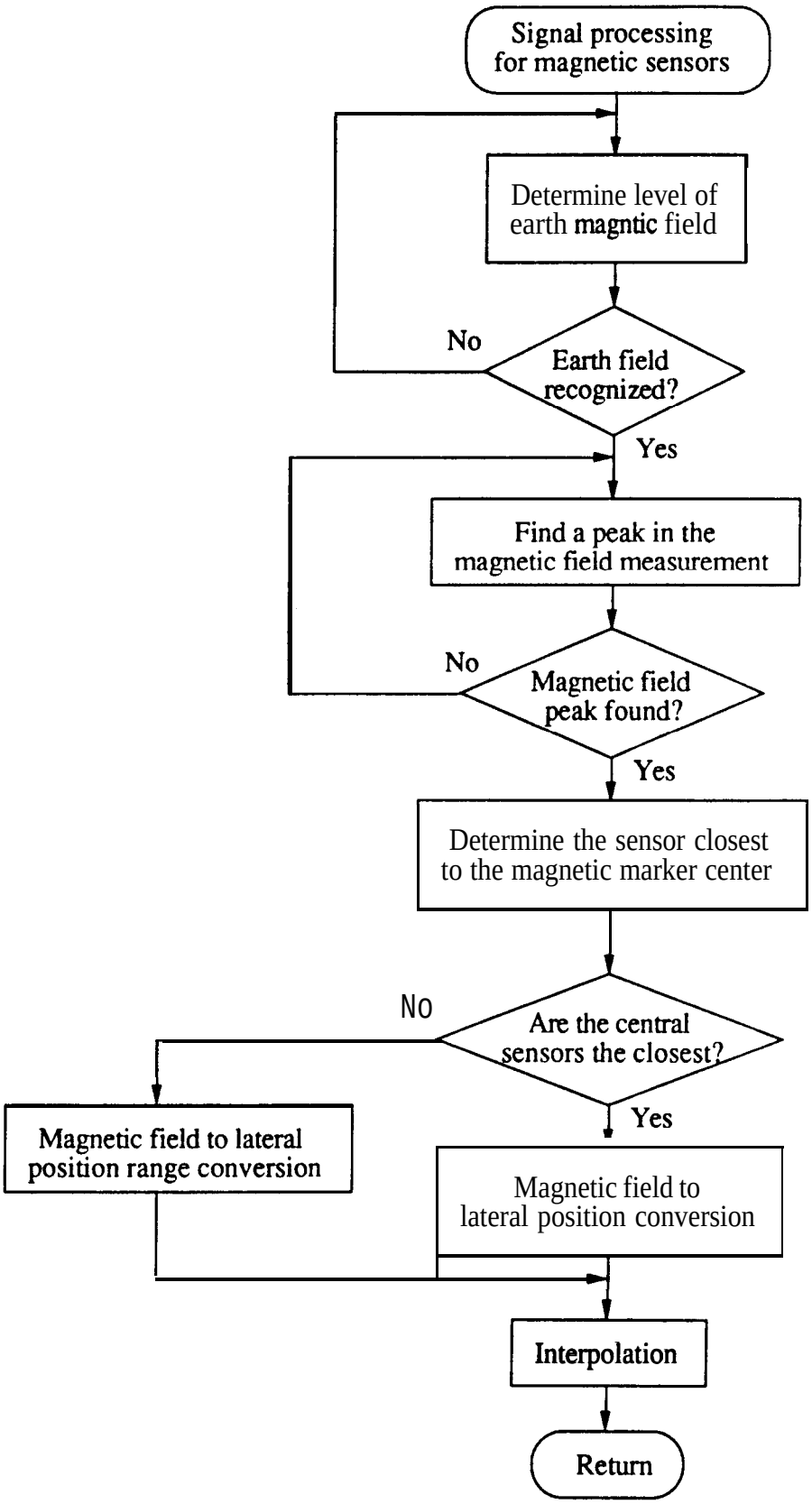

Figure E.8 Flow Chart for Magnetic Measurement Signal Processing

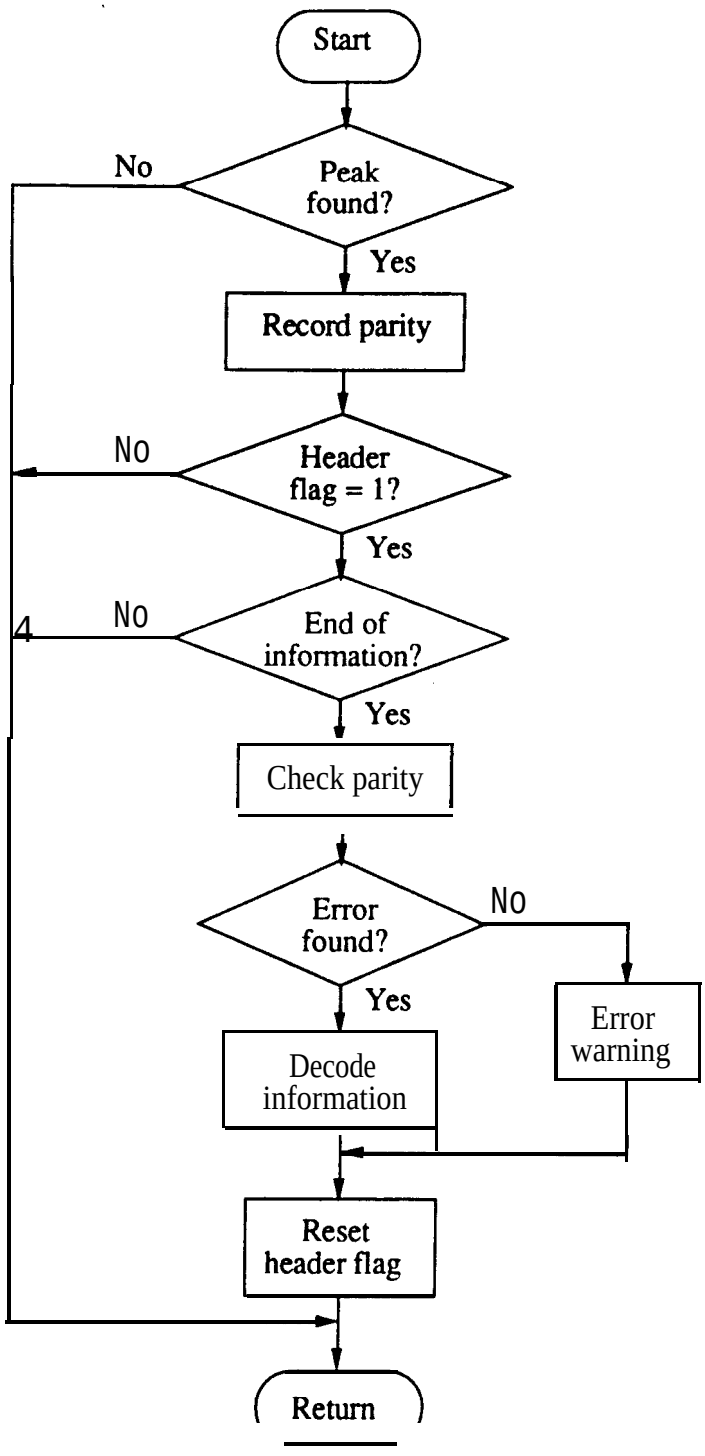

Figure E.9 Flow Chart for Curvature Information Decoding

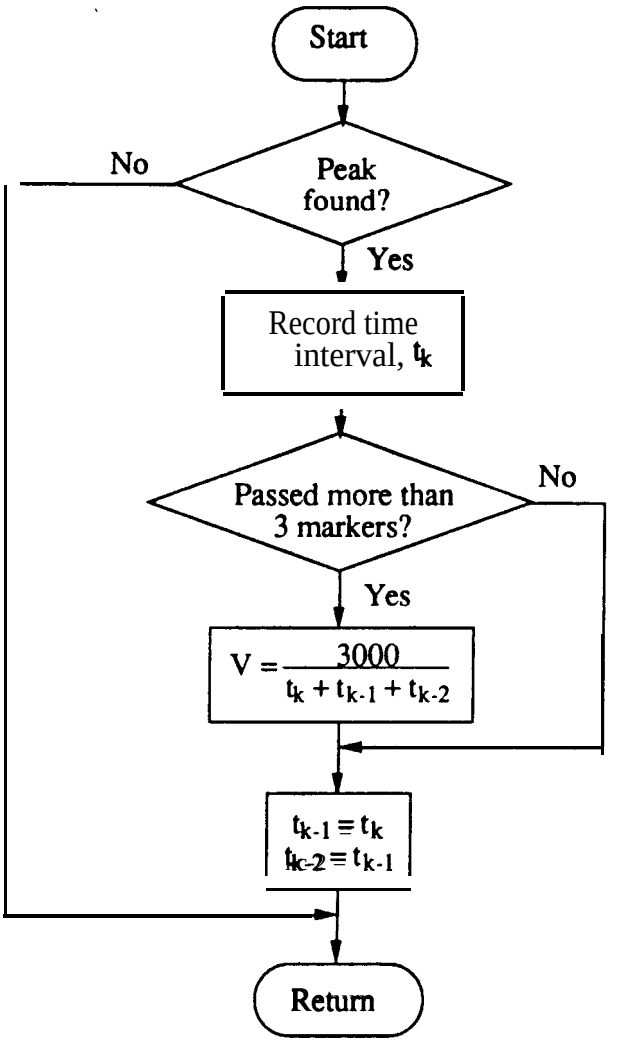

Figure E. 10 Flow Chart for Speed Measurement Algorithm

- **controller()**: Implements FSLQ or PID control, which includes an estimation of vehicle states using the observer, gain scheduling, computation of desired steering angle based on the feedback and preview algorithms, and tire cornering stiffness estimation.

- **steering_actuator()**: Sends the desired steering command through D/A channel 0 to the steering actuator every 21 ms.

- **camera()**: Processes the signals from the two video cameras to obtain front and rear lateral displacements and the vehicle yaw angle.

- **datasaver()**: Saves the desired variables (integer and floating-point) every "**dt_save**" (user assigned value) seconds. The data to be saved are written to both the DSP board memory and a dual-port memory. The latter part of the memory can be accessed by the host PC without interrupting the execution of the DSP. This feature provides a parallel execution ability for the DSP and PC.

- **c_int10()**: An interrupt handier, which is activated every 3 ms in parallel with the main program routine to do data sampling and to scale the input signals by calibration **factors.**

Tie timing sequence for **dsp_con.c is shown** in **Figure** E. 111.

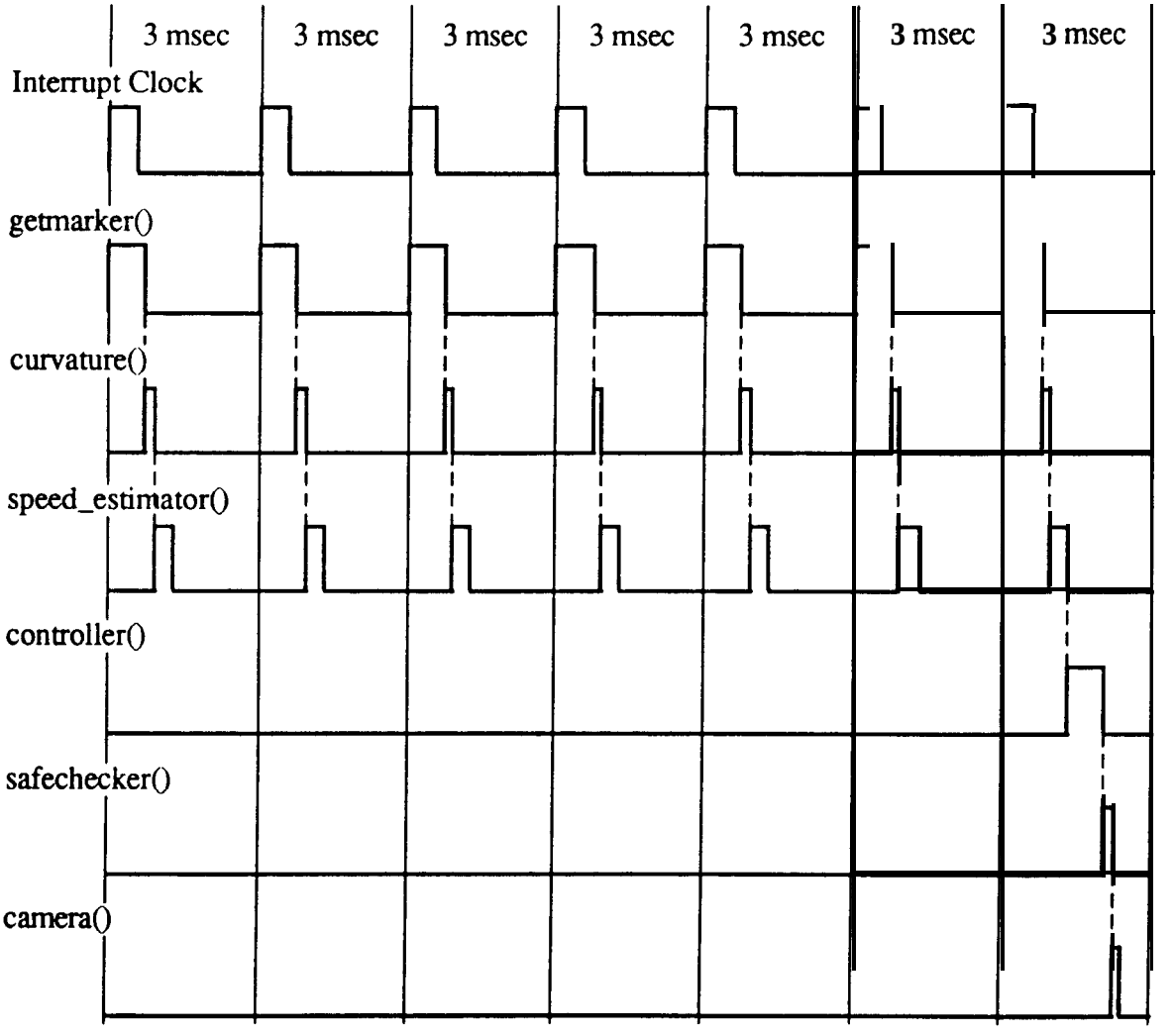

Figure E. 11 Timing Sequence for **dsp_con.c**

E2.13 Simulation programs

These two simulation program are similar to **pc_con.c** and **dsp_con.c**. They are used in the program development stage for debugging. The only differences between these two programs as compared to their respective control versions are:

- **pc_sim.c** will download an extra data file representing the four magnetic signals to the DSP board memory before starting the execution of the DSP.
- **dsp_sim.c** will read four magnetic sensor inputs from its memory instead of from its A/D ports to compute the vehicle lateral displacement.

E.2.2 Input Data Files

Program control file: **dsp_con.in**

The input data file format is as follows:

line #	[data] or [save flag]	Description
1	d t-save	Data sampling in [ms], minimum = main loop time
2	v-start, v-end	Controller initiate and terminate speed [m/s]
3	deltat, previewseg, sampl	Time step [ms], preview steps, control sample time [ms]
4	m, iz	Vehicle mass [kg] and inertia [N-m]
5	marker-spacing, forgetter	Forgetting factor for C_s estimation
6	superon	superon = 1: Taking account super elevation
7	igs, FF_type	FF_type = 1: FF, FF_type = 2: Preview
8	control-type	= 1:FSLQ, ≠ 1: PID
9	kp1, kp0	PID gain: kp = kpl x vspeed+kp0
10	kil, kio	PID gain: ki = kil x vspeed+ki0
11	kdl, kd0	PID gain: kd = kdl x vspeed+kd0
12	x x x x x	A/D scaling factors: channel O-4
13	x x x x x	A/D scaling factors: channel 5-9
14	x x x x x	A/D scaling factors: channel 10-14
15	x x x x x	A/D scaling factors: channel 15- 19
16	x x x x x	A/D scaling factors: channel 20-24
17	x x x x x	A/D scaling factors: channel 25-29
18	x x x x x	A/D scaling factors: channel 30-3 1

19	marker, O/l	variable name, **saveflag** = 1: save this data
20	markflag, O/l	
21	curvflag, O/l	
22	**cstiff,** O/l	
23	marker-count, O/l	
24	**bflag1,** O/l	
25	**bflag2, 0/1**	
26	**bflag3, 0/1**	
27	**bflag4, 0/1**	
28	**bflag5, 0/1**	
29	**bflag6, 0/1**	
30	**bflag7, 0/1**	
31	**bflag8, 0/1**	
32	**bflag9, 0/1**	
33	**bflag10, 0/1**	
34	**bflag11,** O/l	
35	**bflag12, 0/1**	
36	**bflag13, 0/1**	
37	**bflag14, 0/1**	
38	**bflag15, 0/1**	
40	**bv0, 0/1**	Vertical center magnetic sensor signal [G]
41	**bv1, 0/1**	Vertical left magnetic sensor signal [G]
42	**bv2, 0/1**	Vertical right magnetic sensor signal [G]
43	**bh0,** O/l	Horizontal magnetic sensor signal [G]
44	xaccl, O/l	Longitudinal accelerometer signal **[m/s/s]**
45	yaccl, O/l	Lateral accelerometer signal [m/s/s]
46	v-sensor, O/l	Vehicle speed sensor signal **[m/s]**
47	**yawrate,** O/l	Yaw rate sensor signal, **[rad/s]**
50	indep1, 0/1	Front camera input A **[V]**
51	**indep2, 0/1**	Front camera input B **[V]**
52	**indep3, 0/1**	Rear camera input A **[V]**
53	**indep4, 0/1**	Rear camera input B [V]
54	**AD14, 0/1**	A/D channel 14: not used
55	**AD15, 0/1**	A/D channel 15: not used
56	**ycar,** O/l	Vehicle deviation from magnetic system [m]
57	delta-c, O/l	Steering command **[rad]**

58	delta-real, O/l	Actual steering angle [rad]
59	indep_y 1, 0/1	front camera lateral displacement [m]
60	indep_y2, 0/1	rear camera lateral displacement [m]
61	indep_yaw, O/l	yaw angle from camera [rad]
62	vspeed, O/l	speed from magnetic sensor [m/s]
63	variablel, O/l	For debugging
64	variable2, 0/1	For debugging
65	variable3, 0/1	For debugging
66	variable4, 0/1	For debugging
'67	variable5, 0/1	For debugging
68	variable6, 0/1	For debugging
69	variable7, 0/1	For debugging

* save flag = 1 indicates that the data will be saved.

Controller input Data Files

No.	File Name	Usage
1	gain-k.dat	feedback gain
2	gain-qa.dat	value of Qa
3	gain-qy.dat	value of Qy
4	gain-qe.dat	value of Qe
5	gain-qi.dat	value of Qi
6	gain-f 1 .dat	preview gain F1
7	gain_f2.dat	preview gain F2
8	test.dat	test parameters
9	gain-obs.dat	observer gain

E.3 Test Operation Procedure

E.3.1 Independent Measurement System Set Up

Prior to each set of tests the set up routine provided by the camera is used to determine the appropriate exposure time for each camera and download the settings from the PC to the cameras. Two other parameters that may be set by the operator affect the sensitivity of the camera: edge span and edge height.

Edge span describes the sharpness of the edge (1- 10). Small span numbers are used for an image with very sharp edges, but the measurements are subject to noise (false edges, i.e. white spots on the road). Large span values are used to detect gradual edges. Sharp changes are filtered out, but the detection of changes is slower. An edge span of 5 is currently being used.

Edge height is the relative gray scale difference between the object and the background (1-10). Small height values are used when there is very little difference between the target and the background. Larger height values are used when there is a large relative gray scale difference. We are currently using an edge height value of 8.

Under E:\SLS Directory

- Connect RS-232 cable to the J3 connector on the rear of the video camera
- Execute **sls.exe** to start window menu
- Select "Configuration" option
- Under the "Configuration" submenu, choose the "Send" option to first send out the **setup** and then the **run** files. Hit the **Return** key at the following prompt.
- Choose "View" option to view the image quality and to obtain camera exposure time.
- Hit ESC key to exit "Configuration" and return to the DOS environment

E.3.2 Run Vehicle Control Test

Under E:\DATA Directory

- Change input data file **dsp_con.in** to select program options.
- Execute **pc_con.exe** to run the test program.
- Key in test running time in [s] and hit the "Return" key.
- Hit the "Return" key again to start control program on the DSP board.
- After termination, execute **upload.exe** to upload test data from DSP board memory. The integer and floating-point data are stored in **dsp_con.dm1** and **dsp_con.dm2** files in ASCII form, respectively. A prompt on the screen will ask if the user wishes to create two binary files **dsp_con.dm1** and **dsp_con.dm2** for MATLAB processing. It should be pointed out that because of the limitation of the MATLAB data conversion subroutine in the QuickC environment, each variable saved for MATLAB files must be limited to less than

5000 data points. If data points of each variable exceed 5000, the PC will be trapped. In case this happens, just do a **warm** restart, re-run **upload.exe** again and choose "n" to the prompt. Whenever upload.exe is executed, the latest test data will be uploaded from DSP memory and stored in the PC hard disk. The test data on the DSP board will not be lost by a warm reset of the host PC, and can always be retrieved by executing **upload.exe.** But if the PC power is off, the test data on the DSP board will be lost.

A batch file **task.bat** is available to assist test operation and to generate a group of six data fiies after each test with the same file name and a file type of **filename.dil - filename.di6** (integer data, ASCII), **filename.df1 - filename.df6** (floating-point data, ASCII), **filename.mi1 - filename.mi6** (integer data in MATLAB format, if chosen), **filename.mf1 - filename.mf6** (floating-point data in MATLAB format, if chosen).

The command for this batch execution is:

task filename number-of-test-to-run, return.

e.g. task fslq306 4

will results in following data files after four test runs:

fslq306.di1	fslq306.df 1	fslq306.mi 1	fslq306.mf1
fslq306.di2	fslq306.df2	fslq306.mi2	fslq306.mf2
fslq306.di3	fslq306.df3	fslq306.mi3	fslq306.mf3
fslq306.di4	fslq306.df4	fslq306.mi4	fslq306.mf4

F. LINEAR and COMPLEX MODEL DESCRIPTIONS

Two models were developed for the vehicle lateral control problem. A six degree-of-freedom (DOF) nonlinear vehicle model was used to represent the vehicle as realistically as possible. It was used to simulate the response of the vehicle in this report. A simplified model was obtained by linearizing the complex model, retaining only the lateral and yaw motions. The feedback and feedforward control laws are designed based on the simplified model.

The complex model includes the six DOFs (three translational and three rotational) of the mass center of the vehicle. The inputs to this model are the road gradient angle, superelevation angle, road curvature, steering angles, and driving/braking torques of the four wheels. It should be noted that there are fourteen state variables in the complex model; ten for the vehicle sprung mass and four for the tires. The lateral displacement of the vehicle mass center relative to the road is calculated from the vehicle state variables and the road reference.

The simplified model (SIM1) is obtained from the complex model by retaining only the lateral and the yaw motions of the vehicle. The vehicle speed, which is a key parameter affecting the lateral dynamics, is assumed to be constant. The lateral deviation (and rate) and yaw error (and rate) of the vehicle mass center with respect to the road reference are chosen to be the state variables. Therefore, there are only four state variables in the simplified model.

F.l Complex Model

Figure F.l shows the scope of the vehicle complex model. The dynamics of this model are described by fourteen state variables, two in each of the vertical, roll, pitch and yaw directions; one in each of the lateral and longitudinal directions; and four for the tires. The control inputs are the steering angles and traction/braking torques acting on the four tires. The exogenous inputs include the road curvature, gradient angle and superelevation angle.

The dynamic equations are derived based on the results of [14]. A curve fitting technique is applied to a set of tire test data to obtain the tire model. In the following, the roll and pitch motions of the sprung mass are reported relative to their undisturbed positions. The yaw motion of the sprung mass relative to the chassis (unsprung mass) is assumed to be small.

Therefore, the yaw angle is with respect to an inertial coordinate. The nomenclature of the complex model is as follows:

Y_r :	lateral displacement of vehicle c.g. from road center
V_x:	vehicle speed in the longitudinal direction
V_y :	vehicle speed in the lateral direction
z :	displacement in the vertical direction
ϕ :	roll angle displacement of the sprung mass
θ :	pitch angle displacement of the sprung mass
ε :	yaw angle of the vehicle unsprung mass
β :	vehicle side slip angle
φ :	vehicle velocity angle $\varphi = \varepsilon + \beta$
γ :	road superelevation angle
A:	road gradient angle
δ_i :	steering angle of the ith tire
F_{xi} :	traction (braking) force on the *ith* tire
F_{yi} :	side force from the *ith tire*
F_{Ai} (F_{Bi}):	longitudinal (lateral) force from the ith tire
F_{Pi} :	normal force on the *ith tire*
$M_x(M_y)(M_z)$:	external torque input in the x (y)(z) direction
$I_x(I_y)(I_z)$:	moment of inertia of the sprung mass in the x (y)(z) direction
$F_{wx}(F_{wy})$:	wind force in the x (y) direction
$l_1(l_2)$:	distance from c.g. to the front (rear) axle
m:	mass of the vehicle
h_2 :	vertical distance from c.g. to the roll center
$h_4(h_5)$:	vertical (longitudinal) distance from c.g. to the pitch center
$s_{b1}(s_{b2})$:	track of the front (rear) axle
O_s :	c.g. of the sprung mass
O_u :	projection point of unperturbed 0, on the road surface
$O_sX_sY_sZ_s$:	coordinate fixed on the sprung mass
$O_uX_uY_uZ_u$:	coordinate fixed on the unsprung mass

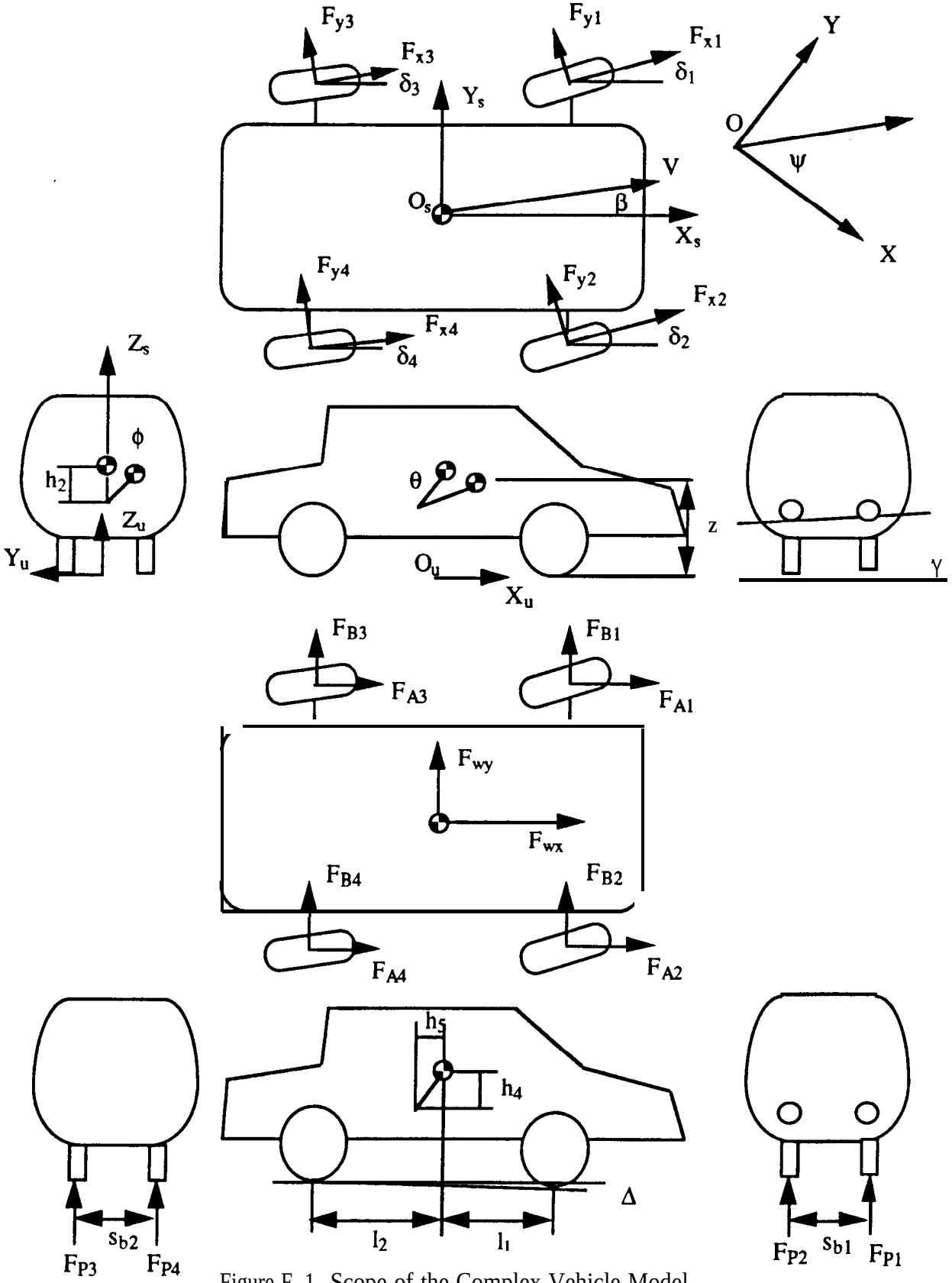

Figure F. 1 Scope of the Complex Vehicle Model

F.1.1 Subsystems of the Complex Vehicle Model

External inputs (forces and moments) enter the vehicle through two ways: wind forces acting on the vehicle body and tire forces entering through the ground. The external force and moment inputs are obtained by constructing the wind force, suspension, and tire models to relate the forces and moments to the states of the vehicle.

F.1.1.1 Wind force model:

A quadratic relationship between the vehicle speed and aerodynamic (wind) force is assumed as:

$$F_{WX} = - K_x V_x^2 \tag{F.1}$$

$$F_{wy} = - K_y V_y^2 \tag{F.2}$$

where F_{wx} and F_{wy} are the wind forces in x and y directions, and K_x and K_y are the wind resistance coefficients. The wind speed is assumed to be zero in Eqs. (F. 1) and (F.2).

F.1.1.2 Suspension model

The suspension of the vehicle is assumed to consist of a spring and a damper at each wheel. The spring and damping forces are determined by the deflections and the deflection rates of the suspension joints. The deflections are calculated from the basic geometry of the car model. Refer to [14] for details.

The spring force is assumed to be governed by:

$$P_{Fi} = C_{1i} (e_i + C_{2i} e_i^5) \qquad i=1\cdots4 \tag{F.3}$$

where C_{1i} and C_{2i} are the spring constants. e_i is the deflection of the ith suspension joint. Positive C_{2i}'s are used producing nonlinear hardening springs. Figure F.2 shows the spring force-deflection characteristics used in the model.

The damping force is modeled as:

$$P_{Di} = D_i \dot{e}_i \qquad |\dot{e}_i| < \overline{w}\ i=1\cdots4 \tag{F.4}$$

$$= D_i \overline{w} + \overline{D}_i(\dot{e}_i - \overline{w}) \qquad \dot{e}_i \geq \overline{w}$$

$$= -D_i\bar{w} + \bar{D}_i(\dot{e}_i + \bar{w}) \quad \dot{e}_i \le -\bar{w}$$

The hysteresis effect is neglected, and the damping force characteristic is represented by three straight lines (Figure F.3).

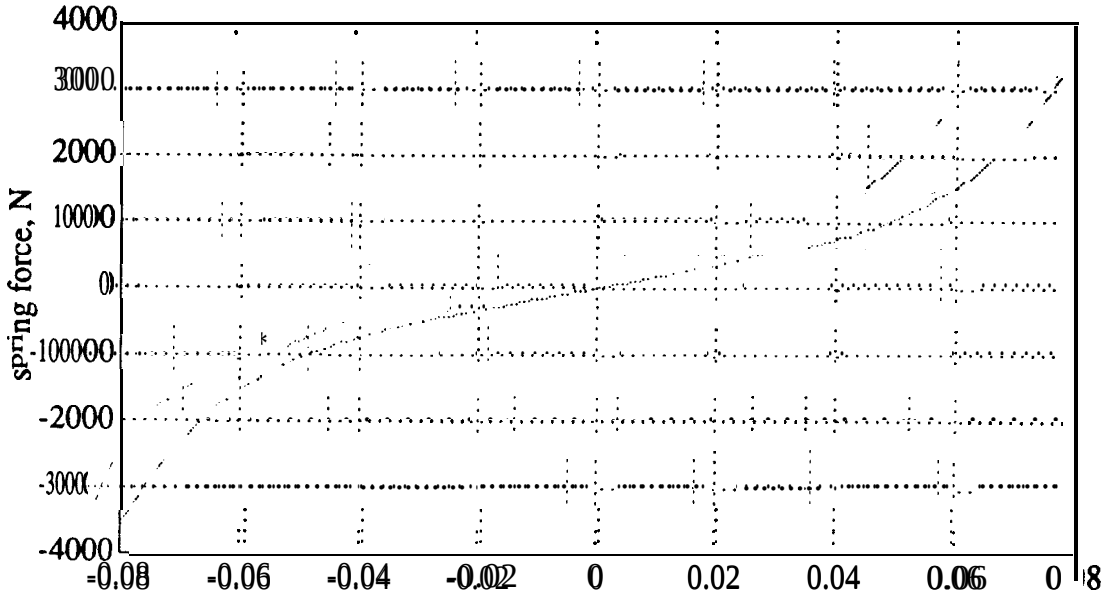

Figure F.2 Suspension Spring Force

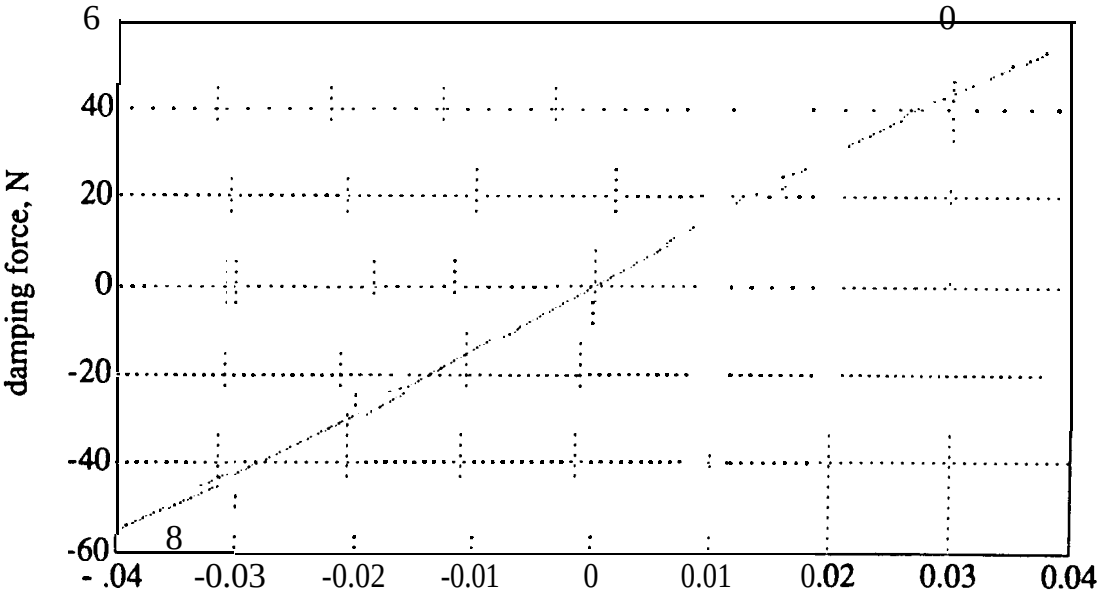

Figure F.3 Suspension Damping Force

By combining the results of the tire and suspension models, the forces and moments entering through the tires can be obtained. The dynamic equations governing the motion of the vehicle center of mass are obtained [14]:

$$m[\dot{V}_x - V_y\varepsilon + h_4\ddot{\theta} + z(\gamma\beta + \dot{\gamma}\beta - \psi\gamma - \psi\dot{\gamma} + \ddot{\Delta}) + h_2\phi\varepsilon + h_2\dot{\phi}\dot{\varepsilon} + \dot{z}\Delta - h_5(\theta\Delta + \theta\ddot{\Delta})] = F_{wx} + mg\Delta + \sum_{i=1}^{4} F_{Ai} \quad \text{(F.5)}$$

$$m[\dot{V}_y + V_x\varepsilon - h_2\ddot{\phi} - z(\dot{\Delta}\beta + \Delta\beta + \dot{\psi}\Delta + \psi\dot{\Delta}) + h_4(\dot{\theta}\varepsilon + \theta\dot{\varepsilon}) - \dot{\gamma}(z - h_5\theta) - \gamma(\dot{z} - h_5\dot{\theta})] = F_{wy} - mg\gamma + \sum_{i=1}^{4} F_{Bi} \quad \text{(F.6)}$$

$$m[\ddot{z} + V_y(\gamma + \Delta\beta + \psi\Delta) - V_x(\dot{\Delta} + \psi\beta - \psi\gamma) - h_5\ddot{\theta} - h_2(\dot{\phi}\gamma + \phi\dot{\gamma}) - h_4(\theta\dot{\Delta} + \theta\ddot{\Delta})] = -mg + \sum_{i=1}^{4} F_{Pi} \quad \text{(F.7)}$$

$$I_x(\dot{\gamma} + \ddot{\phi} - \theta\dot{\varepsilon} - \dot{\theta}\varepsilon + \ddot{\Delta}\beta + \dot{\Delta}\beta + \dot{\psi}\Delta + \psi\dot{\Delta}) - (I_y - I_z)(\dot{\theta} + \dot{\Delta})\varepsilon = M_{xu} - \theta M_{zu} \quad \text{(F.8)}$$

$$I_y(\ddot{\theta} + \ddot{\Delta} + \dot{\gamma}\beta + \gamma\dot{\beta} - \dot{\psi}\gamma - \psi\dot{\gamma} + \phi\dot{\varepsilon} + \dot{\phi}\varepsilon) - (I_z - I_x)(\phi + \gamma)\varepsilon = M_{yu} + \phi M_{zu} \quad \text{(F.9)}$$

$$I_z(\dot{\varepsilon} + \theta\dot{\gamma} + \dot{\theta}\gamma + \theta\ddot{\phi} - \phi\ddot{\theta} - \phi\dot{\Delta} - \dot{\phi}\Delta) - (I_x - I_y)(\phi + \gamma)(\dot{\theta} + \dot{\Delta}) = M_{zu} + \theta M_{xu} - \phi M_{yu} \quad \text{(F. 10)}$$

where M_{xu} ,M_{yu} and M_{zu} are the moments acting on the vehicle through the tires. The complex model simulation is coded using the C programming language. Integration of the ordinary differential equations is performed using the Runge-Kutta method with adjusted integration time step for better accuracy of the simulation results.

F.2 Simplified Model

The simplified model is obtained from the complex model. Assuming that the vertical, roll, and pitch motions can be neglected, the superelevation and gradient of road, side slip angle, and error in yaw angle are small, and the longitudinal speed is constant, the complex model presented in the first part of this appendix can be simplified to a linear model. The number of state variables is four, two in each of the lateral and yaw directions. Referring to Figure F.4, the nomenclature of the simplified model is:

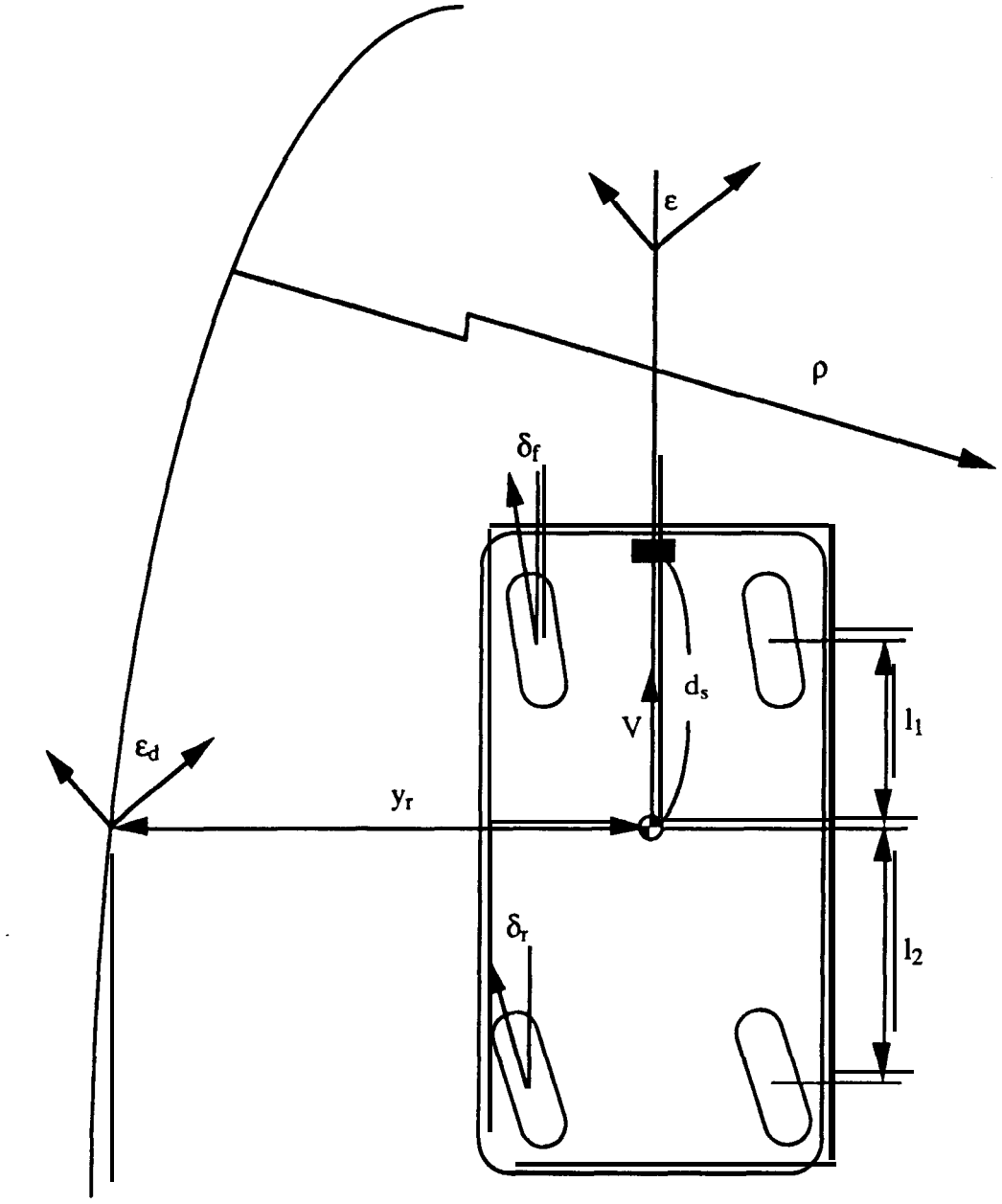

Figure F.4 Scope of the Simplified Model

Yr : lateral distance between the vehicle c.g. and the center line of the road

ε : yaw angle of vehicle body

ε_d : desired yaw angle set by the road

d_s : distance from vehicle mass center to magnetic sensor

v : longitudinal speed of vehicle

ρ : radius of curvature of the road

w : curvature of the road ($= \frac{1}{\rho}$)

δ_f : front wheel steering angle
δ_r : rear wheel steering angle
m: mass of the vehicle
I_z : yaw moment of inertia of the vehicle
l_1 : distance from c.g. to the front axle
l_2 : distance from c.g. to the rear axle

By retaining only the lateral and the yaw motions, the nonlinear vehicle model can be simplified to a fourth order linear model [14]. For front-wheel-steering vehicle, assuming that $\delta_f = 6$ and $\delta_r = 0$, we obtain the following state space equation:

$$\frac{d}{dt}\begin{bmatrix} y_r \\ \dot{y}_r \\ \varepsilon - \varepsilon_d \\ \dot{\varepsilon} - \dot{\varepsilon}_d \end{bmatrix} = \left[\begin{array}{cccc} 0 & 1 & 0 & 0 \\ 0 & \frac{A_1}{V} & -A_1 & \frac{A_2}{V} \\ 0 & 0 & 0 & 1 \\ 0 & \frac{A_3}{V} & -A_3 & \frac{A_4}{V} \end{array}\right] \left[\begin{array}{c} y_r \\ y_r \\ \varepsilon - \varepsilon_d \\ \dot{\varepsilon} - \dot{\varepsilon}_d \end{array}\right] + \begin{bmatrix} 0 \\ B_1 \\ 0 \\ B_2 \end{bmatrix} \delta + \begin{bmatrix} 0 \\ A_2 - V^2 \\ 0 \\ A_4 \end{bmatrix} \frac{1}{\rho}$$

$$= A\chi + B\delta + D\,w \qquad \text{(F.11)}$$

where y_r is the lateral deviation of the mass center from the reference, ε is the yaw angle of the vehicle, and ε_d is the desired yaw angle determined by the road curve. ρ is the radius of curvature, and $w = \frac{1}{\rho}$ is the curvature of the road. A_i's and B_i's depend on vehicle parameters, and are defined as follows:

$$A_1 = \frac{-2(C_{sf} + C_{sr})}{m} \qquad \text{(F.12)}$$

$$A_2 = \frac{2(C_{sr}l_2 - C_{sf}l_1)}{m} \qquad \text{(F.13)}$$

$$A3 = \frac{2(C_{sr}l_2 - C_{sf}l_1)}{I_z} \qquad \text{(F. 14)}$$

$$A_4 = \frac{-2(C_{sf}l_1^2 + C_{sr}l_2^2)}{I_z} \qquad \text{(F.15)}$$

$$B_1 = \frac{2C_{sf}}{m} \qquad \text{(F.16)}$$

$$B_2 = \frac{2l_1C_{sf}}{I_z} \qquad \text{(F.17)}$$

where C_{sf} and C_{sf} are the tire cornering stiffness of the front and rear wheels, respectively. The output y_s, taken as the measurement of lateral deviation from a sensor located at a distance d_s ahead of the mass center, can be expressed as:

$$y_s(t) = y_r(t) + d_s(\varepsilon(t) - \varepsilon_d(t)) = [\, 1, 0, d_s, 0 \,] \underline{x}\,(t) \qquad \text{(F.18)}$$

Now that the vehicle is represented in a linear state space form, linear optimal control theories can be applied to design the feedback and feedforward controllers.

G. FSLQ CONTROL FORMULATION

In the following, the Frequency-Shaped ***Linear Quadratic*** (FSLQ) control theory is introduced for the feedback controller design. The tracking error, passenger ride quality, and robustness with respect to high frequency unmodeled dynamics are included in the performance index for trade-offs. The performance index of the automatic lateral control problem is formulated as follows:

$$J = \frac{1}{2\pi}\int_{-\infty}^{\infty} [a^*(j\omega)\frac{q_a^2}{1+\lambda_a^2\omega^2}a(j\omega) + y_s^*(j\omega)\frac{q_y^2}{1+\lambda_y^2\omega^2}y_s(j\omega) + (\dot{\varepsilon}(j\omega) - \dot{\varepsilon}_d(j\omega))^*\frac{q_\varepsilon^2}{1+\lambda_\varepsilon^2\omega^2}(\dot{\varepsilon}(j\omega) - \dot{\varepsilon}_d(j\omega)) + y_s^*(j\omega)\frac{q_i^2}{(j\omega)^2}y_s(j\omega) + \delta^*(j\omega)R\delta(j\omega)]\,d\omega \tag{G.1}$$

where * denotes a complex conjugate. The coefficient λ_a determines the bandwidth of the weighting on the lateral acceleration, and is crucial for ride quality. Coefficients λ_y and λ_ε are determined by considering both the high-frequency robustness of the controller and the tracking performance. After choosing the values of λ_a, λ_y and λ_ε, the values of q_a, q_y, q_ε and q_i are selected by further tuning. The parameters q_a, q_y, q_ε and q_i are tuned to compromise between the ride quality and the tracking error. At this stage of the experiment, R is fixed to be one for the front-wheel-steering vehicles. The FSLQ problem is transformed to a standard Linear Quadratic (LQ) problem by introducing augmented state variables

$$z_1^* z_1 \equiv a^*(j\omega)\frac{q_a^2}{1+\lambda_a^2\omega^2}a(j\omega) \tag{G.2}$$

$$z_2^* z_2 \equiv y_s^*(j\omega)\frac{q_y^2}{1+\lambda_y^2\omega^2}y_s(j\omega) \tag{G.3}$$

$$z_3^* z_3 \equiv (\dot{\varepsilon}(j\omega) - \dot{\varepsilon}_d(j\omega))^*\frac{q_\varepsilon^2}{1+\lambda_\varepsilon^2\omega^2}(\dot{\varepsilon}(j\omega) - \dot{\varepsilon}_d(j\omega)) \tag{G.4}$$

$$z_4^* z_4 \equiv y_s^*(j\omega)\frac{q_i^2}{(j\omega)^2}y_s(j\omega) \tag{G.5}$$

The performance index, Eq. (G. 1) can be transformed to a standard LQ performance index (does not include frequency as a parameter) using Parseval's theorem [24]:

$$J = \frac{1}{2}\int_{I_0}^{\infty} (z_1^T z_1 + z_2^T z_2 + z_3^T z_3 + z_4^T z_4 + \underline{\delta}^T R \underline{\delta}) \, dt \tag{G.6}$$

$$= \frac{1}{2}\int_0^{\infty} [\underline{x}^T z_1^T \; z_2^T \; z_3^T \; z_4^T \; \underline{\delta}^T] \begin{bmatrix} 0 & 0 & 0 & 0 & 0 & 0 \\ 0 & 1 & 0 & 0 & 0 & 0 \\ 0 & 0 & 1 & 0 & 0 & 0 \\ 0 & 0 & 0 & 1 & 0 & 0 \\ 0 & 0 & 0 & 0 & 1 & 0 \\ 0 & 0 & 0 & 0 & 0 & R \end{bmatrix} \begin{bmatrix} \underline{x} \\ z_1 \\ z_2 \\ z_3 \\ z_4 \\ \underline{\delta} \end{bmatrix} dt \tag{G.7}$$

where $\underline{x}$ is the original fourth order state vector. The augmented system is of eighth order since four extra state variables are introduced. Now that the system equation is in the standard LQ form, the gain vector of the feedback controller can be computed by solving the Algebraic Riccati Equation. For more details, refer to [14].

H. PREVIEW CONTROL FORMULATION

When the future road information is available, the controller can utilize this information to improve the tracking performance of the vehicle. In the following, the preview control theory is studied from a deterministic point of view. That is, the road curvature is obtained without any measurement noise, although quantization error may exist. The preview time is assumed to be finite. That is, at time t, the road curvature in $\tau \in [\, t, t + t_{la}]$ is assumed to be known, where t_{la} is the preview time.

The preview control law is applied to the FSLQ augmented system in this report. The resulting algorithm retains all the advantages of the FSLQ control algorithm as described in Appendix F. Furthermore, the preview action utilizes the future road curvature information so that the transient tracking error and lateral acceleration can be reduced simultaneously. Assuming the system to be controlled is represented in a linear state space form:

$$\dot{\underline{x}}_e(t) = A_e \underline{x}_e(t) + B_e \underline{\delta}(t) + D_e \underline{w}(t) \tag{H.1}$$

and the performance index to be minimized is in a standard quadratic form:

$$J = \lim_{t_f \to \infty} \frac{1}{2} \int_{0-}^{t_f} [\, \underline{x}_e^T(t)\, Q\, \underline{x}_e(t) + \delta^T(t)\, R\, \delta(t)\, 1\, dt \tag{H.2}$$

where $\underline{x}_e(t) = [\, x^T(t), z_1(t), z_2(t), z_3(t), z_4(t)\,]^T$ is the augmented eighth order state vector, and A_e, B_e and De are the augmented system matrices. In the following, the optimal preview control laws are developed where the road curvature, w, is assumed to be available as preview information. Like other linear quadratic optimal control problems, the optimal preview control problem is solved by Dynamic Programming [25]. Recalling that the performance index to be minimized is the one in Eq. (H.2), the following equation can be derived from the principle of optima&y:

$$0 = \min_{\delta(t)} \left\{ \frac{1}{2} \underline{x}_e^T(t)\, Q\, \underline{x}_e(t) + \frac{1}{2} \delta^T(t)\; R\; 6(t) + \frac{dJ^*(t)}{dt} \right\} \tag{H.3}$$

where $J^*(t)$ is the optimal cost function among all J(t) defined in Eq. (H.2), The Hamiltonian H is defined as:

$$H(t) \equiv \frac{1}{2}\,\underline{x}_e^T(t)\,Q\,\underline{x}_e(t) + \frac{1}{2}\,\delta^T(t)\,R\,\delta(t) + \frac{\partial J^*(t)}{\partial \underline{x}_e}(A_e\underline{x}_e + B_e\delta + D_e w) \qquad \text{(H.4)}$$

The optimal control, $\delta_{opt}(t)$, can then be obtained from:

$$\frac{\partial H}{\partial \delta}\Big|_{\delta = \delta_{opt}} = 0 \qquad \text{(H.5)}$$

The minimization of the performance index Eq. (H.2) requires that the disturbance be specified over the problem duration. However, the preview assumption implies that only $\{w(t+\sigma) \mid 0 \le \sigma \le t_{la}\}$ is known at time t. A natural way to specify the disturbance beyond the preview segment is to introduce a disturbance generator described by:

$$\frac{dw(\tau)}{d\tau} = A_w w(\tau) \qquad \tau \ge t + t_{la} \qquad \text{(H.6)}$$

where $A_w \le 0$ governs the decay rate of $w(\tau)$. The optimal preview control algorithm is solved by assuming that the optimal cost function can be expressed by the generalized quadratic form with respect to:

1. the current state vector, $\underline{x}_e(t)$
2. disturbance, $w(t+\sigma)$, in the preview segment $\sigma \in [0, t_{la}]$

The optimal cost function is then expressed as:

$$\begin{aligned} J^*(\underline{x}_e(t), w(t,[0,t_{la}])) = {} & \frac{1}{2}\underline{x}_e^T(t)\,K(t)\,\underline{x}_e(t) \\ & + \frac{1}{2}\int_0^{t_{la}}\int_0^{t_{la}} w^T(t,l_1)\,K_w(t,l_1,l_2)\,w(t,l_2)\,dl_1 dl_2 \\ & + \frac{1}{2}w^T(t+t_{la})\,K_d(t)\,w(t+t_{la}) \\ & + \underline{x}_e^T(t)\int_0^{t_{la}} F_1(t,l)\,w(t,l)\,dl + \underline{x}_e^T(t)\,F_2(t)\,w(t+t_{la}) \end{aligned} \qquad \text{(H.7)}$$

where $w(t, l) \equiv w(t + l)$. The optimal control law can then be derived from Eqs. (H.3)-(H.7):

$$\delta_{opt}(t) = -R^{-1}B_e^T \left[K(t)\, x_e^T(t) + \int_0^{l_a} F_1(t, l)\, w(t, l)\, dl + F_2(t)\, w(t+t_{la})\right] \qquad (H.8)$$

The details to derive Eq. (H.8) and the equations governing the gain matrices K, F_1, and F_2 are presented in [4]. It can be seen from Eq. (H.8) that the preview control law consists of three terms, one feedback term and two feedforward terms. The first term is exactly the same as the feedback control signal in the FSLQ control algorithm without the preview assumption. The second term is the preview action to deal with the disturbance signal (road curvature) within the preview segment. The third term is the preview action to cope with the disturbance beyond the preview segment. For the FSLQ augmented system, the problem duration is infinite. Therefore, time-invariant gains of $F_1(l)$ and F_2 are used:

$$F_1(l) = e^{A_c^T l} K_{ss}\, D_e \qquad (H.9)$$

$$F_2 = -(A_c^T + A_w I)^{-1} e^{A_c^T t_{la}} K_{ss}\, D_e \qquad (H.10)$$

where $A_c \equiv A - B_e R^{-1} B_e^T K_{ss}$ is the closed loop system matrix.